Thermodynamics and Kinetics of Sorption

Charl Guillaume Marais

Thesis presented in partial fulfilment of the requirements for the degree of

Master of Science in Chemistry at Stellenbosch University

Supervisor: Prof. L. J. Barbour

Co-Supervisor: Dr. C. Esterhuysen

December 2008

Declaration

By submitting this thesis electronically, I Charl Guillaume Marais, hereby declare that the entirety of the work contained therein is my own, original work, that I am the owner of the copyright thereof (unless to the extent explicitly otherwise stated) and that I have not previously in its entirety or in part submitted it for obtaining any qualification.

Date: 25 November 2008

Summary

A device was built, described and used to perform volumetric sorption experiments on porous solid host systems, and used to calculate the thermodynamic parameters of solid-gas sorption reactions. The device was tested on six supramolecular host systems to highlight the versatility, advantages and disadvantages of the device. The six systems that were studied are:

- 2,2'-bis-(formyl-1,6,7-trihydroxy-5-isopropyl-3-methylnaphthalene) or gossypol
- *p-tert*-butylcalix[4]arene
- Cu_2(2,3-bis(imidazol-1-ylmethyl)-2,4,6-trimethylbenzene)$_2Cl_4$ or [Cu_2(BITMB)$_2Cl_4$]
- Cd_2(4,4-bis(2-methylimidazol-1-ylmethyl)biphenyl)$_2Cl_4$ or [Cd_2(B2MB)$_2Cl_4$]
- Molecular Sieve 4A
- tris(*o*-phenylenedioxy)cyclotriphosphazene

A novel device to calculate kinetic parameters of solid-gas sorption was built and tested on the following four supramolecular host systems:

- 2,2'-bis-(formyl-1,6,7-trihydroxy-5-isopropyl-3-methylnaphthalene) or gossypol
- *p-tert*-butylcalix[4]arene
- Cu_2(2,3-bis(imidazol-1-ylmethyl)-2,4,6-trimethylbenzene)$_2Cl_4$ or [Cu_2(BITMB)$_2Cl_4$]
- Cd_2(4,4-bis(2-methylimidazol-1-ylmethyl)biphenyl)$_2Cl_4$ or [Cd_2(B2MB)$_2Cl_4$]

The methodology development was undertaken with the aim to gain greater insight into the underlying mechanisms governing the sorption process. Thermodynamic and kinetic data were used in conjunction with standard crystallographic, CP-MAS NMR, computational and sorption techniques to describe a mechanism for gas transport through the crystal lattice of the guest free low density phase of *p-tert*-butylcalix[4]arene.

Opsomming

Die bou, beskrywing en gebruik van ‘n apparaat gepas vir die uitvoering van volumetriesesorpsie eksperimente, asook vir die die bepaling van termodinamiese veranderlikes vir die soliede-gas sorpsiereaksie word hier beskryf. Die apparaat was getoets op ses verskillende supramolekulêre vastetoestand gasheersisteme om die veelsydigheid, voordele en nadele aan te spreek. Die ses bestudeerde sisteme is:

- 2,2'-bis-(formiel-1,6,7-trihidroksi-5-isopropiel-3-metielnaftaleen) or gossiepol
- *p-ters*-butielkaliks[4]areen
- Cu_2(2,3-bis(imidasool-1-ylmethiel)-2,4,6-trimethielbenseen)$_2Cl_4$ or $[Cu_2(BITMB)_2Cl_4]$
- Cd_2(4,4-bis(2-methielimidasool-1-ylmethiel)bifeniel)$_2Cl_4$ or $[Cd_2(B2MB)_2Cl_4]$
- Molekulêresif 4A
- tris(*o*-fenieleendioksi)siklotrifosfaseen

Die doel van die metodiekontwikkeling was om tot beter insig te kom aangaande die onderliggende meganismes wat die sorpsieproses bepaal. Termodinamiese – en kinetiese data word gebruik saam met standaard kristallografiese -, vastetoestand KMR-, rekenaar - en sorpsietegnieke om 'n meganisme van gasvervoer deur die kristalrooster van die gasvrye, laedigtheid fase van *p-ters*-butielkaliks[4]areen.

Posters and Seminars

Parts of this work have been presented at the following conferences as a poster presentation:

- International Symposium on Inclusion Compounds (ISIC) 11, Kiev, Ukraine, 2007.
- The Annual Polish Crystallographic Conference, Wrocław, Poland, 2007.
- 24th European Crystallographic Meeting (ECM), Marrakech, Morocco, 2007.

Parts of this work have been presented in the form of an oral presentation at the following conferences:

- South African Chemical Institute (SACI) Young Scientist Symposium, Cape Town, 2007.
- Carman National Physical Chemistry Symposium, Cape Town, 2007.

Acknowledgements

None of this work would have been possible without the constant guidance and patience my supervisor, Prof L.J. Barbour and co-supervisor, Dr. C. Esterhuysen have given me during the course of my research. Thank you both for not only steering a project, but for steering and guiding my education in such a manner that I leave here with a sincere appreciation for science, knowing that what we know now is only a scratch at the surface of what lies waiting to be found. A sincere word of thanks to my adopted Polish supervisors Prof J. Lipkowski and Dr. K. Suwińska, at the Institute of Physical Chemistry, Polish Academy of Science. It was a fantastic experience working with both of you. Thank you Dr. Agnieszka Szumna for your help and assistance regarding the synthesis of isopropylcalix[4]arene. Thank you Dr. Mariusz Pietrzak for your assistance in running the solid-state CP-MAS NMR experiments.

The following people helped provide samples of the compounds which were studied as part of this work and without their assistance none of this work would have been possible. Tia Jacobs for the synthesis and crystallisation of $[Cd_2(B2MB)_2Cl_4]$. Gareth Lloyd and Liliana Dobrzańska for the synthesis and crystallisation of $[Cu_2(BITMB)_2Cl_4]$. Prof L. R. Nassimbeni and Dr. Tanya le Roex for providing the Gossypol. Dr. Dinabandhu Das for synthesising tris(*o*-phenylenedioxy)cyclotriphosphazene. Prof L. J. Barbour and Bettinah Chipimpi for providing the *p*-*tert*-butylcalix[4]arene.

Dr. J.-A. Gertenbach must be especially thanked for his advice and his technical expertise, and all those weekends of training in the early days. All gravimetric sorption experiments were performed with the kind assistance of Dr. Gertenbach. Prof L. R. Nassimbeni must be thanked for his invaluable input regarding the kinetic experiments and Prof J. Dillen must be thanked for his input regarding all matters computational and for his input concerning the chemical activity of a solid.

Throughout this work my friends and colleagues in the Supramolecular Materials Group have provided tremendous moral support which does not go unnoticed or unappreciated. Much thanks then to Tia Jacobs, Storm Potts, Leigh Loots, Jan Gertenbach, Martin Bredenkamp, Bettinah Chipimpi, Dinabandhu Das, Tanya le Roex, Delia Haynes, Eustina Batisai and Marlene Milani.

“Would you tell me, please, which way I ought to go from here?”

‘That depends a good deal on where you want to get to,’ said the Cat.

“I don’t much care where-” said Alice.

‘Then it doesn’t matter which way you go,’ said the Cat.

“- so long as I get *somewhere*,” Alice added as an explanation.

‘Oh, you’re sure to do that,’ said the Cat, ‘if you only walk long enough.’

Lewis Carol, *Alice’s Adventures in Wonderland*.

List of Abbreviations

a	A van der Waals constant for a real gas
A	Absorbance
Å	Ångström = 10^{-10} m
a	Chemical activity
A	Preexponential constant in the Arrhenius equation
A_M	Maximum absorbance
ar	Aryl
b	A van der Waals constant for a non-real gas
B2MB	4,4-bis(2-methylimidazol-1-ylmethyl)biphenyl
bar	Bar of pressure (1 bar ≈ 1/1.01325 atmosphere = 100 kPa)
BITMB	1,3-bis(imidazol-1-ylmethyl)-2,4,6-trimethylbenzene)
c	Ordinate intercept of a straight line for the equation $y=mx+c$
CP-MAS	Cross polarisation magic angle spinning
CSD	Cambridge Structural Database
e	Exponent
E_a	Activation energy
E_{FF}	Total force field potential energy
etc	*et cetera*
f	Fugacity
g	Gas
G	Guest
H	Host
H•G	Host-guest complex
IR	Infra-red
IUPAC	International Union of Pure and Applied Chemistry
k	Boltzmann's constant
K	Kelvin
k_a	Rate constant for adsorption
kcal	Kilocalorie
k_d	Rate constant for desorption
K_{eq}	Rate constant for the reaction under equilibrium conditions
k_f	Rate constant for the forward reaction

k_H	Henry's Law constant
kJ	Kilojoule
k_r	Rate constant for the reverse reaction
ln	Natural logarithm
m	Gradient of a straight line for the equation $y=mx+c$
mbar	Millibar
min	Minutes
mmol	Millimoles
MOF	Metal-organic framework
mol	Moles
M_R	Molecular weight
n	Guest-host ratio
n	Number of moles
N	Surface concentration of a sorbed species
NMR	Nuclear magnetic resonance
NPT	Isothermal-isobaric ensemble
NVE	Microcanonical ensemble
NVT	Canonical ensemble
P	Pressure
p	Pressure
$P°$	Standard pressure (1 bar)
P_A	Pressure transducer A monitoring pressure in the gas reservoir
P_B	Pressure transducer B monitoring pressure in sample chamber
PXRD	Powder X-ray diffraction
R	Gas regulator
R	Universal gas constant (8.3145 $J.mol^{-1}.K^{-1}$)
R_{des}	Rate of desorption
s	Solid
SIT	Sorption isosteric technique
T	Temperature in Kelvin (unless another unit is specified)
t	Time
TPD	Temperature programmed desorption
TPP	Tris(*o*-phenylenedioxy)cyclotriphosphazene
V	Volume

$V_{1\text{-}3}$	Valves numbered one, two or three
V_A	Volume A of the gas reservoir
V_B	Volume B of the sample chamber
V_D	Volume of the "*dead space*"
V_s	Specific retention volume
vs	*versus*
V_S	Volume of the sample
V_x	Volume of aluminium rod
x	Kinetic order of desorption
XRD	X-ray diffraction
z	The molecular partition function
α	Alpha, extent of reaction
δ	Density
$\Delta G°_{ad}$	Standard Gibbs free energy
$\Delta G_{reaction}$	Gibbs free energy of the reaction
$\Delta H°_{ad}$	Standard enthalpy of adsorption
$\Delta S°_{ad}$	Standard entropy of adsorption
ΔY	Thermodynamic parameters
ε	Energy state
ε_D	Total potential energy
θ	Degree of coverage
μ	Chemical potential

THERMODYNAMICS AND KINETICS OF SORPTION I

DECLARATION II

SUMMARY III

OPSOMMING IV

POSTERS AND SEMINARS V

ACKNOWLEDGEMENTS VI

LIST OF ABBREVIATIONS VIII

CHAPTER 1. INTRODUCTION AND OBJECTIVES. 1

CHAPTER 2. LITERATURE STUDY 3

2.1. HISTORICAL OVERVIEW OF SUPRAMOLECULAR CHEMISTRY 3
2.2. HOST-GUEST CHEMISTRY 5
2.3. SORPTION 8
2.4. POROSITY 12
2.4.1. Conventional Porosity 13
2.4.2. Virtual Porosity 14
2.4.3. Transient Porosity 14
2.5. THERMODYNAMICS AND KINETICS OF GAS SORPTION 14
2.5.1. Methods to Determine Thermodynamic Parameters of Solid-Gas Sorption Reactions. 17
2.5.1.1. Computational Methods 17
2.5.1.2. Calorimetric Methods 18
2.5.1.3. Chromatographic Techniques 18
2.5.1.4. Born-Haber-type Thermodynamic Cycles 18
2.5.1.5. Variable Temperature Infra-Red Spectroscopy (VTIR) 19
2.5.1.6. Gravimetric and Volumetric Sorption Isosteric Techniques 20
2.5.2. Methods to Determine Kinetic Parameters of Solid-Gas Sorption Reactions. 20
2.5.2.1. Computational Methods 21
2.5.2.2. Temperature Programmed Desorption (TPD) 21
2.5.2.3. Volumetric and Gravimetric Methods 22
2.6. COMPUTATIONAL CHEMISTRY OVERVIEW 23
2.6.1. Force Field Methods (Molecular Mechanics) 24
2.6.2. Energy Minimisation 25
2.6.3. Molecular Dynamics 26

CHAPTER 3. MATERIALS AND METHODS 28

3.1. SINGLE-CRYSTAL X-RAY DIFFRACTION 28
3.2. POWDER X-RAY DIFFRACTION (PXRD) 28
3.3. SOLID-STATE CP-MAS NMR 28
3.4. SOLUTION STATE NMR 29
3.5. VOLUMETRIC SORPTION 29
3.6. GRAVIMETRIC SORPTION 29
3.7. COMPUTER PACKAGES 29
3.7.1. Cerius^2 29
3.7.2. XPREP 29
3.7.3. SHELX-97 29
3.7.4. POV-Ray 30
3.7.5. SQUEEZE 30
3.7.6. Cambridge Structural Database (CSD) 31
3.7.1. X-Seed 31
3.7.2. MSROLL 31
3.7.3. WebLab ViewerPro 31
3.8. COMPOUNDS STUDIED 31
3.8.1. 2,2'-bis-(formyl-1,6,7-trihydroxy-5-isopropyl-3-methylnaphthalene): Gossypol 31

3.8.2. p-tert-butylcalix[4]arene 33
3.8.3. Cu_2(1,3-bis(imidazol-1-ylmethyl)-2,4,6-trimethylbenzene)$_2Cl_4$: [Cu_2(BITMB)$_2Cl_4$] 36
3.8.4. Cd_2(4,4-bis(2-methylimidazol-1-ylmethyl)biphenyl)$_2Cl_4$ [Cd_2(B2MB)$_2Cl_4$] 37
3.8.5. Molecular Sieve 4A 39
3.8.6. Tris(o-phenylenedioxy)cyclotriphosphazene (TPP) 40
3.8.7. p-isopropylcalix[4]arene 42

CHAPTER 4. METHODOLOGY DEVELOPMENT FOR DETERMINING THERMODYNAMIC PARAMETERS OF SOLID-GAS SORPTION REACTIONS. 44

4.1. THE CONSTRUCTED VOLUMETRIC SORPTION DEVICE 44
4.2. A TYPICAL EXPERIMENT: THEORY AND PRACTICE 50
4.2.1. The Sorption Reaction to Equilibrium 51
4.2.2. Determining the Thermodynamic Parameters $\Delta G°_{ad}$, $\Delta H°_{ad}$, and $\Delta S°_{ad}$ 53
4.3. ADVANTAGES & DISADVANTAGES OF THE VOLUMETRIC SIT DEVICE. 61
4.4. RESULTS AND DISCUSSION 61
4.4.1. Gossypol 62
4.4.2. p-tert-Butylcalix[4]arene 66
4.4.3. Cu_2(1,3-bis(imidazol-1-ylmethyl)-2,4,6-trimethylbenzene)$_2Cl_4$ [Cu_2(BITMB)$_2Cl_4$] 68
4.4.4. Cd_2(4,4-bis(2-methylimidazol-1-ylmethyl)biphenyl)$_2Cl_4$ [Cd_2(B2MB)$_2Cl_4$] 70
4.4.5. Molecular Sieve 4A 73
4.4.6. Tris(o-phenylenedioxy)cyclotriphosphazene (TPP) 74
4.5. CONCLUSION 76

CHAPTER 5. METHODOLOGY DEVELOPMENT FOR DETERMINING KINETIC PARAMETERS OF SOLID-GAS SORPTION REACTIONS. 78

5.1. INSTRUMENT DESCRIPTION 78
5.2. A TYPICAL EXPERIMENT: THEORY & PRACTICE 82
5.3. RESULTS AND DISCUSSION 89
5.3.1. [Cu_2(BITMB)$_2Cl_4$] 89
5.3.2. Gossypol 94
5.3.3. p-tert-butylcalix[4]arene 95
5.4.3. [Cd_2(B2MB)$_2Cl_4$] 97
5.4. CONCLUSION 98

CHAPTER 6. CARBON DIOXIDE GAS-TRANSPORT IN *P-TERT*-BUTYLCALIX[4]ARENE. 101

6.1. POSTULATING A POSSIBLE PATH FOR GAS MOVEMENT 101
6.2. CHOICE OF FORCE FIELD 105
6.3. BUILDING THE CRYSTAL LATTICE 105
6.4. INCORPORATION OF THE GUEST IN THE HOST STRUCTURE 106
6.5. EXECUTING THE CALCULATION 107
6.6. RESULTS AND DISCUSSION 110
6.7. CONCLUSION 118

CHAPTER 7. CONCLUSION 121

CHAPTER 8. REFERENCES 124

CHAPTER 1. Introduction and Objectives.

Porous solids have attracted widespread attention owing to their unusual physico-chemical properties [1] and are of particular economic interest with regard to their potential applications in gas storage [2, 3], gas separation [4] and sensing [3, 5]. Industrial applications in the manufacturing sector often require the ready availability of pure gas and it is thus necessary to devise new methods for the effective separation of gaseous mixtures and the safe storage of purified gas. With fossil fuels fast becoming depleted as an energy source, a drive toward a renewable alternative has become the research focus of many academic and non-academic research groups, with particular attention focussed on the possible exploitation of hydrogen gas as an alternate energy carrier. Greenhouse gas emission regulations have been highly topical among environmentalists and politicians as the effects of climate change become ever more prominent. Understanding mechanisms of gas transport, gas storage and the weak interactions governing solid-gas interactions has consequently become imperative to solving problems facing today's society, and has become key in the exploitation of applied technologies. The study and rational design of property-specific supramolecular materials has therefore become a rapidly growing research field.

This study primarily concerns itself with gaining greater understanding of the physico-chemical mechanisms involved in the transport and storage mechanisms associated with the sorption of gas by porous supramolecular assemblies in the solid-state. Volumetric and gravimetric sorption results are interpreted in conjunction with crystallographic and computational techniques in order to postulate feasible transport mechanisms. Methodology development for the determination of thermodynamic and kinetic parameters was also undertaken to further our current understanding of underlying solid-gas interactions and mechanisms of sorption observed for various porous systems. With a better comprehension of sorption mechanisms we can move closer to the goal of developing rationally designed and functional "*smart*" materials.

CHAPTER 2 contains a general introduction to the field of supramolecular chemistry, discussing its origins and development in **Section 2.1.** Important concepts used throughout this study such as the idea of host-guest chemistry (**Section 2.2.**), the distinctions made between physisorption and chemisorption (**Section 2.3.**), and the different classifications of

porosity (**Section 2.4.**) are discussed. A brief introduction to the thermodynamics and kinetics of sorption (**Section 2.5.**) is given as a prelude to the discussions on methodology development regarding the calculation of thermodynamic (**CHAPTER 4**) and kinetic (**CHAPTER 5**) parameters of solid-gas sorption reactions. An overview of computational procedures used as a part of this study is discussed in **Section 2.6**.

CHAPTER 3 briefly discusses experimental methods and materials.

CHAPTER 4 concerns itself with the development, construction and testing of an instrument used to determine thermodynamic parameters of a solid-gas sorption reaction. The mechanical description of the device (**Section 4.1.**) and the theory behind a typical experiment (**Section 4.2**) are discussed. The primary advantages and disadvantages of this technique are mentioned in **Section 4.3**. Results of six different supramolecular compounds are shown and discussed in **Section 4.4.** A conclusion regarding the method and the results is given is **Section 4.5**.

A novel method of calculating kinetic parameters of solid-gas sorption reactions is outlined in **CHAPTER 5**. Results are discussed and the method is seen to be a viable alternative to current commercial methods. Future experiments and adjustments to the instrumental design are recommended.

CHAPTER 6 discusses the postulation of a possible gas transport mechanism inherent to a transiently porous crystal by employing standard crystallographic, computational and solid-state CP-MAS NMR techniques in addition to the methods discussed in **CHAPTERS 4** and **5**.

A conclusion of the work comprising this study is given in **CHAPTER 7** and also highlights shortcomings and provides suggestions for future work regarding the development and postulation of gas transport mechanisms in porous solids.

CHAPTER 2. Literature Study

2.1. Historical Overview of Supramolecular Chemistry

The field of supramolecular chemistry is a relatively young branch of chemistry having undergone its primary development in the latter quarter of the 20th century [6]. The Nobel laureate Lehn said that supramolecular chemistry concerns itself with "*chemistry beyond the molecule*" [7] and can be viewed as the "*chemistry of molecular assemblies and of the intermolecular bond*" [7]. The principal reason for its late development is that a thorough understanding of synthetic methods is necessary when designing large supramolecular systems. In addition, powerful analytical technology is needed for supramolecular structure elucidation and for the investigation of physical, physico-chemical and dynamic properties of supramolecular assemblies [8].

The notion of individual molecules aggregating to form a distinct supramolecular assembly with novel and unique physico-chemical properties dates back to the early 19th century with the discovery of chlorine hydrate by Davy [6, 9] and the correct assignment of its chemical formula by Faraday [6, 10]. The pioneering contribution made by Werner [11] in the field of coordination chemistry facilitated the development of further conceptualisation with regard to how chemists view, understand and describe intermolecular interactions and observed phenomena [6, 11, 12].

Following the concepts put forward by Werner, Ehrlich introduced the idea of a molecular "*receptor*" which is receptive for interactions with new and unique chemical species introduced into the system [13]. Concurrently, biochemists began to observe that enzymatically catalysed reactions were often much faster and more selective than similar reactions performed without enzymatic catalysis. This led to the groundbreaking "*lock and key*" model proposed by Fischer [14]. The early 20th century saw the word "*supermolecule*" or "*Übermoleküle*" being used for the first time by Wolf [15] to describe ordered structural entities resulting from the association of many coordinatively saturated chemical species [6]. Considerable advances were made by Curtis, Busch, Jäger and Pedersen with developments in macrocyclic ligands. These ligands were designed for metal cations following Cram's work on cyclophanes, spherands and carcerands in the 1950s and 1960s and Lehn's work on

cryptands in the late 1960s [6]. These groundbreaking contributions to supramolecular chemistry earned Pedersen, Cram and Lehn the Nobel Prize in Chemistry in 1987.

The sorptive properties of certain compounds were known and utilised by the ancient Egyptians, Greeks and later the Romans [16]. There were a wide array of applications of certain clays and charcoal, including the clarification of fat and oil and the purification of water [16]. Although applications of supramolecular systems have been known for centuries [17], an increased understanding regarding the nature of supramolecular systems has led to an increase in the development of industrial applications from within the supramolecular field. The ability of solid-state supramolecular entities to remove colour from solutions containing dyes and the removal of unsavoury odours from air have been known since the 19th century. Charcoal was used in gas masks during World War I and bone char was used for refining sugar, oil and waxes, although the mechanism of action was poorly understood at the time [17]. With the development of synthetic zeolites and their myriad industrial applications came a greater understanding of solid-state chemistry.

Understanding the intermolecular forces that govern the formation of supramolecular entities, including the mechanisms involved in their observed novel properties is the first step toward the rational design of property-specific supramolecular entities. Ironically, these intermolecular forces, the "*cement*" that holds the supramolecular entities together, are weak interactions which were poorly understood until recently [18]. Yet, it is the nature of the weak hydrogen bond that causes ice to be less dense than water, preventing the earth's oceans from irreversibly freezing from the bottom up, thus permanently changing the face of the earth. The importance of the weak hydrogen bond is thus irrefutable. Powerful analytical techniques needed to be developed in order to gain better insight into the nature of these important weak intermolecular forces governing supramolecular assembly. Techniques that have successfully been employed include UV-visible-, fluorescence- and infra-red spectrophotometry, nuclear magnetic resonance spectroscopy, powder X-ray diffraction and, most prominently, single-crystal X-ray diffraction [12]. Single-crystal X-ray diffraction has made the most significant contribution to successfully understanding the intermolecular interactions in a supramolecular entity primarily owing to the crystal's periodic and ordered structure [19]. Dunitz [20] described the crystal as "*one of the finest examples of a supermolecule*" and a "*supermolecule par excellence*". Thus, studying this "*supermolecule par excellence*" by means of X-ray diffraction has led to the greatest improvement in the understanding of the forces that govern

supramolecular assembly. Dunitz further noted that only through the successful control of these intermolecular interactions could one design property-specific supramolecular entities [20].

Today supramolecular chemistry is one of the fastest growing and most interdisciplinary areas in chemistry with many exciting challenges to face. The quest to be able to manipulate and predict the nature of intermolecular forces in the design of property-specific supramolecular entities remains one of the greatest scientific challenges [21-24]. In this study we aim to gain greater understanding of the mechanisms associated with sorption of gas by solid-state supramolecular systems. A comprehensive understanding of solid-gas host-guest interactions will bring scientists one step closer to the rational design and synthesis of property-specific or *"smart"* materials.

2.2. Host-Guest Chemistry

Supramolecular chemistry concerns itself with the aggregation, binding or complexation of molecules *via* non-covalent interactions to form a larger conglomerate or supermolecule [6]. In order to conceptualise a model of the possible mechanisms involved in this process it is imperative to define which molecule is doing the binding and which molecule is being bound [6]. Following the work of Erhlich [13] and Wolf [15] it has become generally accepted to define a "*host*" as a molecule having *convergent* binding sites and the "*guest*" as a molecule containing *divergent* binding sites [6, 8, 25]. The interplay between "*host*" and "*guest*" molecules to form a structurally unique "*host-guest*" system is predominantly the result of a plethora of non-covalent interactions such as van der Waals interactions, hydrogen bonding, metal-ligand interactions, electrostatic interactions and π-acid and π-base interactions, to name but a few [25]. Understanding host-guest systems provides an ideal platform from which the tailored design and synthesis of property-specific supramolecular assemblies can develop in the future.

Host-guest systems may be classified into those that are stable in solution such as crown-ethers, cryptands and cryptophanes, and those that are stable only in the solid-state such as urea clathrates and gas hydrates [6]. The focus in this thesis will be on solid-state host-guest chemistry, which is the chemistry of the crystal forms of inclusion compounds or clathrates [12]. The earliest examples of such compounds date back to the 19th century but it has only

been in the latter half of the 20th century that these dynamic systems have become better understood with the advent of modern analytical techniques [12].

An important concept in host-guest chemistry is that of "*hole size*" [8]. It is unequivocally analogous to the "*lock and key*" concept proposed by Fischer [14]. The "*lock and key*" model was expounded when it was seen that host compounds containing two or more separate binding sites could show varying degrees of cooperativity and was consequently termed the "*induced fit*" model [8, 26]. The "*induced fit*" model or MWC model, proposed by Monod, Wyman and Changeux, postulates that a lithe interaction between the host enzyme and the guest ligand induces a conformational change in the structure of the host, initiating enhanced guest binding affinity [27]. The hypothesis was later confirmed by X-ray crystallography [27]. Further development by Koshland, Nemethy and Filmer led to the hypothesis of the "*sequential*" or KNF model [27, 28]. The KNF model proposed that guest binding to the enzyme host induces a conformational change in a subunit of the supramolecular host system causing cooperative interactions with neighbouring subunits of the supramolecular host enzyme. Effectively, the number of guests interacting with the host influences the host's ability to bind the guest [27].

Analogous solid-state host-guest chemistry systems involving solid-solid and solid-gas reactions need to be developed in the light of the socio-economic interest in gas separation, sequestration and sensing technologies. There are many potentially industrially relevant applications such as chiral recognition and the design of chiral phases for chromatographic use, enantiomer separation, autocatalysis and molecular switching [8]. Current understanding of the underlying processes and mechanisms are poorly evolved, at best [29].

In this study, solid-gas host-guest sorption reactions are investigated. A typical reaction can be viewed as follows:

$$\mathrm{H}\,(s) \quad + \quad \mathrm{nG}\,(g) \quad \underset{k_r}{\overset{k_f}{\rightleftharpoons}} \quad \mathrm{H{\cdot}G_n}\,(s) \qquad \textbf{(2.1)}$$

where $H_{(s)}$ is the solid host compound, n is the number of moles of guest, $G_{(g)}$ is the gaseous guest compound and $H{\cdot}G_{(s)}$ is the solid host-guest inclusion compound that is formed.

Since all phases of a solid will not necessarily display porosity it is imperative to define what phase of the compound one is working with. A description by Nassimbeni [30] concerning the classification of host phases in host-guest chemistry is followed in order to maintain clarity, and is shown in **Figure 2.1**. In this treatment, the *general* formation of the host-guest complex can be viewed as follows [30]:

$$H_{(s,\alpha)} + nG_{(l)} \text{ or } {}_{(g)} \# H{\cdot}G_{n(s,\beta)} \qquad \textbf{(2.2)}$$

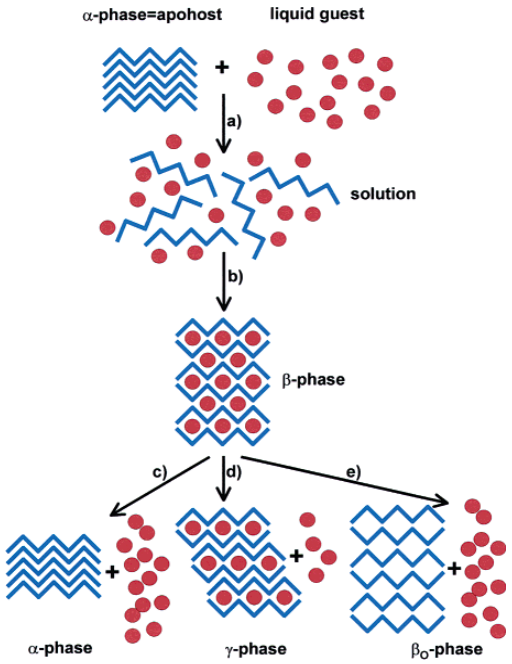

Figure 2.1. A schematic representation showing the differences between the α, β, β_0 and γ-phases of inclusion compounds [30, 31]. (**a**) Shows the α-phase (the non-porous solid host compound) dissolving into a liquid guest and (**b**) the formation of an inclusion compound, the β-phase. Processes (**c-e**) indicate the possible products that can be formed upon guest removal from the β-phase. (**c**) Shows guest removal to again yield the α-phase and guest. (**d**) Shows partial guest removal causing a structural change to the host framework, to yield a new form of the inclusion compound, the γ-phase. (**e**) Shows guest removal without a discernable change to the host framework, yielding the β_0-phase of the host.

From **Figure 2.1** it can clearly be seen that the different phases of the host solid (α, β, β_0 and γ-phases) may display different affinities for guest uptake depending on their inherent stacking arrangements in the solid-state. Porosity and sorption are two topics relevant to solid-

state host-guest chemistry that are closely linked to the development and understanding of the kinetic and thermodynamic phenomena, and are discussed below.

2.3. Sorption

The study of the sorptive properties of a solid can arguably be traced back to the "*experiments*" by Gideon on fleece in 1100 BCE [32] but most assuredly from the early experiments of Scheele [33] and Fontana [34, 35]. The process of sorption has been subdivided into two principal types, namely adsorption and absorption. The former term was first used by Kayser in 1881 [36, 37] to best describe the observation concerning the condensation of gas onto a surface [38]. This was done to distinguish adsorption from absorption, where the latter describes the phenomenon of gas molecules penetrating the mass of the absorbing phase [38]. Adsorption is viewed as a surface phenomenon and is related to the concentration of the adsorbent relative to that of the adsorbate. Adsorption occurs when the concentration of the adsorbate species at the adsorbent-adsorbate boundary region is higher than that in the bulk volume of the system. One of the chief differentiating factors observed experimentally between adsorption and absorption is that the former is necessarily exothermic, whereas the latter can be either endo- or exothermic [38]. This can be attributed to the entropy effect necessarily associated with adsorption. As the adsorbate molecules are stabilized on the adsorbent surface, relative to the bulk phase, energy is released, which can be experimentally observed by plotting isotherms of adsorption [39]. Brunauer, Emmet and Teller [40] classified adsorption isotherms into five categories and this was later expanded to the six standard IUPAC isotherms. The shapes of the isotherms are indicative of the mechanism of sorption associated with a particular system [41].

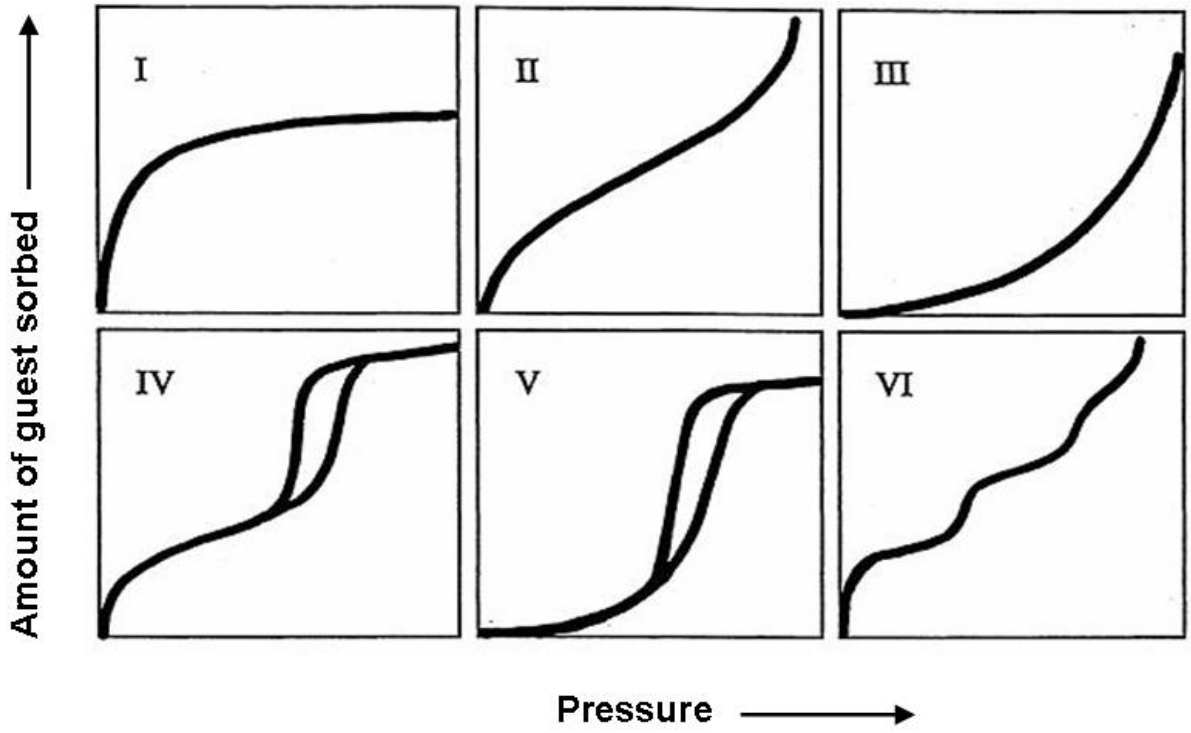

Figure 2.2. The six standard IUPAC adsorption isotherms [42].

Type I isotherms are generally attributed to systems where the pore size of the adsorbent is similar to the dimensions of the sorbate molecule since a definite saturation limit exists due to the filling of adsorbent pores [41]. Types II and III are observed when a varying degree of pore size is inherent to the adsorbent. The initial adsorption process is a monolayer of adsorbate molecules interacting with the adsorbent, followed by multilayer adsorption due to by varying pore size and, finally, capillary condensation [41]. Type IV isotherms have been rationalized by suggesting that there are two distinct surface layers and that the pore size is much larger than the sorbate molecule. Type V isotherms are a variation on Type I and occur when the intermolecular attractive interactions are very strong [41]. Type IV and V isotherms in **Figure 2.2** show hysteresis (*i.e.* where the isotherms of sorption and desorption are non-overlapping. The type VI isotherm was introduced as a hypothetical isotherm whose shape is the result of monomolecular layers forming completely before the next layer is formed. The models discussed above were all developed on the assumption that the adsorbent inherently consists of well defined pores and were almost exclusively developed with reference to the field of zeolite chemistry. Recent studies by Barbour [43-48] and co-workers have shown, by means of gas sorption isotherms, that this supposition is false and that seemingly non-porous supramolecular systems can indeed display porosity. The concept of porosity will be discussed below.

Sorption can further be divided into physisorption and chemisorption. Physical sorption involves relatively weak intermolecular forces, while chemisorption involves the formation of a chemical bond between the sorbate molecule and the surface of the adsorbent [39]. This differentiation depends largely on how one classifies a chemical bond. Pauling described the chemical bond as follows [49]:

"*We shall say that there is a chemical bond between two atoms or groups of atoms in case that the forces acting between them are such as to lead to the formation of an aggregate with sufficient stability to make it convenient for the chemist to consider it as an independent molecular species* ."

Weak interactions were not previously considered to constitute formal chemical bonds. However, this view is changing, as the host-guest supramolecular entity can be regarded as "*an independent molecular species*" according to Pauling's definition. Thus, what is deemed physical adsorption (physisorption) and what is deemed chemical absorption (chemisorption) becomes obscure. Owing to the structural types of the many compounds discussed here, and the occasional confusion regarding the definition of adsorption and absorption, all gas uptake processes will henceforth be termed "*sorption*".

The energetics of a sorption reaction can be discussed in terms of the Lennard-Jones treatment shown in **Figure 2.3.a** or as a contour map of potential energy as shown in **Figure 2.3.b** [50].

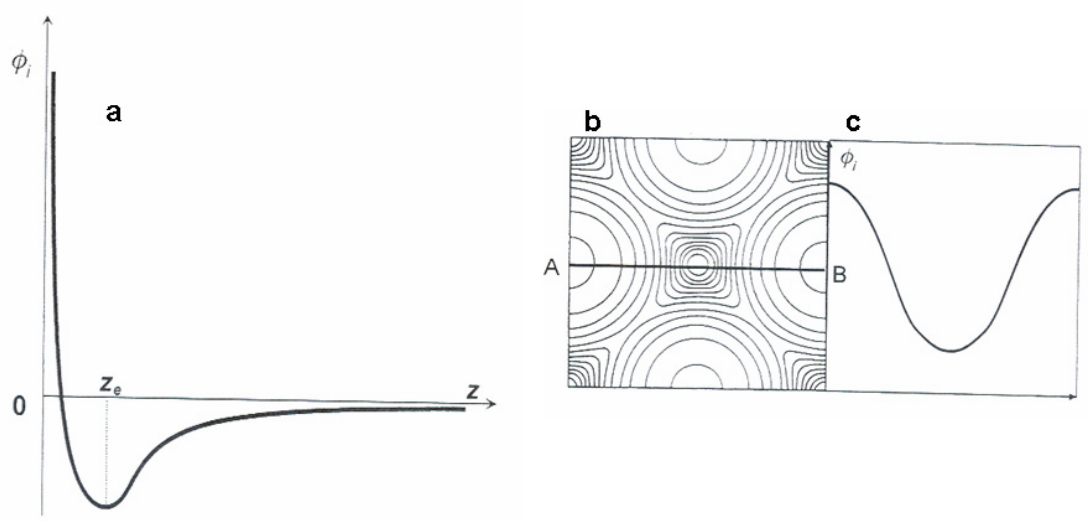

Figure 2.3. (**a**)The energetics of a sorption reaction viewed in terms of a Lennard-Jones treatment, where the potential energy for the molecule *i*, Φ_i, is given as a function of the distance *z* from the host surface. (**b**) Shows the contour map of a guest molecule, *i*, being sorbed onto a surface and (**c**) shows the potential energy, Φ_i, of the guest molecule *i* as it moves from position **A** to **B** [16].

In the case of a solid-gas sorption reaction, the sorbate molecule experiences attractive forces as it nears the solid surface. These forces are due to van der Waals effects and electrostatic polarization [50] between the sorbate and sorbent. When the sorbate comes into closer contact with the solid sorbent it experiences repulsive forces and there is an associated increase in potential energy. This repulsive force exists because of Pauli's exclusion principle, as the outer atomic orbitals of the sorbate and sorbent are in close proximity to one another [50]. Consequently, there exists a minimum energy where the sorbed molecule can reside. In the case of chemisorption, this minimum potential energy is generally > 50 kJ.mol^{-1} and for physisorption < 50 kJ.mol^{-1} [50]. The forces that are at play during a sorption reaction are numerous and their description becomes complex when taking into account adsorbent-adsorbate, adsorbate-adsorbate, and adsorbent-adsorbent interactions [16]. Dispersion attractive forces and short-range repulsion are the two main opposing forces that need to balance out in order to yield a minimum energy potential as shown in **Figure 2.3.a**. The dispersion attractive forces arise owing to fluctuations in electron density of one atom which induce an electrical dipole moment in an adjacent atom [16], and were first described by London [51]. The total potential energy, accounting for both the attractive and repulsive forces can be described in terms of the Lennard-Jones potential [16, 52] shown in **Equation 2.3**.

$$\varepsilon_D(r) = \frac{B}{r^{12}} - \frac{C}{r^6} \qquad \textbf{(2.3)}$$

where r is the distance between two atoms, B is an empirical constant and C is a measure of polarisability between the adsorbent and adsorbate. The first term, $B \cdot r^{-12}$, represents the repulsive interactions and the second term, $C \cdot r^{-6}$, represents the attractive interactions. The Lennard-Jones potential is a very simplified view of the forces at play. More complex mathematical descriptions exist to take into account the energy contributions of dipole-quadrupole and quadrupole-quadrupole interactions to mention a few [16].

2.4. Porosity

The notion of certain materials being porous dates back to ancient times [38]. Conventionally porous materials are either amorphous or crystalline compounds that contain pores for the reversible passage of gas or fluid [53]. These compounds have been categorised on the basis of pore size diameter: macroporous (>500Å), mesoporous (15-500Å) and microporous (<15Å) [53]. Of the classes of porous compounds studied to date, zeolites, first described by Cronstedt [54, 55] in 1756, have undoubtedly had the most significant impact on industry, with a plethora of applications as discussed below [56, 57].

Zeolites are aluminosilicate supramolecular entities with rigid open-frameworks that are capable of sorbing guest molecules. With applications in catalysis, adsorption and ion exchange in the agriculture, aquaculture, horticulture, water treatment, petrochemical and construction industries [58] to mention a few, zeolites have become a major commodity. Conventional porosity, as understood within the zeolite research community, functions on a molecular level and necessitates infinite channels of at least 3Å in diameter within the rigid aluminosilicate host framework [58, 59]. Molecular crystals with zeolite-like properties are rare in nature and are difficult to synthesise in the laboratory. This relates to Aristotle's "*Horror vacui*" philosophy purporting that "*Nature abhors a vacuum*" [60]. Molecular building blocks forming the supramolecular crystal pack as close to one another as possible in order to exist in the lowest energetic state in accordance with the second law of thermodynamics. Consequently, molecular crystals with infinite channels, such as those found in zeolites, are atypical; indeed research into molecular crystals that are analogous to zeolites as porous materials was sparse until fairly recently [58]. Owing to their vast structural

versatility, metal-organic frameworks (MOFs), also termed coordination polymers, have proven to be a successful alternative to molecular crystals in emulating the porosity of zeolites [58]. Research into the design of property-specific "*smart*" materials has intensified tremendously with possible applications in ion exchange [61], gas storage [2, 3, 62, 63], sensing [5] and drug delivery [64-66]. Phenomenal success has been achieved in the last decade and the study of porous materials is now such a highly active field of research [1, 5, 48, 67, 68] that the terms "*porous*" and "*porosity*" have become the subject of some debate (and abuse).

A dictionary definition [69] of the word "*pore*" suggests "*a minute passage or interstice*". It is thus implied that a supramolecular entity can be deemed porous if it contains interstitial passages or openings within the bulk. Recent papers by Barbour [58] and Kitagawa [70-72] state that, for a compound to be deemed "*porous*", it must be unambiguously demonstrated experimentally that guest uptake can take place. Furthermore, Barbour [58] purports that for porosity to be viewed as a conceptually meaningful term it must describe the property of a specific host phase of the supramolecular compound under investigation and not the bulk host material in general. Additionally, the host structure must not be substantially affected by the sorption process. Barbour distinguishes three classes of "*porosity*":

1. Conventional Porosity,
2. Virtual Porosity and
3. Transient Porosity

that are often incorrectly grouped under the umbrella concept of "*porosity*".

2.4.1. Conventional Porosity

Conventional porosity is used to describe a situation where guest molecules found within the discrete channels of the supramolecular host can be removed or exchanged with another type of guest molecule without compromising the integrity of the host structure. The shape and structure of the host framework can be used to rationalise the type of guest compound that could be sorbed. Zeolites are the best example of this type of porosity [71, 73].

2.4.2. Virtual Porosity

Virtual porosity is generally an *in silico* phenomenon seldom supported by an *in situ* demonstration of porosity [58]. This is achieved by ignoring certain atoms within the host framework (*e.g.*, counter ions or solvent molecules) when generating an image *in silico*, or by misrepresenting a model by employing ball-and-stick and capped-stick diagrams instead of space-filling diagrams [58].

2.4.3. Transient Porosity

This situation occurs when there are discrete voids within the crystal lattice that are not permanently interconnected to form channels large enough for the passage of guest molecules. Despite the lack of channels, it is observed that some compounds nevertheless undergo sorption *in situ*. There is thus a physical mechanism inherent to the system for the successful uptake of gas to occur. The best studied example of such a phenomenon is the sublimed apohost β_0 phase of *p-tert*-butylcalix[4]arene, **2a**, [45-48, 74] where it was shown unambiguously that sorption occurs despite the absence of discrete pores within the crystal structure. A physico-chemical phenomenon termed "*gating*" is often associated with such compounds, owing to a temporary pore forming in the host framework, thus allowing the passage of gas [67, 75-78]. Consequently, the phenomenon cannot be viewed as conventional porosity, despite porosity being demonstrated *in situ*. Other examples studied that fall within the ambit of this thesis are the metallacycles $[Cu_2(BITMB)_2Cl_4]$ (**3**) and $[Cd_2(B2MB)_2Cl_4]$ (**4**). Potential gating mechanisms are investigated in this work through the use of sorption, computational, and crystallographic techniques.

2.5. Thermodynamics and Kinetics of Gas Sorption

Kinetics stands in direct contrast to thermodynamics. Kinetics involves a dynamic process, concerning itself with the rate of reaction and with relating this rate to the reaction mechanism. In contrast, thermodynamics is concerned only with the initial and final states of the system under study [79, 80]. Consider the illustration of a dam above a valley in **Figure 2.4**: the presence of the dam implies the potential of a river to flow from it (thermodynamics) whereas the dam wall and the size of the openings within the dam wall determine the rate of flow of the river to the valley below (kinetics).

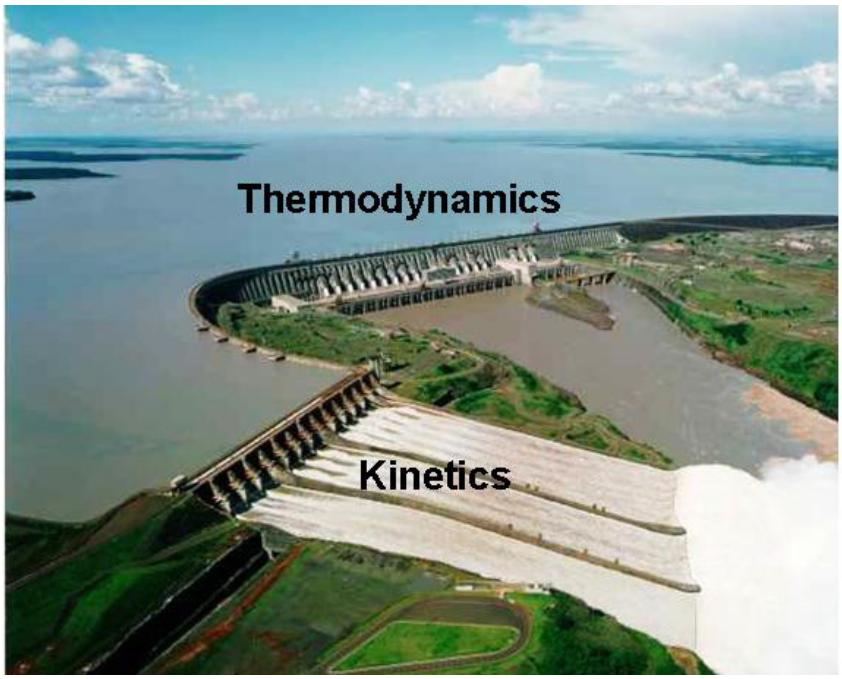

Figure 2.4. The Itaipu Hydroelectric Project, illustrating the relationship between kinetics and thermodynamics [81].

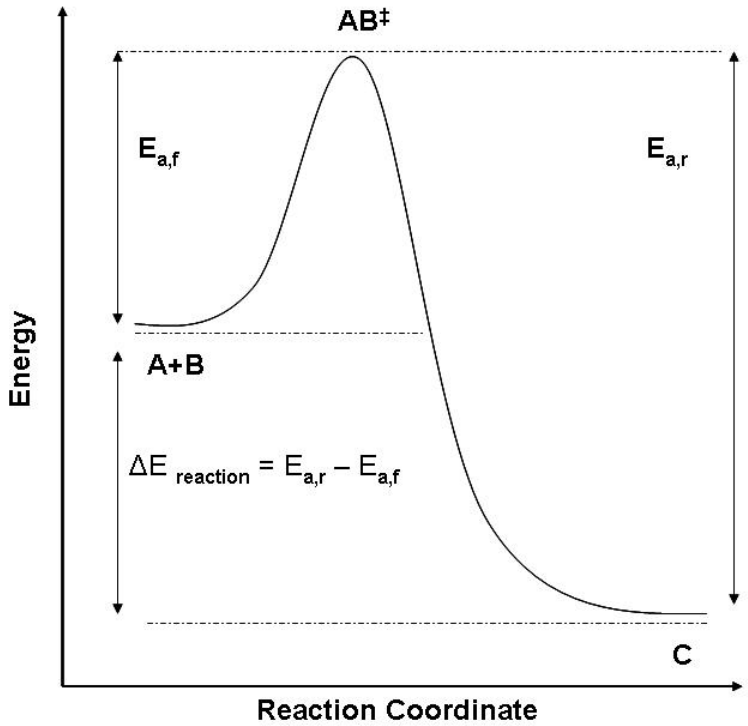

Figure 2.5. Reaction coordinate diagram [82] showing the energy profile for a reaction A + B # $AB^{‡}$ # C. The activation energy for the forward reaction, $E_{a,f}$, is the difference in energy between the reactants, A and B, and the transition state complex $AB^{‡}$. The activation energy for the reverse reaction, $E_{a,r}$, is given by the difference in energy between C and $AB^{‡}$. The energy for the reaction, $\Delta E_{reaction}$, is the difference between $E_{a,r}$ and $E_{a,f}$.

Figure 2.5 relates the energy of the system under study to a particular geometry along one possible reaction path. The activation energy E_a is a kinetic parameter and represents the minimum energy required by the reactants to be converted into product. $E_{a,f}$ is the activation energy for the forward reaction and $E_{a,r}$ for the reverse reaction. The transition state, $\mathbf{AB}^{\ddagger}$, is the point on the energy surface where there is an unstable activated complex which is the transitory state between reactants **A+B**, and product **C**.

The kinetics of the system include the rate constant, k, which gives information concerning the rate of the reaction and is related to the activation energy, E_a, *via* the Arrhenius equation,

$$k = Ae^{\frac{-E_a}{RT}} \qquad \textbf{(2.4)}$$

where A is the preexponential constant , R is the universal gas constant and T is the temperature in Kelvin.

The thermodynamics of the system are related to the free energy of the reaction, $\Delta G_{reaction}$,

$$\Delta E_{reaction} = E_{a,r} - E_{a,f} = \Delta G_{reaction} \qquad \textbf{(2.5)}$$

As mentioned above, adsorption is necessarily exothermic and agrees, in principle, with the reaction coordinate diagram shown in **Figure 2.5**. Generally, the rate of reaction is directly proportional to the reaction temperature and is termed Arrhenius behaviour, however, certain compounds display anti-Arrhenius behaviour, where the rate of reaction is inversely proportional to the reaction temperature [83].

Quantifying the thermodynamic and kinetic parameters of weak solid-gas interactions that influence sorption capacities and rates is critical to understanding the underlying processes governing sorption [84]. Novel methods for determining thermodynamic and kinetic parameters that govern sorption phenomena in solid transiently porous materials were developed as part of this study and are described in **Chapters 4** and **5**.

Barrer [85] and Hey [86] pioneered the measurement of thermodynamic and kinetic parameters of solid-gas interactions (mostly using zeolite hosts [57]). They constructed

volumetric sorption systems for the determination of the isosteric heat of adsorption (ΔH_{ad}). This was a major contribution to the understanding of solid-gas interactions and provided new insight into the nature of the reaction itself. This ΔH_{ad} is the amount of heat that is evolved during the course of a chemical reaction and reveals a great deal about the energetics and possible mechanisms that govern the reaction. The ΔH_{ad} value serves as a measure of the affinity that a particular guest has for a specific host. In order to develop property-specific functional supramolecular systems, it is imperative to understand the energetic implications and the mechanism of guest uptake between a solid host and a gas.

2.5.1. Methods to Determine Thermodynamic Parameters of Solid-Gas Sorption Reactions.

Currently, the six main methods for determining ΔH_{ad} of a solid-gas sorption reaction are:

1. Computational Methods;
2. Tian-Calvet Calorimetry [87];
3. Gas Chromatography methods [88];
4. Born-Haber-type Thermodynamic Cycles [29];
5. Variable Temperature Infra-Red Spectroscopy (VTIR) [84] and
6. Volumetric [86, 89] and Gravimetric Sorption Isosteric Techniques (SIT) [90].

2.5.1.1. Computational Methods

Modern high speed computers have led to the possibility of predicting sorption phenomena in host-guest systems using molecular modelling [16]. In order to do this, a complete description of the adsorbent regarding its solid structure, pore size and solid-state packing arrangements is required. Algorithms describing sorbate-sorbate and sorbent-sorbate interaction must exist for the system under study in order to determine potential energies for the different stages of the reaction.

2.5.1.2. Calorimetric Methods

Four general types of calorimetric techniques are available for the study of gas sorption [16], but they will not all be discussed individually as part of this work. The most useful of the four techniques for solid-gas sorption studies is the diathermal-conduction technique during which the sample temperature follows the temperature of the surroundings by means of conduction. Notably relevant is the Tian-Calvet type calorimeter [16, 91, 92] which has the ability to measure heat flux for changes in temperature as small as 10^{-6} K.

2.5.1.3. Chromatographic Techniques

This technique is based upon the correlation between temperature dependence of Henry's law constant, k_H, and the value for $\Delta H°_{ad}$ at zero coverage, θ, [16] expressed in **Equation 2.6**,

$$\Delta H^{o}_{ad} = RT^{2}\left(\frac{\partial(\ln k_H)}{\partial T}\right)_n \qquad \textbf{(2.6)}$$

where n is the number of moles of substance.

Purnell [93] and Littlewood [94] have shown, however, that at low pressures the specific retention volume, V_S, is a linear function of k_H. Thus, **Equation 2.6** becomes **Equation 2.7**, and it is possible to determine values for $\Delta H°_{ad}$ [16].

$$\Delta H^{\circ}_{ad} = RT^{2}\left(\frac{\partial(\ln V_S)}{\partial T}\right)_n \qquad \textbf{(2.7)}$$

The main disadvantage is that the carrier gas must not be sorbed [16]. The most prominent contribution in recent literature in the field of inclusion chemistry has come from Gorbatchuk employing head space gas chromatography[95-97].

2.5.1.4. Born-Haber-type Thermodynamic Cycles

Buschmann [29] recently reported an indirect approach using Born-Haber-type thermodynamic cycles to calculate values for thermodynamic parameters of solid-gas sorption reactions. Their method rests upon the hypothesis that the equilibrium for the complexation

reaction in solution, and that of the solid-gas reaction are related through a Born-Haber-type thermodynamic cycle shown in **Figure 2.6**.

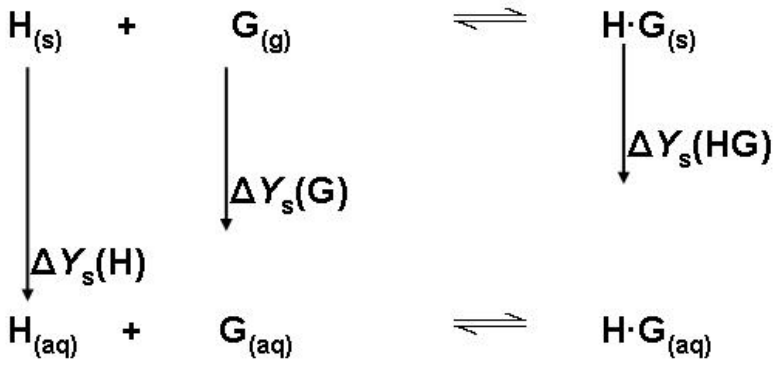

Figure 2.6. Born-Haber-type thermodynamic cycle employed by Buschmann [29] to indirectly calculate thermodynamic parameters of solid-gas reactions. $H_{(s)}$ is the solid host, $H_{(aq)}$ is the aqueous host. Similarly, $G_{(g)}$ is the gaseous guest, $G_{(aq)}$ the aqueous guest, $HG_{(s)}$ the solid host-guest complex and $HG_{(aq)}$ the aqueous host-guest complex. ΔY_s represents the thermodynamic parameters.

The method relies on the prior calculation of thermodynamic parameters of the complexation reaction in solution [29]. This method becomes cumbersome as prior studies on solution reactions must be performed. The disadvantage is that the thermodynamic parameters are inferred in an indirect manner, which may not necessarily be an accurate description of the system under investigation.

2.5.1.5. Variable Temperature Infra-Red Spectroscopy (VTIR)

In detailed reviews by Areán [84, 98] it was shown that thermodynamic parameters of solid-gas sorption reactions can be calculated given **Equation 2.8**,

$$\ln\left[\frac{A}{(A_M - A)P}\right] = \left(\frac{-\Delta H^{\circ}_{ad}}{RT}\right) + \left(\frac{\Delta S^{\circ}_{ad}}{R}\right) \qquad \textbf{(2.8)}$$

where A is the IR absorbance, A_M is the maximum absorbance, P is the pressure relative to P° and ΔS°_{ad} is the standard entropy of adsorption.

This system relies on certain conditions being fulfilled, namely that the sorption process causes or changes a characteristic IR sorption band in the sorbed molecule, or a change in the sorption band of the active site of sorption [98]. The main advantage of this method is that it

enables one to differentiate between the types of sorption sites that may be present in the host and can, in certain cases, give specific thermodynamic data regarding specific active sites of sorption [98]. A disadvantage is that only Langmuir-type sorption is defined for this method in order to yield meaningful results due to **Equation 2.8** being developed from the well known Langmuir equation [98].

2.5.1.6. Gravimetric and Volumetric Sorption Isosteric Techniques

For solid-gas sorption reactions the sorption process can be monitored by recording the gas pressure in a reaction flask, as a function of time, at a specific constant temperature until the pressure reaches a constant value, signifying equilibrium reaction conditions. By conducting a set of experiments yielding different equilibrium pressures, and by varying the temperature of the experiment, thermodynamic parameters can readily be calculated. In a volumetric system the pressure drop must occur in a constant volume reaction flask to determine the amount of gas sorbed. The gravimetric method relies on a high precision analytical balance to measure the change in mass of a host sample as a function of guest pressure in order to determine the amount of guest being sorbed. A detailed description concerning the volumetric isosteric method is presented in **Chapter 4** of this work.

A volumetric SIT device, as described by Barbour [99], was constructed as part of this study, and the validity of the method investigated using six different supramolecular systems as discussed in **Chapter 4**.

2.5.2. Methods to Determine Kinetic Parameters of Solid-Gas Sorption Reactions.

Kinetic parameters for solution-phase host-guest complexation reactions have been well studied, in contrast to those for solid-gas inclusion processes [29]. Breck [56] and Barrer [57] provide comprehensive information of how various kinetic parameters such as diffusion coefficients and activation energies of diffusion processes can be calculated. For the effective study of kinetics, *direct* measurements of mass transport into, and out of, the porous host framework are usually studied [57]. Information regarding the amount of guest sorbed can be calculated in a number of ways:

i. By monitoring the change of the volume of gas or vapour in the reaction flask containing the porous host, as a function of time, while keeping the pressure and temperature constant [57];
ii. By monitoring the change in pressure of the gas or vapour around the host, while keeping the volume constant [57];
iii. By monitoring the mass of the host-guest complex, while the host is surrounded by a constant vapour pressure [57].

Sorption kinetics can also be inferred *indirectly* [57] by using optical and NMR techniques, to name a few, but these techniques will not be discussed.

The three principal methods for determining the activation energy (E_a, a kinetic parameter) of a solid-gas sorption reaction are:

1. Computational Methods;
2. Temperature Programmed Desorption [100].
3. Volumetric and Gravimetric methods [57]

2.5.2.1. Computational Methods

As mentioned in **Section 2.5.1.1**, modern high-speed computing and sophisticated computational chemistry packages readily allow the calculation of interactions between guest and host and enable the calculation of kinetic parameters of reactions, including solid-gas sorption reactions.

2.5.2.2. Temperature Programmed Desorption (TPD)

TPD is a technique for determining thermodynamic [98] and kinetic [101] parameters for a desorption reaction. Using this approach, the host-guest complex is heated under vacuum whilst being connected to a mass analyser [102]. With a rise in temperature, the sorbed species will gain enough energy to escape from the host lattice, and this process will be detected by the mass analyser [102]. Clearly, this technique is not suited to physisorption systems where the guest will desorb with vacuum being applied to the host-guest system. The technique is thus only suited to host-guest systems where chemisorption takes place. The technique rests upon the theoretical premise that the rate of desorption, R_{des}, is

$$R_{des} = k_{des}\ N^{x} \qquad \textbf{(2.9)}$$

where k_{des} is the rate constant for the desorption process, N is the surface concentration of the sorbed species and x is the kinetic order of desorption. Following the Arrhenius equation, **Equation 2.4**, one arrives at the following expression,

$$k_{des} = A e^{\left(\frac{-E_a^{des}}{RT}\right)} \qquad \textbf{(2.10)}$$

The rate of desorption, R_{des}, can thus be given by **Equation 2.11**,

$$R_{des} = -\frac{dN}{dt} = A N^{x} e^{\left(\frac{-E_a^{des}}{RT}\right)} \qquad \textbf{(2.11)}$$

TPD has proven to be very useful [98, 103], but clearly has limitations (i) being suited mainly to chemisorption and (ii) only able to provide thermodynamic parameters for the desorption reaction.

2.5.2.3. Volumetric and Gravimetric Methods

Early volumetric methods to calculate the kinetics of desorption were pioneered by Walker [104] and Nelson [104]. Gravimetric methods were pioneered by Barrer [105] and Fender [105]. The volumetric method aims to determine the parameters for diffusion kinetics of reactions with gases and zeolite hosts, whereas the gravimetric method focussed on the sorption reactions of liquid guests into zeolite hosts [57]. Although their approach was ground breaking, their lack of high precision equipment hindered their attempts to obtain accurate data.

In this study we propose a novel, simple and direct method for determining E_{a} of a solid-gas host-guest sorption reaction as discussed in **Chapter 5**. It is important to note that the theory and practice of our technique discussed in Chapter 5 rests upon the following assumptions:

i. That the particle size of the host sample, which is an important factor in determining kinetic parameters, does not change with the repetition of experiments.
ii. That activation energy, E_a, remains independent of particle size
iii. That no significant local heating of the sample occurs during the experimental process.
iv. That the host volume remains constant (*i.e.* guest-induced transformations possibly affecting the host volume are ignored).

Results obtained using this new method led to the postulation of possible interactions playing a role in the sorption processes. This has furthered our understanding of gas sorption by transiently porous supramolecular systems and affords new insight into how we can confront the challenge of designing "*smart*" materials.

2.6. Computational Chemistry Overview

The development of theoretical molecular models provides an invaluable method for describing what is observed in Nature, and thus forms a crucial part of the development of our understanding of solid-gas interactions. Computational chemistry has gained substantial relevance in predicting chemical and physical properties of compounds, especially when used in conjunction with complementary experiments [106].

Computational chemistry rests upon the hypothesis that all molecular properties are related to molecular structure [106], and that inherent properties of molecules can be calculated from the structure, and *vice versa*. The chemistry of a system is thought to be related to the energy of a specific geometry [107]. The energy of a system can be calculated, given that the atomic coordinates and that an algorithm exists to describe the system. In this study computational chemistry (*i.e.* molecular modelling) was employed to describe the lowest energy pathway that gas molecules can follow through a *transiently* porous crystal system. These results were used to postulate a possible transport trajectory intrinsic to the system. Molecular modelling is generally classified into the following three distinct groups, all based on different approaches:

1. Force Field Methods
2. Quantum Mechanical Methods and
3. Semi-empirical methods.

This study employs only force field methods, which will be described below. Quantum mechanics utilises the Schrödinger equation and the semi-empirical method uses both the Schrödinger equation and classical Newtonian mechanics. These two techniques are used extensively in the field of computational chemistry but fall beyond the ambit of this work.

2.6.1. Force Field Methods (Molecular Mechanics)

A molecular force field is a term that refers to the functional form and parameter sets used to describe the potential energy of a molecule or molecular system in the electronic ground state. Since the potential energy of an isolated geometry is the result of inter-atomic interactions, it is not affected by the translation or rotation of the molecule. A molecular force field may be described as the relationship between the potential energy of a molecule and its internal coordinates [108].

The potential energy of an isolated molecule in the electronic ground state is determined using the coordinates of the nuclei alone [108]. Electrons are not considered to affect the potential energy explicitly as it is assumed that they will find their optimum distribution once the positions of the nuclei are fixed. This assumption is based on the Born-Oppenheimer approximation of the Schrödinger equation which states that nuclei, which are much heavier, move far slower than electrons [109].

Consequently, nuclear translations, rotations and vibrations can be studied independently from electrons as it is assumed that the electrons are able to move rapidly enough to adjust to any movement of the nuclei [106]. This is in direct contrast to quantum mechanical methods. In force field methods molecules are therefore modelled as balls held together by springs and the interactions between atoms are calculated using classical mechanics. Nuclear interactions amongst different classes of molecules: organic, inorganic, metallic, polymeric *etc*, are most accurately described using different functional forms and different parameter sets to best approximate the potential energy. This is due to the different chemical and physical properties of different elements. Force fields are thus explicitly designed to study specific types of molecules [110]. The choice of which force field to implement rests upon its performance in predicting the chemical and physical properties of the studied set of molecules, and on computational efficiency.

In order to use techniques such as energy minimisation and molecular dynamics, the first and second derivatives of the energy with respect to the atomic coordinates are needed, and must be calculated within a reasonable time span if the force field is to be a practical tool in gaining understanding of chemical interactions. The total force field potential energy is the sum of several terms called force potentials, which define the potential energy of a molecule as shown in **Equation 2.12**. Each individual force potential is an equation associated with a specific internal interaction [111]:

$$E_{FF} = \sum E_{str} + \sum E_{bend} + \sum E_{tors} + \sum_{oop} + \sum_{vdW} + \sum E_{coul} + \sum_{cross} \qquad \textbf{(2.12)}$$

where E_{FF} is the total force field potential energy, E_{str} represents the energy function for stretching a bond between two atoms, E_{bend} the energy for bending an angle, E_{tors} the torsional energy, E_{oop} the energy from out of plane deformations, E_{vdW} the energy due to van der Waals non-bonded interactions, E_{coul} the energy due to Coulombic non-bonded interactions and E_{cross} represents the energy from cross terms which are coupled to the first three terms, which affect one another experimentally. Using the above force potentials, the relative energy and geometry of a molecule or supramolecular entity can be calculated by minimising E_{FF} as a function of the atomic coordinates.

2.6.2. Energy Minimisation

According to the second law of thermodynamics, a molecule or a molecular system in Nature will always strive to exist in the lowest possible energy state. To determine the structure with the lowest possible potential energy, the equilibrium structure, an energy minimisation must be performed. A minimum in a potential energy function can be described mathematically as a point where the first derivative of the function, with respect to each of the variables, is zero and the second derivatives are all positive as shown in **Equation 2.13** [112]. Energy minimisation is the process of slightly altering the geometry of the molecule or molecular system in order to reduce the energy of the conformation until any further change leads to an increase in energy. It is then said that *convergence* has occurred. A minimisation algorithm is used to determine this.

$$\frac{\partial f}{\partial x_i} = 0 \text{ and } \frac{\partial^2 f}{\partial x_i^2} > 0 \qquad \textbf{(2.13)}$$

Care must be taken when selecting an algorithm to use for the minimisation calculation. A compromise is made between the computational efficiency and the accuracy of the algorithm. The ideal algorithm is one that provides an accurate equilibrium structure within a short period of time. Whether one is working with force field methods or quantum mechanical methods plays a determining role in the choice of algorithm. The two methods require different amounts of computational time in order to accurately calculate energies of the various configurations of the molecule or molecular system under investigation. Minimisation algorithms tend to follow a downhill path on the energy surface, locating the minimum that is closest to the starting point. In order to locate both local minima and the global minimum, the algorithm must be designed in such a fashion that it can generate multiple starting points. Minimisation algorithms can be classified into two groups: those that utilise derivatives of the energy with respect to the coordinates and those that do not [113]. Non-derivative methods are computationally less expensive, but fall short in providing accurate results. Derivative methods, such as the method of steepest descent and the Newton-Raphson method, are computationally more expensive but yield more accurate results.

2.6.3. Molecular Dynamics

"*…everything that living things do can be understood in terms of the jiggling and wiggling of atoms*."

-Richard Feynman [114]

Molecular dynamics is a computational simulation technique mostly utilising force field methods, where the time evolution of a set of interacting atoms is followed by integrating their equations of motion according to Newton's laws [115]. The result is a trajectory that specifies how the positions and velocities of the particles in the system vary with time [116]. The principles of molecular dynamics are governed by the Born-Oppenheimer approximation, which supposes that the movement of atoms and electrons can be treated independently [106, 117, 118]. The nuclei are much heavier than the electrons and are easily described in terms of Newtonian mechanics whereas the effect of the electrons is approximated. Different conditions can be simulated for a specific system by keeping different parameters constant and varying others within the system under study. The differing parameter sets define what is termed an *ensemble*.

Ensembles are typically described by an abbreviation of the parameters kept constant when employing such an ensemble during an experiment. Common ensembles include the microcanonical (NVE), canonical (NVT) and the isothermal-isobaric (NPT) ensembles where N is the number of moles, V is volume, E is energy, T is temperature and P is pressure.

In this study molecular dynamics simulations are used to explain the mechanisms associated with the sorption of gas in transiently porous supramolecular entities using an NVT ensemble. The simulated behaviour of the supermolecule is investigated and the results are used to explain the inherent ability of the system to sorb gas.

CHAPTER 3. Materials and Methods

A description of the analytical instruments that were used during the course of this study are given, in addition to a description of software packages used, and that may not be familiar to the reader. Methods of sample preparation and the synthesis of samples are also briefly outlined.

3.1. Single-Crystal X-Ray Diffraction

Selection of crystals for single-crystal X-ray diffraction experiments was based on their ability to extinguish plane-polarised light uniformly, and on their size. Diffraction data were collected on a Bruker SMART Apex CCD or a Bruker-Nonius Kappa Apex II CCD single-crystal X-ray diffractometer [119] using graphite monochromated Mo-K_α radiation (λ = 0.71073 Å) and equipped with an Oxford Cryostream cooling system. Reduction of the collected data was carried out using SAINT [120] or Denzo and Scalepack [121], and empirical corrections were made using SADABS [122]. Structures were solved and refined using the SHELX-97 [123] suite of programs and the X-Seed [124] graphical user interface. In general, non-hydrogen atoms were located by direct methods (SHELXS-97) and the structures were expanded using difference electron density maps (SHELXL-97). Where atomic coordinates could not be obtained for solvent molecules by direct methods, difference Fourier maps were employed to account for diffuse electron density (SQUEEZE [125]). Structures were refined anisotropically against F^2 using full-matrix least squares calculations. Where feasible, hydrogen atoms were placed in calculated position using riding models.

3.2. Powder X-Ray Diffraction (PXRD)

A Bruker D8 Advance powder diffractometer with Bragg-Brentano geometry and Cu-K_α (40 kV; 30 mA) X-ray radiation was used. The diffractometer is equipped with a dynamic scintillation (point type) detector. A step size of 0.04 degrees and a scan-speed of 2 sec per step were used during experimental measurements.

3.3. Solid-State CP-MAS NMR

A Bruker Avance II 500 MHz solid-state CP-MAS spectrometer was used at the Institute of Physical Chemistry, Polish Academy of Sciences.

3.4. Solution State NMR

A Varian Unity INOVA 400 MHz spectrometer was used at the University of Stellenbosch. A Varian Unity Gemini 200 MHz was used at the Institute of Organic Chemistry, Polish Academy of Sciences.

3.5. Volumetric Sorption

A volumetric sorption analyser previously described by Barbour [99] was constructed. A detailed description of its construction and operation is given in **Chapter 4**.

3.6. Gravimetric Sorption

An Intelligent Gravimetric Analyser (IGA-002) by Hiden Analytical (Ltd) was used for all gravimetric studies performed as part of this work. The system allows sorption experiments to be studied up to a pressure of 20 bar. Gas buoyancy effects are taken into account and the temperature is kept within ± 0.05°C of the desired temperature. The experimental data are monitored in real-time by software [126-128].

3.7. Computer Packages

3.7.1. Cerius^2

Cerius^2 3.8 [129] was used for all computational molecular modelling. A detailed account of the force fields and techniques used is given in **Chapter 6**.

3.7.2. XPREP

The space group determination of crystal structures was made using XPREP [130]. The program was also used in order to set up the SHELX input files.

3.7.3. SHELX-97

SHELX-97 [123] was used for crystal structure solution and refinement. SHELX is comprised of a set of six computer programs (SHELX, SHELXL, CIFTAB, SHELXA, SHELXPRO and SHELXWAT) routinely used for the determination of crystal structures from single-crystal diffraction data [131]. As part of this work SHELX was used for structure solution using

direct methods and SHELXL was used for structure refinement by employing full-matrix least squares calculations always refining against F^2.

3.7.4. POV-Ray

All of the crystal structure figures were generated using POV-Ray™ for Windows 3.6 [132]. POV-Ray™ renders images using a technique called *ray-tracing*, which is a method used to produce high quality graphics. The program works by reading a text file describing the position of a hypothetical camera, the lighting of the object and the object itself [133]. Algorithms then generate a set of mathematical descriptions that are used to render an image of the object from the camera's point of view [133].

3.7.5. SQUEEZE

SQUEEZE [125, 134] is a program designed to detect electron density due to solvent within solvent-accessible "*voids*" of crystal structures. The computational method rests upon the premise that the total electron density of a correctly phased Fourier map can be separated into two parts [134]:

i. a part that represents the disordered solvent and,

ii. a part that represents the atomic parameters for the ordered region of the crystal structure.

Thus, the calculated structure factor F_h^c for the reflection **h** is a function of F_h^m (the structure factor contribution for the ordered part of the crystal structure), and F_h^s ,(the structure factor contribution for the disordered solvent) [125, 134]. F_h^m is easily obtained from the structural parameters of the structure, and F_h^s is calculated by employing electron-density difference mapping techniques [134]. The primary disadvantage of the program is that the number of electrons found within an identified void is heavily dependent on the quality of high-angle reflections, thus necessitating high quality and complete data sets from single-crystal X-ray diffraction studies [125].

3.7.6. Cambridge Structural Database (CSD)

The CSD [135] was used to retrieve published crystal data for comparison with experimental results.

3.7.1. X-Seed

X-Seed [124] was used as a graphical interface for SHELX-97, POV-RAY and MSROLL.

3.7.2. MSROLL

The program MSROLL [136-138] was originally designed by Michael Connolly to study cavities in protein structures. The program was incorporated into X-Seed in order to calculate the volume of void spaces in a structure and to calculate the pore sizes if conventional pores are present. MSROLL works on the premise of a spherical probe with a designated radius mapping the free volume. The original software calculated the *contact* surface of the spherical probe with a preset radius. To calculate pore sizes efficiently it is necessary to not just calculate the *contact* surface, but the guest *accessible* surface. After MSROLL was incorporated into X-Seed it was appropriately modified to enable the calculation of both the *contact* and *accessible* surfaces.

3.7.3. WebLab ViewerPro

WebLab ViewerPro 3.7 [139] was used to render certain graphics.

3.8. Compounds Studied

3.8.1. 2,2′-bis-(formyl-1,6,7-trihydroxy-5-isopropyl-3-methylnaphthalene): Gossypol

Gossypol, **1**, is a yellow polyphenolic organic pigment obtained from cottonseed oil [140]. The pigment is toxic and confers natural protection to the plant against insects and disease. It has been found to display an array of biological activities including acting as an antimicrobial, antimalarial and anti-HIV agent [140]. Research regarding the potential biological applications of **1** surged in recent years following the discovery that **1** exhibits male oral contraceptive properties [6]. Chemically, **1** is a symmetrically substituted 2,2′-binaphthalene, and was first described by Adams in the 1940s [141]. It is reported that **1** can form inclusion

compounds with 120 different solvents, and is consequently viewed as an extremely versatile host compound [140].

In solid-gas inclusion processes, the host β_0 phase of **1** (*i.e.* **1a**), can be viewed as an organic zeolite with associated zeolite-like properties [140]. When crystallised from dichloromethane three different inclusion compounds can be formed. One of these forms channels from which **1a** can be readily obtained by evacuation of the guest molecules. Guest removal does not cause a discernable collapse of the host framework, yielding a β_0 phase with discrete channels stabilised by weak van der Waals interactions. It has been shown that the channels of **1a** have a pore diameter of ~6Å and selectively include linear guests such as carbon dioxide [140].

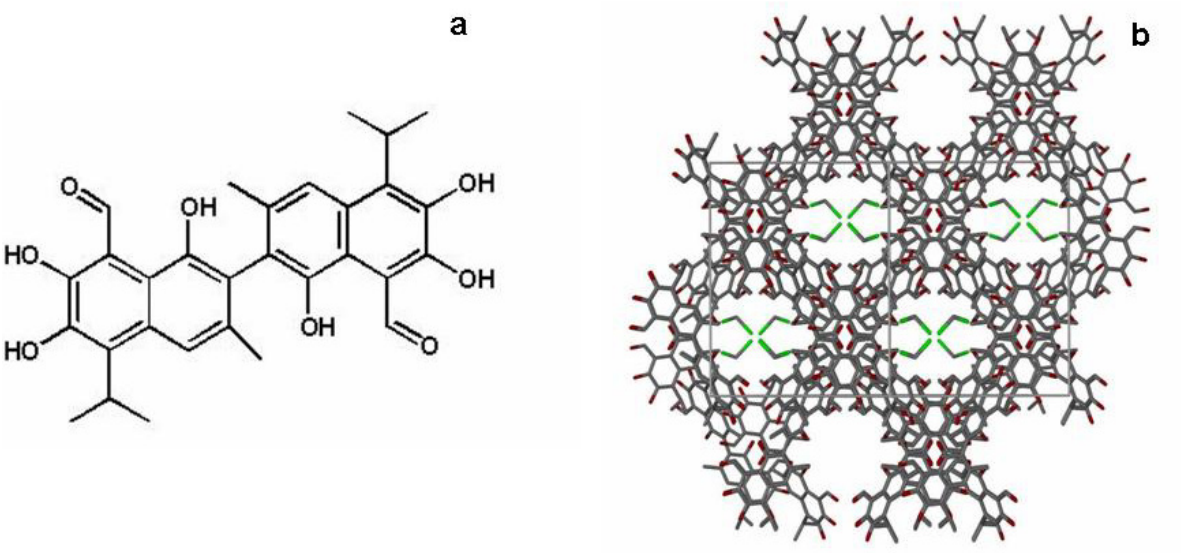

Figure 3.1. (**a**) Schematic structure of gossypol and (**b**) a view along [101] of the crystal structure with CH_2Cl_2 as guest molecules in the pores of the structure given as reference code JIDTOF10 [142] in the CSD [135].

Table 3.1 Crystallographic Information for **1**.

Molecular Formula	$C_{30}H_{30}O_8$
Molecular Weight (M_R) ($g.mol^{-1}$)	516.56
Density (δ) ($g.cm^{-3}$)	1.213
Space Group	C2/c
Unit Cell (*a, b, c* in Å and β in °)	a = 21.320(4) b = 19.199(6) c = 15.765(2) β = 113.05(2)

The compound was supplied as the β_0 phase by Dr. T. le Roex. Prior to performing experiments the sample was evacuated overnight to ensure the correct phase was employed as host. The guest-host ratio was inferred from gas sorption results as 1:1, and is an important parameter for thermodynamic studies discussed in **Chapter 4**.

3.8.2. *p-tert*-butylcalix[4]arene

The synthesised material of *p-tert*-butylcalix[4]arene, **2**, was provided by Prof L.J. Barbour in the form of a white powder. A detailed synthetic procedure has been described by Gutsche [143] and later by Arduini [144] and is simplified in **Scheme 3.1**. Two guest free polymorphs of **2** exist, namely the kinetic form **2a** and the thermodynamic form, **2b**. It was observed, as part of this work, that both forms **2a** and **2b** can form concomitantly by sublimation at 270°C under reduced pressure. It is well known that **2a** is a transiently porous structure and that **2b** does not display inherent porosity at low pressures.

Compound **2** has been the subject of exhaustive studies, yet it continues to be shrouded in controversy and continually yields interesting finds [145-147]. After much debate, it is now generally accepted that two apohost phases of the compound exist at room temperature [12, 148, 149]. Atwood *et al.* [48] first described the ability of one of the apohost phases, the sublimed, low-density β_0 phase, **2a**, to sorb gas without possessing discrete pores within the structure. This ultimately led to the re-evaluation of the concept of porosity by Barbour [58] and the sublimed, low density **2a** to be classified as a *transiently porous* supramolecular system.

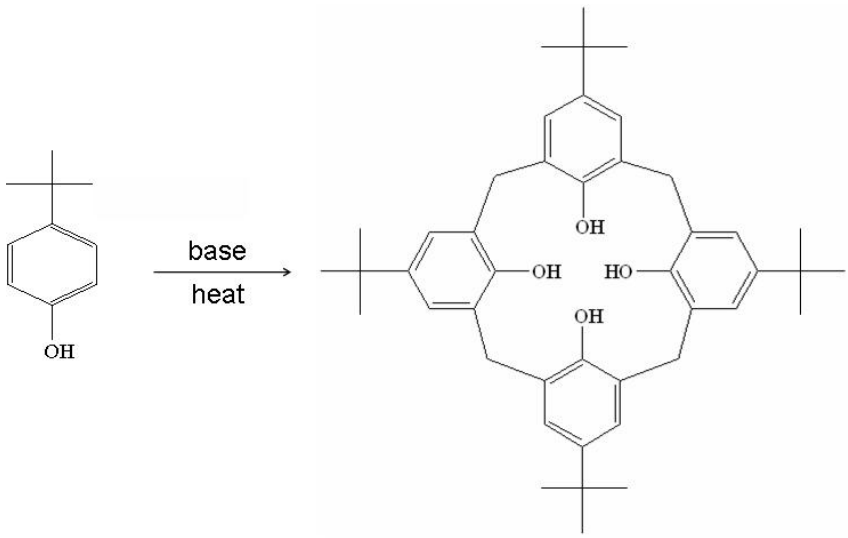

Scheme 3.1. The basic synthetic strategy [150] for synthesising *p-tert*-butylcalix[4]arene, **2**, from *tert*-butylphenol.

From single-crystal diffraction data it is known that the sublimed, low-density β_0 form of **2** crystallises in the space group $P2_1/n$ where the asymmetric unit consists of an entire molecule of **2** with $Z = 4$. The molecules of **2a** are in the cone conformation, which is stabilised by a cyclic arrangement of O–H···O hydrogen bonds between the hydroxyl groups at the base of the calixarene cup. It is well-documented that the structure is packed in an **abcd** bilayer fashion without any interdigitation [12], such that pairs of calix[4]arenes face one another, but are slightly offset. The lack of interdigitation results in the formation of an unoccupied cavity of *ca* 234 $Å^3$ at -100°C. Surprisingly, although this void is sufficiently large to accommodate two molecules of CO_2, we have established that only a maximum of one CO_2 molecule will occupy the volume at any given time and confirms results of previous studies [12]. When viewing **2a** in the light of host-guest chemistry, the host was taken as one double cup of facing, paired calix[4]arene molecules and the guest as one carbon dioxide molecule. This choice is arbitrary, but is important in the light of thermodynamic studies performed in **Chapter 4**. The guest-host ratio is thus 1:1 in the case of carbon dioxide, and is used as such throughout this study.

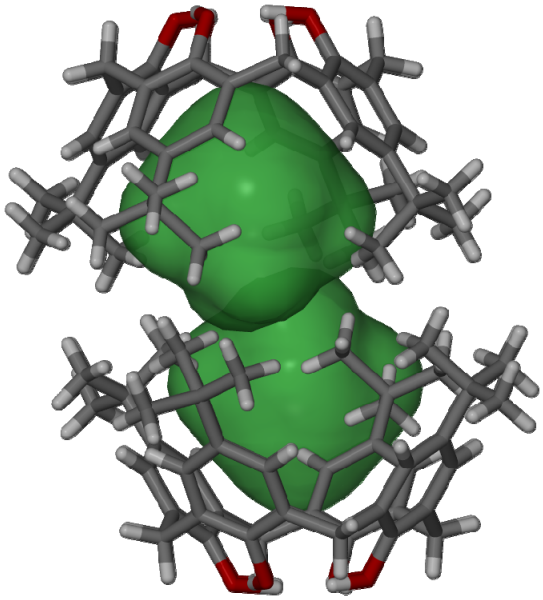

Figure 3.2. A perspective view along [001] showing the void space as mapped by MSROLL (1.5 Å probe radius).

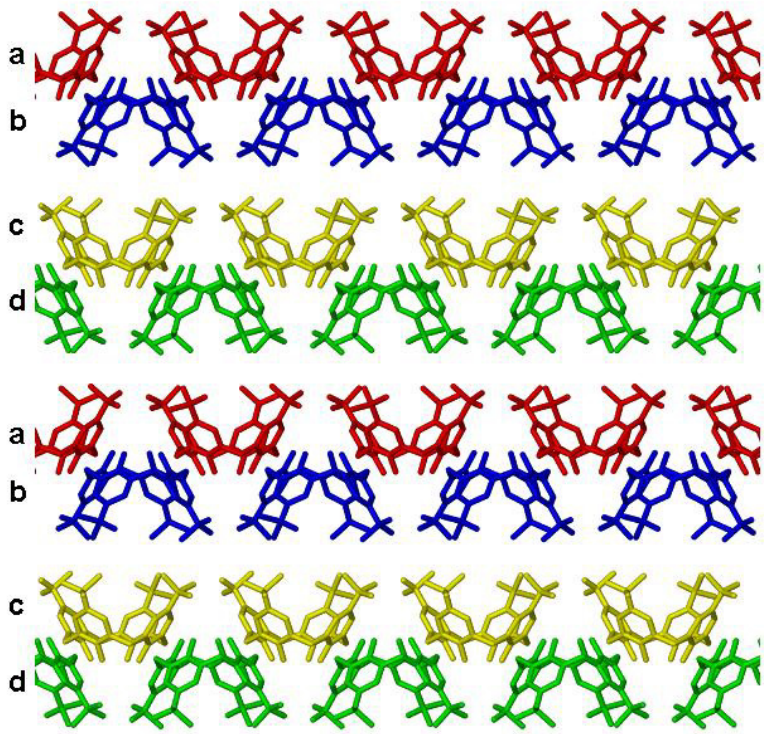

Figure 3.3. The **abcd** bilayer structure of **2a** viewed along [001]. Two distinct bilayers, **ab** and **cd**, can be distinguished. Molecules are shown in capped-stick representation with hydrogen atoms omitted for clarity.

Table 3.2 Crystallographic Information for **2a** and **2b**.

	2a	**2b**
Molecular Formula	$C_{44}H_{56}O_4$	$C_{44}H_{56}O_4$
Molecular Weight (M_R) ($g.mol^{-1}$)	648	648
Density (δ) ($g.cm^{-3}$)	1.0334	1.157
Space Group	$P2_1/n$	$P2_1/c$
Unit Cell (*a, b, c* in Å & β in °)	a=12.804(3) b=25.769(5) c=12.646(2) β = 90.03(1)	a=9.588(<1) b=30.500(1) c=13.541(<1) β = 109.85(<1)

3.8.3. Cu_2(1,3-bis(imidazol-1-ylmethyl)-2,4,6-trimethylbenzene)$_2Cl_4$: $[Cu_2(BITMB)_2Cl_4]$

The synthesis of BITMB [151], and the consequent crystallisation of the dinuclear metallacycle, $[Cu_2(BITMB)_2Cl_4]$, **3**, from methanol and water, was carried out by Dobrzańska and Lloyd [12, 152]. The green-blue crystals were shown to undergo guest removal by evacuation without any noticeable loss of single crystallinity, and a guest free structure was thus determined by single-crystal X-ray diffraction [12]. The distorted square planar arrangement of **3** is can be seen in **Scheme 3.2**, which shows that each copper ion is coordinated to two BITMB ligands and two chloride anions. The doughnut-shaped metallacycles are inclined by 40° relative to the crystallographic *a*-axis along which they pack to form linear columns [152], shown in **Figure 3.4**. The structure was shown to lack discrete pores or channels, but did display discrete void spaces created by the doughnut-shaped metallacycle [12]. The void spaces were mapped using MSROLL and were found to have a volume of ~110 $Å^3$ using a probe radius of 1.4 Å for the crystal structure determined under vacuum. This β_0 phase of **3**, namely **3a**, was obtained by placing the sample under vacuum overnight. Previous *in situ* controlled pressure single-crystal X-ray studies have indicated that the void can host one carbon dioxide molecule disordered over two positions [12] with the void space increasing to ~116 Å (probe radius 1.4 Å) when under carbon dioxide pressure. A guest-host ratio of 1:1 was thus inferred from the crystallographic studies where the host is arbitrarily identified as one complete metallacyclic ring and the guest as one carbon dioxide molecule.

Table 3.3. Crystallographic Information for **3a**.

Molecular Formula	$C_{34}H_{40}Cl_4Cu_2N_8$
Molecular Weight (M_R) ($g.mol^{-1}$)	829.65
Density (δ) ($g.cm^{-3}$)	1.4095
Space Group	$P2_1/c$ (No. 14)
Unit Cell (*a, b, c* in Å & β in °)	$a = 8.362(6)$ $b = 10.550(8)$ $c = 22.438(16)$ $\beta = 99.093(14)$

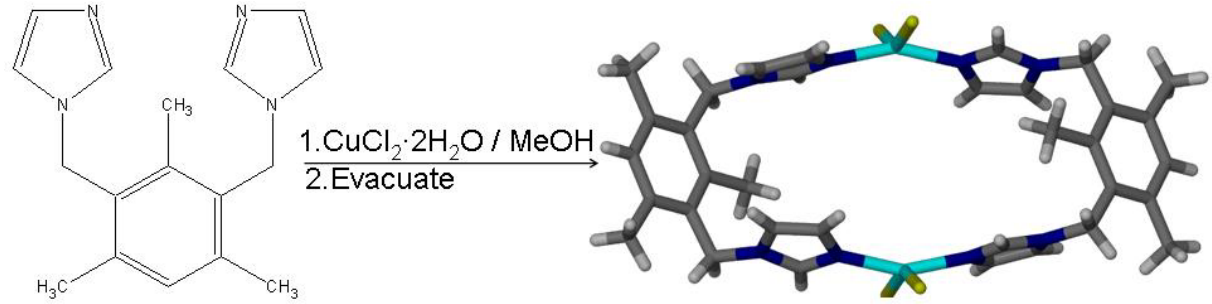

Scheme 3.2. The crystallisation of **3a** [44]. In step **1**, the BITMB ligand complexes to copper chloride in the presence of methanol to form the β-phase inclusion compound. In step **2**, the methanol solvent is removed and the guest free, β_0-phase of the metallacycle, **3a**, is formed, and is shown as a capped stick diagram (colours: ● copper; ● nitrogen; ● chloride anions; ● carbon and ○ are hydrogen).

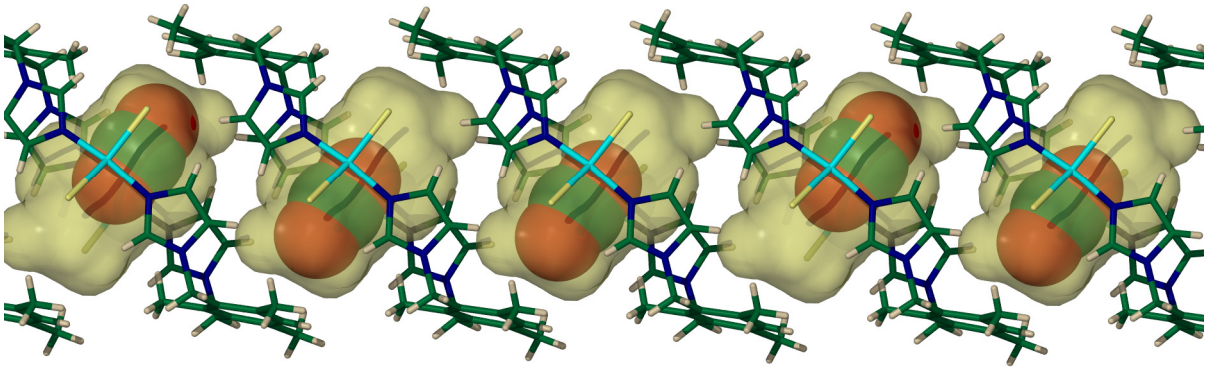

Figure 3.4. The discrete voids created by metallacycle **3a** are mapped in semi-transparent yellow surfaces. The disordered carbon dioxide molecule is shown inside the void (in space filling representation), at randomly selected atomic positions [12] (colours: ●copper, ● nitrogen, ● chloride anions, ● carbon, ● oxygen and ○ hydrogen).

3.8.4. Cd_2(4,4-bis(2-methylimidazol-1-ylmethyl)biphenyl)$_2Cl_4$ [$Cd_2(B2MB)_2Cl_4$]

The synthesis of the ligand B2MB and the crystallisation of $Cd_2(B2MB)_2Cl_4$, **4**, was performed by Jacobs [53]. The two discrete cadmium atoms forming part of the metallacycle **4** are tetrahedrally coordinated to two chloride anions and two bridging B2MB ligands, as seen in **Scheme 3.3**. The molecules stack along the crystallographic *c*-axis, with no pores, but display solvent filled voids between adjacent metallacycles [53], shown in **Figure 3.5**. The guest free structure **4a** was obtained by evacuating the crystals. It has been shown that **4a** displays *transient* porosity, hosting guest molecules in its void pockets. The size of the void

pocket increases from 106 Å under vacuum to 154 Å under carbon dioxide pressure using MSROLL to map the void (probe radius 1.4 Å). *In situ* carbon dioxide pressure-controlled single-crystal diffraction studies performed by Jacobs have shown two discrete carbon dioxide molecules in each void pocket [53]. A guest-host ratio of 2:1 was thus inferred from the crystallographic studies. Here the host is identified as one complete metallacyclic ring and the guest as one carbon dioxide molecule. In this study **4a** is used extensively in thermodynamic and kinetic studies of gas sorption. The sample was evacuated for 10 hours prior to experimentation to ensure the guest free **4a** crystal form.

Table 3.4. Crystallographic Information for **4a**.

Molecular Formula	$C_{44}H_{44}N_8Cd_2Cl_4$
Molecular Weight (M_R) ($g.mol^{-1}$)	1051.52
Density (δ) ($g.cm^{-3}$)	1.4570
Space Group	*C*2/*m*
Unit Cell (*a, b, c* in Å & β in °)	*a* =18.2002(3) *b* =15.5252(2) *c* =9.3605 (1) β = 115.029 (3)

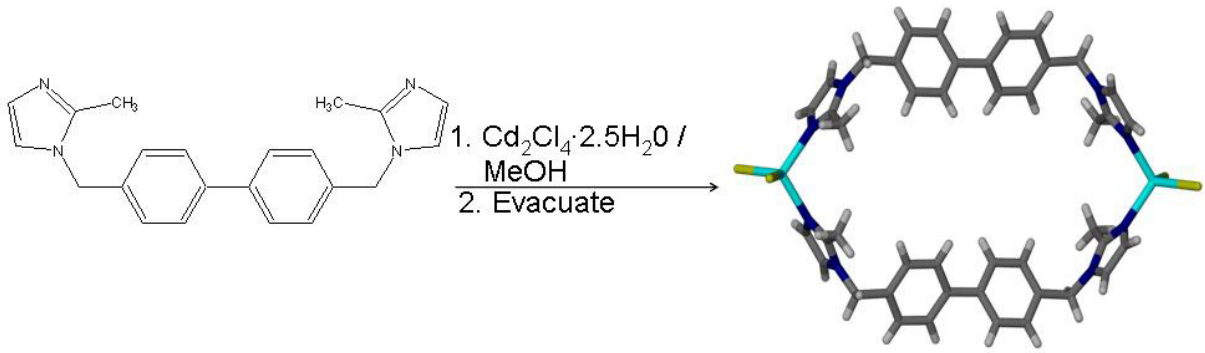

Scheme 3.3. The crystallisation of **4a** [53]. In step **1**, the B2MB ligand complexes to cadmium chloride in the presence of methanol to form the β-phase inclusion compound. In step **2**, the methanol solvent is removed and the guest free, β_0-phase of the metallacycle, **4a**, is formed, and is shown as a capped stick diagram (colours: ● are cadmium atoms; ● are nitrogen atoms; ● are chloride anions; ● carbon atoms and ○ are hydrogen atoms).

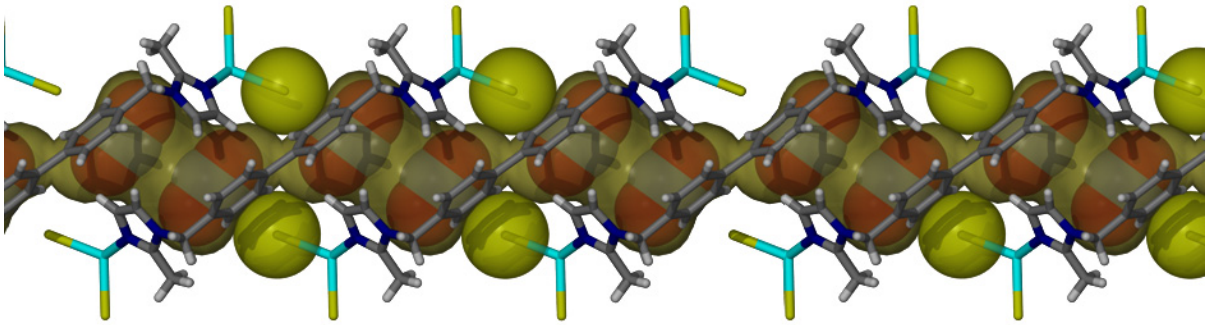

Figure 3.5. Metallacycle **4a** displaying the void spaces mapped in transparent light yellow. The chloride anion and carbon dioxide molecules are shown in space filling representation (colours: ● are cadmium atoms; ● are nitrogen atoms; ● are chloride anions; ● carbon atoms, ● are oxygen atoms and ○ are hydrogen atoms).

3.8.5. Molecular Sieve 4A

Molecular Sieve 4A (**5**) was purchased from Sigma-Aldrich. Molecular sieve 4A is an aluminosilicate framework of aluminium and silica tetrahedra. The solid-state structure forms distinct pores of 4 Å in diameter. Industrially, it is primarily used for the sorption of ethylene, ethanol, methanol, water and carbon dioxide. Molecular sieve 4A is a particularly effective desiccant and is used extensively in industry for this purpose.

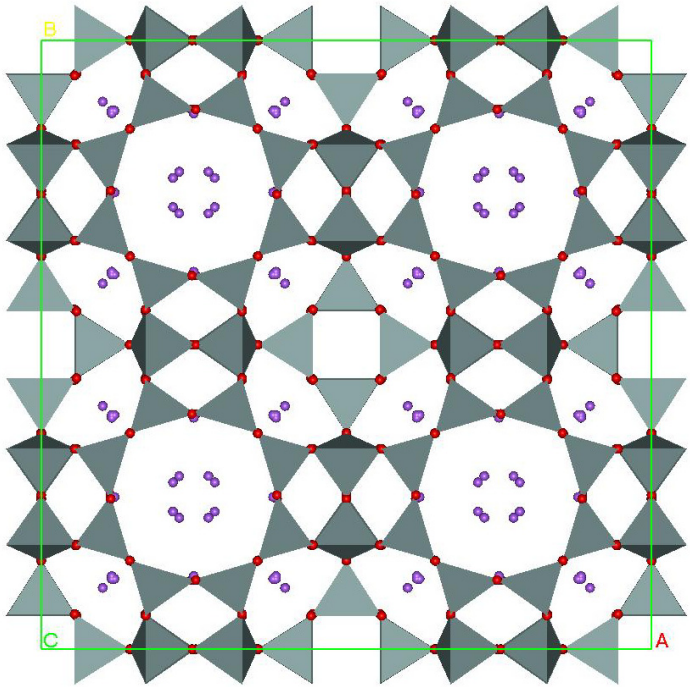

Figure 3.6. The structure of molecular sieve 4A [153] (colours: ● are sodium anions; ● are silicon atoms; ● are oxygen atoms and ● are aluminium atoms which are disordered over the same position as one of the silicon atoms and they are thus not visible).

The guest-host ratio was inferred from sorption experiments (see **Section 4.4.5**). The host is treated as one formula unit of **5** and the guest as one carbon dioxide molecule.

Table 3.5. Crystallographic Information for **5** [153-155].

Molecular Formula	$1Na_2O:1Al_2O_3:2.0\pm1SiO_2:4.5H_2O$
Molecular Weight (M_R) ($g.mol^{-1}$)	365.1772
Density (δ) ($g.cm^{-3}$)	0.66 ±0.04
Space Group	*Fm*3c
Unit Cell (*a,* in Å°)	*a* =24.5920(2)

3.8.6. Tris(*o*-phenylenedioxy)cyclotriphosphazene (TPP)

The synthesis of **6** was performed by the author and later by Dr. Dinabandhu Das following the method used by Allcock [156]. The material was sublimed in order to remove all guest material. Compound **6** is known to display porosity, sorbing gases such as oxygen, argon, methane and carbon dioxide [157]. The empty pore has a diameter of ~4.6 Å [157]. The host framework is held together by weak van der Waals interactions, while it is thought that weak π-interactions stabilize host-guest interactions.

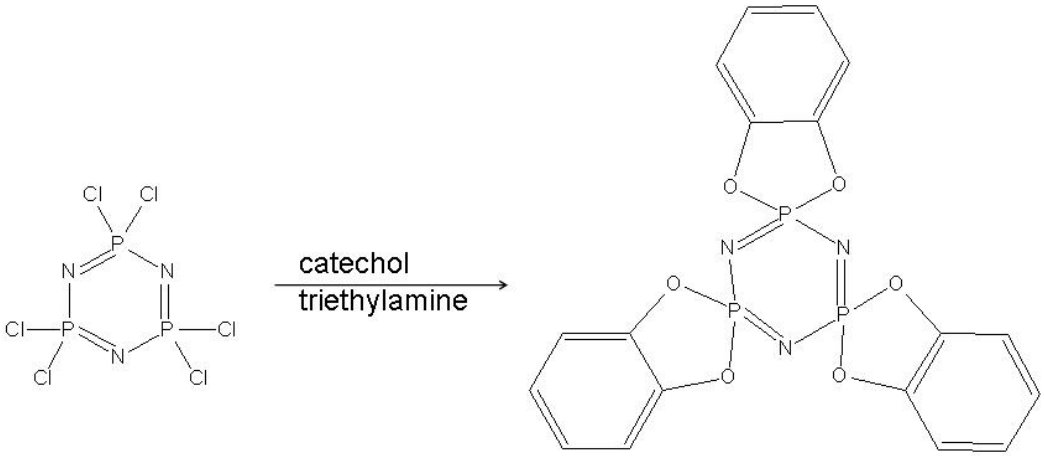

Scheme 3.4. The general synthetic procedure for TPP [156]. Hexachlorotriphosphazene reacts with catechol in the presence of triethylamine to yield TPP.

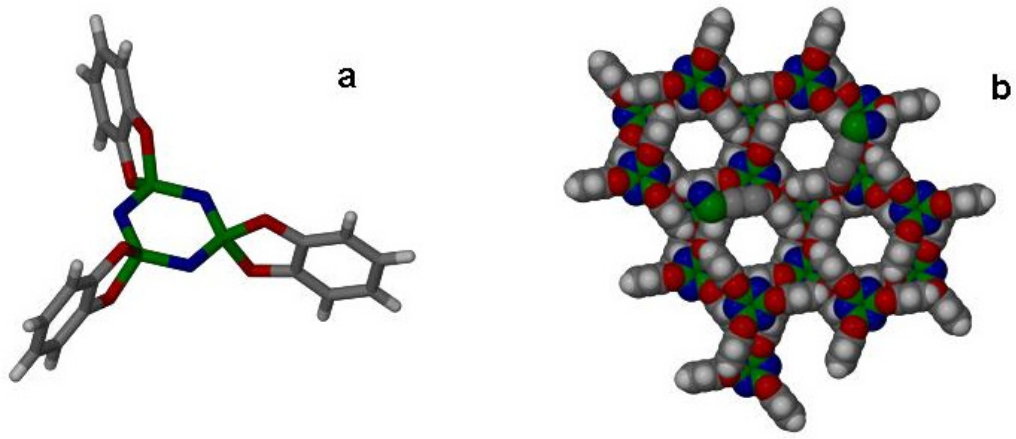

Figure 3.7. (**a**) Shows a molecule of **6** and (**b**) shows a space filling diagram of **6** viewed along [001] clearly highlighting the 4.6 Å discrete pores. (colours: ● are phosphorous atoms; ● are nitrogen atoms; ● are oxygen atoms; ● are carbon atoms and ○ are hydrogen atoms).

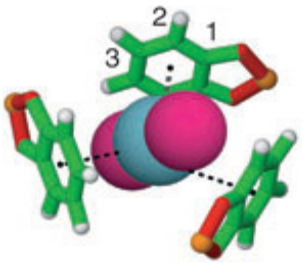

Figure 3.8. Weak C-π interactions are thought to stabilise the carbon dioxide inside the pore of **6** [157]. (colours: ● are nitrogen atoms; ● are oxygen atoms; ● are carbon atoms and ○ are hydrogen atoms).

Table 3.6. Crystallographic Information for **6**.

Molecular Formula	$C_{18}H_{12}N_3O_6P_3$
Molecular Weight (M_R) ($g.mol^{-1}$)	459.23
Density (δ) ($g.cm^{-3}$)	1.321
Space Group	$P6_3/m$
Unit Cell (*a, b, c* in Å & γ in °)	$a=b=11.454(4)$ $c=10.160(4)$ $\gamma = 120$

3.8.7. *p*-isopropylcalix[4]arene

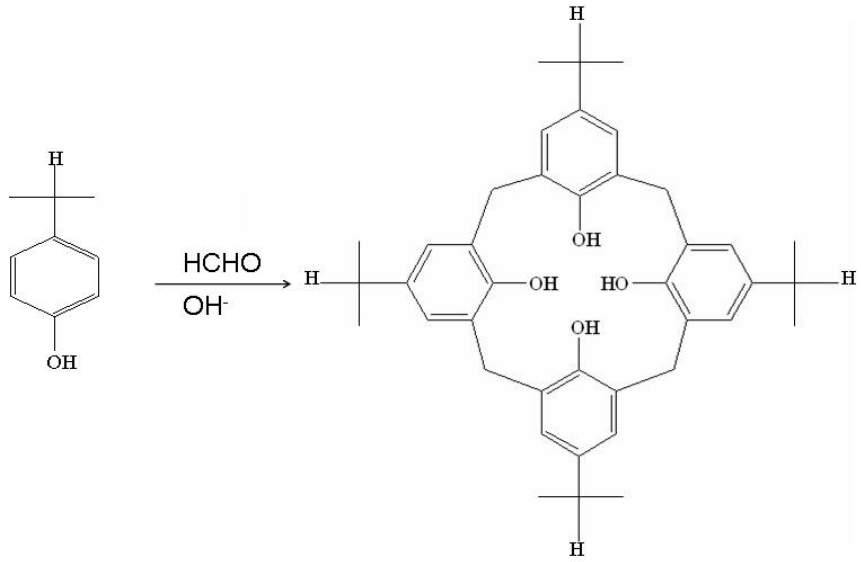

Scheme 3.5. Synthetic procedure followed to yield **7**.

The synthesis of 7 was performed the author and Dr Agnieszka Szumna by modifying the procedure followed by Gutsche [143] to produce a record yield of 29%.

4-isopropylphenol (27.238g or 1eq), formaldehyde (20.6 ml), sodium hydroxide (0.36g or 0.45 eq) and water (1 ml) were added to a three-neck 1 litre round bottomed flask and placed in an oil bath with a mechanical stirrer to stir at room temperature for 15 minutes.

The mixture was then regulated to between 110-120°C and the clear mixture was stirred for 2 hours. After 20 minutes the mixture turned yellow and eventually developed into a thick slurry of a deep yellow-brown hue. Stirring was discontinued and the reaction mixture was allowed to cool to room temperature. The resulting residue was dissolved in warm diphenyl ether over a period of 2 hours.

The three-neck round bottomed flask was then fitted with a nitrogen gas inlet and a Dean-Stark apparatus. Whilst stirring, the contents were heated to between 110-120°C with nitrogen gas flowing over the reaction mixture to facilitate the removal of water. As the water was removed a solid precipitate started to form. Once all the water was successfully removed, the Dean-Stark apparatus was replaced with a condenser and the reaction mixture was heated to between 150°C and 160°C and left to reflux for 3-4 hours under nitrogen gas flow. The solid precipitate dissolved to form a grey-black solution. The reaction mixture was then cooled to

room temperature overnight. 500 ml ethyl acetate was added to the solution to precipitate out the product. The mixture was first stirred for 30 minutes and then allowed to stand for 30 minutes.

The resulting precipitate was filtered and then washed twice with 30 ml ethyl acetate; once with 60 ml acetic acid; twice with 30 ml water and twice with 15 ml acetone. The resulting white solid product was dissolved in 500 ml boiling toluene. Upon cooling the product was obtained as clear crystals.

^{1}H NMR and mass spectrometry confirm the synthesis of **7** (see **Addenda**). Guest removal was achieved by sublimation at reduced pressure at 260°C. Concomitant polymorphism was observed yielding two non-porous crystal structures **7a** and **7b**. Crystallographic data are available in the **Addenda**.

Table 3.7. Crystallographic Information for **7a** and **7b**.

	7a	**7b**
Molecular Formula	$C_{40}H_{48}O_4$	$C_{40}H_{48}O_4$
Molecular Weight (M_R) ($g.mol^{-1}$)	592.82	592.82
Density (δ) ($g.cm^{-3}$)	1.1836	1.1824
Space Group	*C*2/*c*	$P2_1/n$
Unit Cell (*a, b, c* in Å & β in °)	*a*=24.851(3) *b*=9.412(1) *c*=29.215(4) β= 103.211 (2)	*a*=17.681(2) *b*=9.525(8) *c*=19.984(2) β= 98.363 (2)

CHAPTER 4. Methodology Development for Determining Thermodynamic Parameters of Solid-Gas Sorption Reactions.

Quantifying the thermodynamic parameters of weak solid-gas interactions is imperative in understanding the underlying processes governing sorption, as mentioned in **Chapter 2**. The primary aim of the work described in this chapter was to develop and construct a simple and effective system suitable for use with *transiently* porous host systems to convincingly determine the thermodynamic parameters $\Delta H°_{ad}$, $\Delta S°_{ad}$, and $\Delta G°_{ad}$ within a reasonable allowed margin of error, where $\Delta H°_{ad}$ is the standard enthalpy of adsorption, $\Delta S°_{ad}$ is the standard entropy of adsorption and $\Delta G°_{ad}$ is the standard Gibbs free energy for the adsorption reaction. The accuracy and precision of the constructed device were then tested using six different supramolecular host-guest systems. The results from this study assist in ascertaining whether enthalpic or entropic parameters are the primary contributing factors facilitating the sorption reaction in the studied host systems. Potential sorption processes were also postulated from the results and are discussed here. The advantages and disadvantages of the volumetric SIT method are highlighted, with particular focus on its application in studying *transiently* porous solids. A discussion regarding the use of complementary techniques is also given.

4.1. The Constructed Volumetric Sorption Device

The notion of obtaining thermodynamic parameters for solid-gas interactions was pioneered by Barrer whilst working on conventionally porous zeolite systems and using volumetric and gravimetric SIT methods [57, 85, 105, 158].

There are six main methods currently in use for determining the thermodynamic parameters for sorption reactions, as discussed in **Chapter 2**. Most of these techniques have been developed for use on conventionally porous systems and require the accurate determination of specific parameters, particularly the degree of coverage, θ. The degree of coverage is a parameter that may be obtained by solving the Langmuir Equation, **Equation 4.1**, and represents the degree of available sorption sites inherent to the host surface area that are occupied by guest molecules.

$$\theta = \frac{\left(\frac{k_a}{k_d}\right)P}{1+\left(\frac{k_a}{k_d}\right)P} \qquad \textbf{(4.1)}$$

where k_a and k_d are the adsorption and desorption rate constants and P is the gas pressure.

The Langmuir equation was developed to describe monolayer adsorption within the vacant space of *conventionally* porous materials. It is thus not sensible to employ the Langmuir model when studying *transiently* porous systems as there are no pores within the supramolecular host framework, thus rendering the concept of monolayer sorption void. Since many of the current methods used to determine thermodynamic parameters for solid-gas sorption reactions stem from the further development of the Langmuir mathematical model, a means of circumventing the necessity of finding θ is needed in order to calculate thermodynamic parameters for transiently porous host compounds.

In this study we constructed a volumetric SIT device previously described by Barbour [99]. The method is based on measuring gas pressure changes in a calibrated and constant volume over a period of time [16]. Basic physical chemistry principles are then applied in such a manner to avoid the necessity of determining θ, whilst ensuring the effective use of the instrument for the study of *transiently* porous compounds and *conventionally* porous compounds alike.

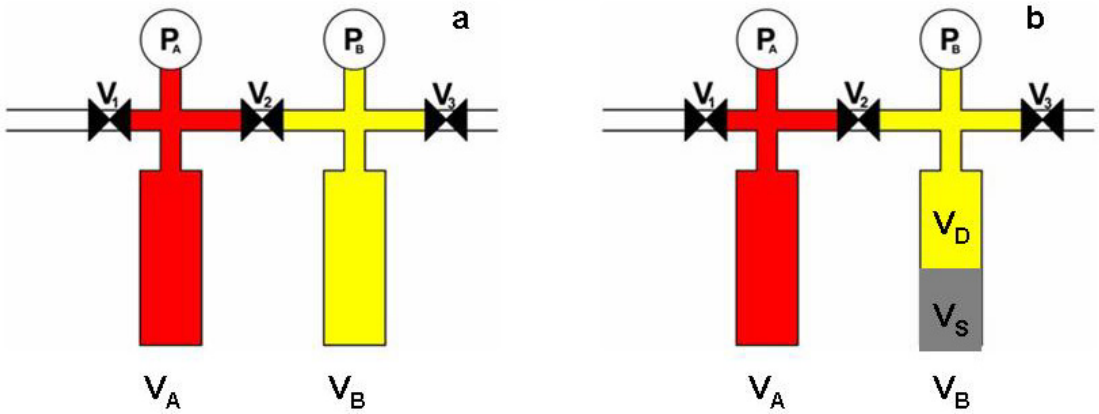

Figure 4.1. The volumetric SIT device shown in (**a**) without sample and (**b**) with sample. In (**a**) P_A and P_B are pressure transducers; V_1, V_2 and V_3 are ball valves; V_A represents the gas reservoir volume (shaded red) and V_B the empty sample chamber volume V_B (shaded yellow). In (**b**) V_S (shaded grey) is the sample volume and V_D (shaded yellow) is the "dead volume" where $V_D = V_B - V_S$.

Figure 4.1.a shows a schematic diagram of the constructed volumetric SIT device. The device was constructed from modular brass Swagelok® components and consists of two chambers A and B with volumes V_A and V_B respectively. Each chamber incorporates its own pressure transducer (P_A and P_B respectively) to monitor gas pressure. The chambers are separated from the environment and from one another using ball valves, V_1-V_3. High precision Wika® Eco-1 pressure transducers are used to measure the pressures. The valves V_1 and V_3 can be used to connect the system to either a high pressure gas cylinder or to a vacuum pump. The device, is mounted against a wooden board, as shown in **Figure 4.2**, which in turn is housed in a thermostated cabinet insulted with polyethylene.

Generally the host sample under investigation is placed in chamber B, with volume V_B, and the chamber is evacuated. Chamber A, with volume V_A, is filled with gas, keeping chamber B under vacuum. By briefly opening and closing V_2 the amount of gas supplied to the sample can be determined using a suitable equation of state. If the sample in V_B is porous, the pressure in V_B will drop and this will be monitored *in situ* by P_B, which is recorded using appropriate software.

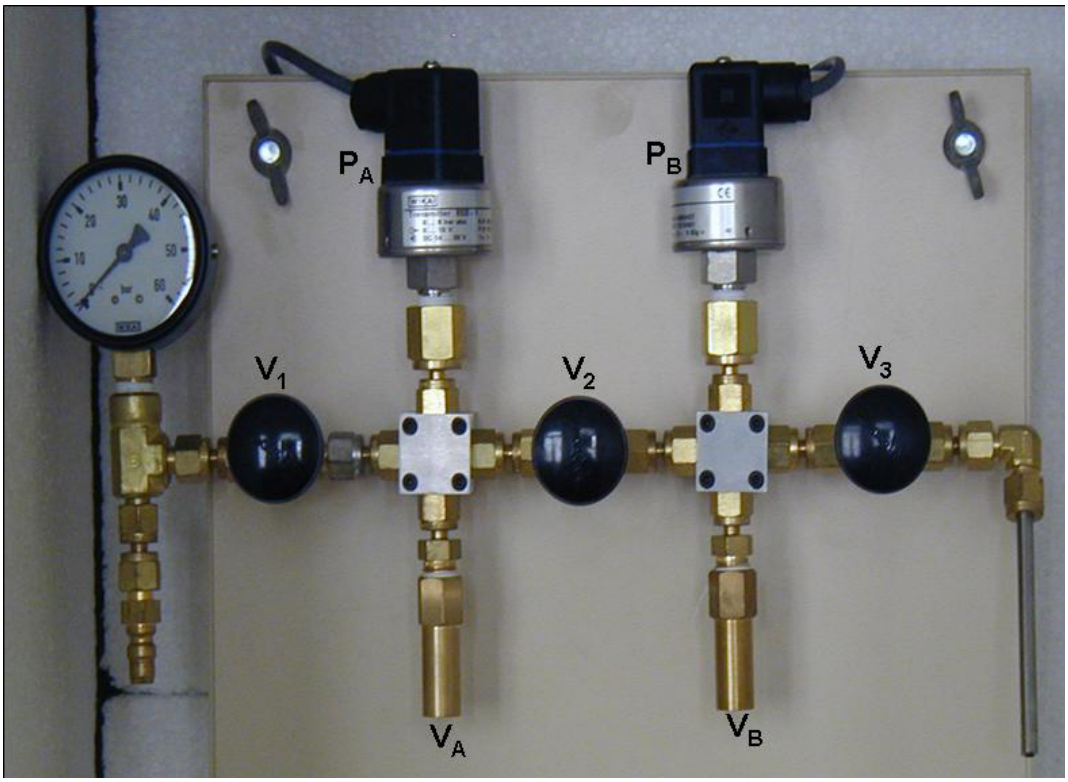

Figure 4.2 A photograph of the volumetric SIT device.

Volumetric SIT methods all rely on an equation of state to relate pressure measurements to n, the number of moles of guest. In order to achieve this, certain variables in the different state functions must remain constant. In this study two equations of state were employed, namely, the Ideal Gas Equation, **Equation 4.2**, and the van der Waals Equation, **Equation 4.3** shown below.

$$PV = nRT \qquad \textbf{(4.2)}$$

where n is the number of moles of gas, P is the pressure, V is the volume, T is temperature in Kelvin and R is the gas constant, and

$$\left(P + \frac{n^2 a}{V^2}\right)(V - nb) = nRT \qquad \textbf{(4.3)}$$

where a and b are constants specific to the gas employed. The constant a is a measure of the attraction between particles, and b represents the volume excluded by a mole of the specific gas particles.

It becomes evident that for a sorption reaction measuring a drop in pressure, the variables of temperature and volume must be kept constant to mathematically relate pressure to number of moles. Thus it is of the utmost importance to thermostat the device and to accurately determine the volumes V_A and V_B.

The greatest contribution to statistical uncertainty in the data obtained using a volumetric SIT arises from an error in the calculated values for the volumes V_A and V_B [159]. Furthermore, when this technique was first developed by Barrer and Hey, the pressure measurements were made using a mercury burette and manometer [16, 85, 86]. This method was neither accurate nor precise, but the development of electronic pressure transducers have overcome this problem to a large extent.

For any general volumetric SIT device to be useful there are a few crucial features that the device must comply with, namely [16]:

1. The accurate determination of V_A and V_B as mentioned above where V_A is the volume of the gas reservoir (chamber A) and V_B is the sample chamber (chamber B) volume.

2. The accurate determination of the sample volume (V_S) (shaded grey in **Figure 4.1.b**). This was generally achieved by using the calculated density from crystallographic studies, and the mass measured using a four decimal place analytical balance.

3. Accurate determination of the "*dead volume*" (V_D) where $V_D = V_B - V_S$, where V_B is the empty sample chamber volume and V_S is the volume of the sample.

4. The device should be thermostated. This ensures that the gas in the different modular parts is at the same constant temperature (this was achieved by placing the device in a thermostated cabinet insulated with polyethylene).

5. Accurate pressure measurements (this was achieved by using Wika® Eco-1 high precision electronic pressure transducers designed for specific pressure ranges).

6. Long-term stability of the instrument with regard to all electronic and physical components as a typical sorption reaction can take several hours to reach equilibrium.

The most sensitive and accurate device can still yield meaningless results if the theoretical model used to fit the experimental data is incorrect. Thus, the equation of state used to relate pressure, temperature, volume and number of moles *n* becomes important. In this study the Ideal Gas Equation was used when working with nitrogen gas and the van der Waals Equation of state when working with carbon dioxide.

Before volume calibrations were performed to determine V_A and V_B, the pressure sensors were calibrated against a highly accurate 0-10 bar Wika® reference gauge (accuracy of ± 0.3%) using nitrogen gas at room temperature. The contribution of local atmospheric pressure on the calibration was taken into account by consulting a local weather station. A thorough leak test was performed prior to loading each sample into chamber B.

The calibration of the volumes V_A (shown in **Figure 4.1.a** in red) and V_B (shown in **Figure 4.1.a** in yellow) are determined using low-pressure transducers and nitrogen gas at room

temperature. Nitrogen gas is used as it exhibits near ideal gas behaviour in low pressure ranges. The Ideal Gas equation, **Equation 4.2**, was then employed to derive values for the volumes V_A and V_B.

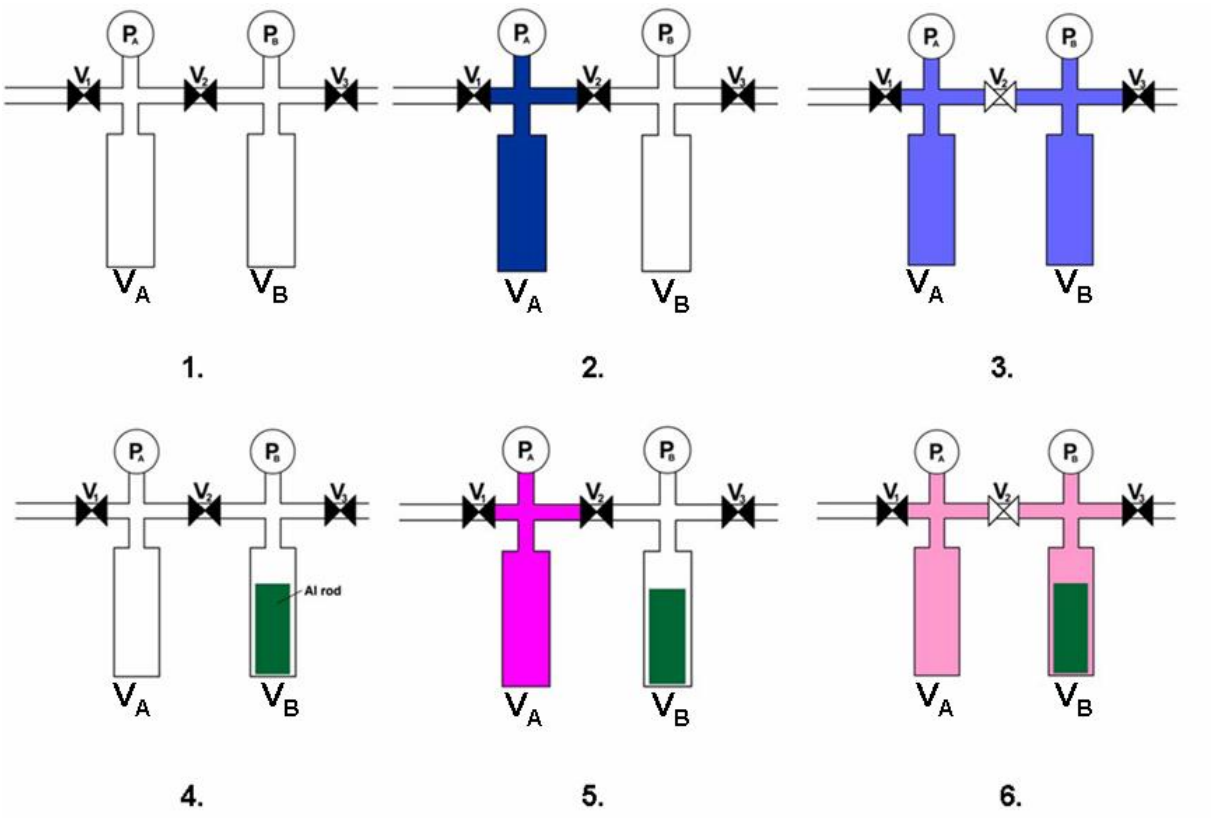

Figure 4.3. A schematic sequence indicating the method used to calculate the volumes V_A and V_B.

The procedure that was followed is illustrated in **Figure 4.3**. Firstly, the temperature is thermostated at 25°C. Both chambers A and B are evacuated and the valves are all closed as indicated in **Figure 4.3.1**. Nitrogen gas is then introduced into V_A and the system is allowed to stabilise at 25°C before a pressure is recorded from P_A as shown in **Figure 4.3.2**. The pressure reading from P_A is recorded as P_1. Valve V_2 is then opened, allowing the nitrogen gas to fill both chambers V_A and V_B as shown in **Figure 4.3.3**. The pressure reading (which should be the same for both pressure transducers) is recorded as P_2. From the recorded pressures we have

$$P_1 V_A = P_2 (V_A + V_B) \qquad \textbf{(4.3)}$$

that on rearrangement yields:

$$\frac{P_1}{P_2} = \frac{(V_A + V_B)}{V_A} = 1 + \frac{V_B}{V_A} \qquad \textbf{(4.4)}$$

The procedure is repeated, but with an aluminium rod of known dimensions (*i.e.* volume V_x, determined from its known density and mass) placed in chamber V_B as shown in **Figure 4.4.4 – Figure 4.4.6**. The two pressures are recorded as P_3 and P_4. From these readings we now have the following information,

$$P_3 V_A = P_4 (V_A + V_B - V_X) \qquad \textbf{(4.5)}$$

which on rearrangement yields,

$$\frac{P_3}{P_4} = \frac{(V_A + V_B - V_X)}{V_A} = 1 + \frac{V_B}{V_A} - \frac{V_X}{V_A} \qquad \textbf{(4.6)}$$

Both V_A and V_B can now be calculated. The procedure is repeated a number of times so that a standard deviation of the volumes can be determined. When performing an experiment with a sample in chamber B it is imperative to subtract the volume of the sample, V_S, from the calculated volume, V_B, in order to arrive at a value for the so-called "*dead space*", V_D, of the sample chamber. This is because once the sample chamber V_B contains a solid sample, the pressure transducer P_B monitors the pressure in the volume V_D, where $V_D = V_B - V_S$. It is imperative to use pressure sensors that are specifically designed to function within the ranges used experimentally. Low pressure sensors exhibit a higher sensitivity yielding more accurate and precise data for the determination of the volumes as compared to high pressure sensors.

4.2. A Typical Experiment: Theory and Practice

The experimental method rests upon two important assumptions:

i. that nitrogen gas behaves as an ideal gas for the accurate volume determination, and
ii. that the sample volume remains constant throughout the experiment (*i.e.* that there is no appreciable gas-induced structural phase change).

4.2.1. The Sorption Reaction to Equilibrium

In a typical isothermal experiment, a known amount of sample (V_S) is placed in the sample chamber, V_B, and the system is evacuated at room temperature for a specific period of time. All the valves are then closed. The selected gas is then introduced into the reservoir chamber, V_A. The system is then allowed to equilibrate at room temperature, after which, the pressure reading of P_A is recorded as P_{Astart}. The valve V_2 is then briefly opened and then closed. Assuming the sample, of volume V_S, in chamber B is porous, sorption will take place with the monitored pressure reading of P_B dropping with time until equilibrium is reached. Once equilibrium is reached, the pressure reading of P_A is recorded as P_{Aend}, and the pressure reading of P_B, monitoring the pressure decrease in chamber B, is recorded as P_{Beq}.

By solving the van der Waals Equation of state it is possible to calculate the amount of gas for all recorded gas pressures P_{Astart}, P_{Aend} and P_{Beq}. The number of moles of guest introduced to the sample is then calculated as,

$$n_{intro} = n(P_{Astart}) - n(P_{Aend}) \qquad \textbf{(4.7)}$$

Thus, the total number of moles of guest being sorbed by the porous sample at a particular equilibrium loading pressure can be given by **Equation 4.8**,

$$n_{total} = n_{intro} - n(P_{Beq}) \qquad \textbf{(4.8)}$$

The experimental procedure is followed in real-time using a computer interface that allows one to monitor various physical conditions (*i.e.* temperature and pressure) of the sorption experiment.

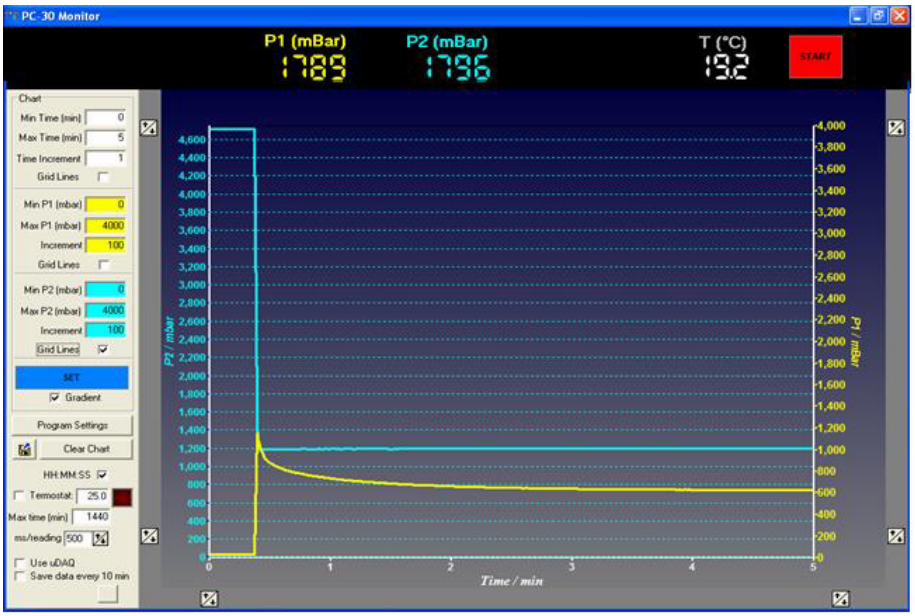

Figure 4.4 The computer interface showing the different pressure readings taken during the course of a typical sorption experiment.

The computer interface in **Figure 4.4** shows the pressure in the pressure transducers P_A (plotted in blue as P_2 in mbar) and P_B (plotted in yellow as P_1 in mbar) as a function of time. The temperature is also monitored to ensure that it remains constant. The amount of gas sorbed by the sample can then be expressed in terms of moles of gas sorbed per gram of substrate (mmol.g^{-1}); as percentage occupancy (%); as a mass ratio (g.g^{-1}) or as mmol guest per mmol host (mmol G / mmol H). If the experimental procedure is repeated by varying the input gas pressure in P_A, it is possible to plot a curve of the amount of gas sorbed by the sample as a function of the equilibrium loading pressure, P_{Beq}, as shown in **Figure 4.5**. When performing an experiment the pressure readings, their corresponding number of moles of gas, the n_{intro} and nV_{Beq} values are tabulated and used to plot the graph shown in **Figure 4.5**. All tabulated sorption data can be viewed in the **Addenda**.

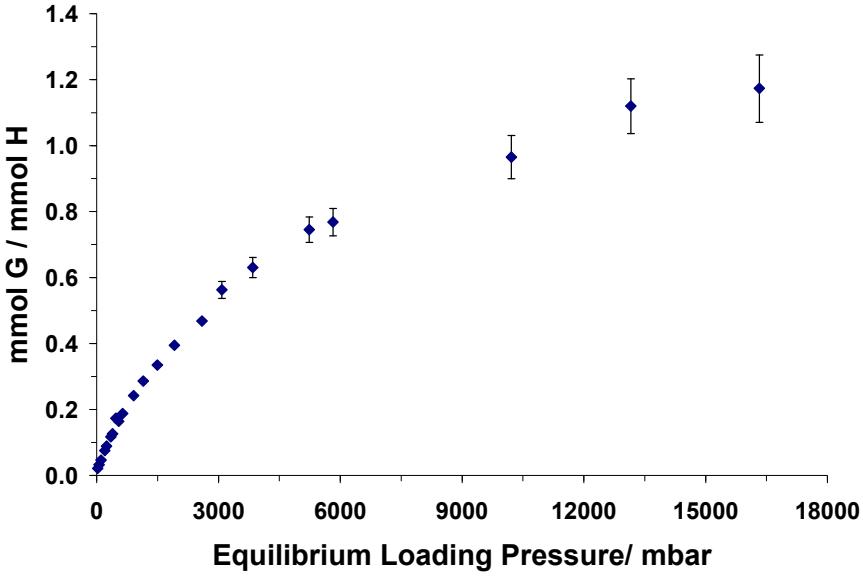

Figure 4.5. A plot of mmol G / mmol H against equilibrium loading pressure.

Figure 4.5 shows the results of a series of typical sorption experiments where the guest-host ratio is plotted as a function of equilibrium loading pressure. The values for the standard deviations are obtained by taking into account the deviation in the values for the volumes V_A and V_B. It should be noted, however, that there are a number of additional factors that contribute to the overall standard deviation on the ordinate values, such as temperature and pressure. In this study, only the standard deviations in the volumes were considered when calculating errors for the ordinate values.

4.2.2. Determining the Thermodynamic Parameters $\Delta G°_{ad}$, $\Delta H°_{ad}$, and $\Delta S°_{ad}$

The thermodynamic parameters $\Delta G°_{ad}$, $\Delta H°_{ad}$, and $\Delta S°_{ad}$ can be experimentally determined for each point on the curve in **Figure 4.5**. This is achieved by recording the equilibrium pressure as a function of temperature for specific quantities of gas and porous sample. The first part of the experiment involves monitoring a sorption reaction until equilibrium has been established, as described in **Section 4.2.1**. After equilibrium has been reached the temperature is ramped at a constant ramp rate from 25°C to 50°C and back down to 25°C while simultaneously monitoring the pressure reading of P_B. As temperature and pressure are related to one another by an equation of state, it is important to choose a ramp rate that will allow the system to reach equilibrium at each temperature recorded. Data from such an experiment can

be used to determine $\Delta G°_{ad}$, $\Delta H°_{ad}$, and $\Delta S°_{ad}$ based on the following physico-chemical principles of a system at equilibrium: Consider the host guest reaction,

$$\mathrm{H}\,(s) \quad + \quad \mathrm{nG}\,(g) \underset{k_r}{\overset{k_f}{\rightleftharpoons}} \quad \mathrm{H{\cdot}G_n}\,(s) \tag{4.7}$$

The equilibrium constant for the total reaction is thus

$$K_{eq} = \frac{k_r}{k_f} = \frac{a_{GH}}{a_H\, a_{G_n}} \tag{4.8}$$

where a_{GH} is the activity for $H{\cdot}G_{n(s)}$, a_H is the activity for $H_{(s)}$ and a_{Gn} is the activity for $nG_{(g)}$.

Activity, a_i, is a way of simply expressing the chemical potential, μ_i, of a species in a mixture [160]. The well-known Maxwell relationship [160], shown in **Equation 4.9**, can be integrated to give an expression to calculate the Gibbs free energy of a reaction, **Equation 4.10**, in terms of pressure.

$$\left(\frac{\partial G}{\partial P}\right)_{T,n} = V \tag{4.9}$$

$$\int_{G^0}^{G_1} dG = \int_{P^0}^{P_1} V dP \tag{4.10}$$

In the situation where the guest gas is an ideal gas, $V = nRT/P$, and **Equation 4.10** becomes **Equation 4.11** at constant temperature,

$$G_1 = G^0 + nRT \ln\left(\frac{P_1}{P^0}\right) \tag{4.11}$$

where P is the pressure in bar and P^0 is the pressure at standard conditions (*i.e.* $P^0 = 1$ bar $\approx$ 1/1.01325 atm).

In the case of a real gas where the van der Waals equation of state is employed, P must be replaced by the fugacity, f, so that **Equation 4.11** becomes,

$$G_1 = G^0 + nRT\ln\left(\frac{f}{P^0}\right) \qquad \textbf{(4.12)}$$

where $f = Pe^{\left[\left(b-\frac{a}{RT}\right)\left(\frac{P}{RT}\right)\right]}$ and a and b are the van der Waals constants for the specific gas under consideration.

For a solid the integrated form of **Equation 4.10** can be expressed as follows, owing to a negligible change in the molar volume of the material,

$$G_1 = G^0 + V\left(P_1 - P^0\right) \qquad \textbf{(4.13)}$$

The Gibbs free energy of a reaction, **Equation 4.11**, can now be expressed in terms of chemical potential, μ_i, and as a function of activity, a_i.

$$\mu_i = \mu_i^0 + RT\ln\left(a_i\right) \qquad \textbf{(4.14)}$$

where $a_i = \frac{P}{P^0}$ for an ideal gas, and $a_i = \frac{f}{P^0}$ for a van der Waals gas.

For a solid, $RT\ln\left(a_i\right) = V\left(P - P^0\right)$ and thus, $a_i = e^{\left[\frac{V\left(P-P^0\right)}{RT}\right]}$.

The equilibrium constant for the reaction shown in **Equation 4.8**, reduces to **Equation 4.15**, when a real gas is used and the pressure is measured in bar.

$$K_{eq} = \frac{k_r}{k_f} = \frac{a_{GH}}{a_H\, a_{G_n}} = \frac{e^{\left[\frac{V\left(P-P^0\right)}{RT}\right]}}{e^{\left[\frac{V\left(P-P^0\right)}{RT}\right]}\left(\frac{f}{P^0}\right)^n} = \frac{1}{f^n} \qquad \textbf{(4.15)}$$

The Gibbs free energy for a reaction can now be given by **Equation 4.16**,

$$\Delta G_{reaction} = \Delta G^{\circ}_{ad} + RT \ln K_{eq} \qquad \textbf{(4.16)}$$

At equilibrium $\Delta G_{\text{reaction}} = 0$, therefore Equation **4.16** reduces to

$$\Delta G^{\circ}_{ad} = -RT \ln K_{eq} \qquad \textbf{(4.17)}$$

but

$$\Delta G^{\circ}_{ad} = \Delta H^{\circ}_{ad} - T\Delta S^{\circ}_{ad} \qquad \textbf{(4.18)}$$

Therefore it follows that

$$\Delta G^{\circ}_{ad} = -RT \ln K_{eq} = -RT \ln(\frac{1}{f^{n}}) = \Delta H^{\circ}_{ad} - T\Delta S^{\circ}_{ad} \qquad \textbf{(4.19)}$$

Upon rearrangement of Equation **4.19** to the general form of $y = mx + c$, the following relationship is obtained,

$$n \ln f = \frac{\Delta H^{\circ}_{ad}}{RT} - \frac{\Delta S^{\circ}_{ad}}{R} \qquad \textbf{(4.20)}$$

where the gradient, m, and the intercept, c, are given by

$$m = \left[\frac{\partial \ln f}{\partial(\frac{1}{T})} \right]_{Volume} = \left[\frac{\Delta H^{\circ}_{ad}}{R} \right]_{Volume} \text{ and } c = \left[\frac{\Delta S^{\circ}_{ad}}{R} \right]$$

Consequently a plot of $n\ln f$ as a function of $\frac{1}{T}$ should yield a linear curve with a gradient of $\frac{\Delta H^{\circ}_{ad}}{R}$ and an intercept $-\frac{\Delta S^{\circ}_{ad}}{R}$. The experiment can be monitored *in situ* using a computer interface as shown in **Figure 4.6**.

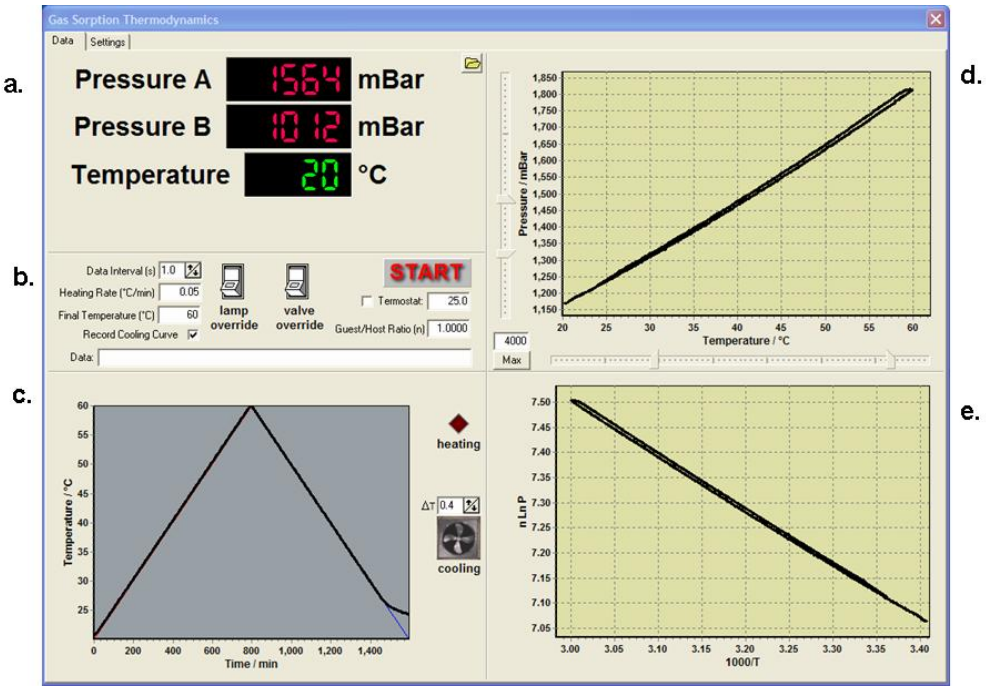

Figure 4.6. A computer interface for *in situ* monitoring of the pressures in order to determine the thermodynamic parameters of a solid-gas sorption reaction. (**a**) This block permits the researcher to monitor the pressures in both chamber A (Pressure A) and chamber B (Pressure B). The temperature of the instrument is also be monitored. (**b**) This block allows one to select a heating ramp rate and to set the upper temperature limit. The interval at which the data are recorded can also be specified. (**c**) This block shows whether the system is reaching the set temperatures at the selected ramp rate. (**d**) Plots the pressure as a function of temperature for heating and cooling of the system. Finally, (**e**) plots $n\ln p$ *vs* $1000/T$ plot for the heating and cooling curves. Values for ΔH°_{ad} and ΔS°_{ad} are obtained from the gradient and intercept values of the plot of $n\ln f$ *vs* $1000/T$ obtained respectively.

Typical experimental results are shown in **Figure 4.7** where **Figure 4.7.a** shows the initial drop in pressure at 25°C until the system reaches equilibrium. **Figure 4.7.b** shows the plot of $n\ln f$ *vs* $1000/T$ yielding the linear plot used to determine ΔH°_{ad} and ΔS°_{ad} at a particular equilibrium loading pressure. Consequently, by performing experiments at varying equilibrium loading pressures, entropic and enthalpic contributions to ΔG°_{ad} can be investigated for a system at equilibrium as shown in **Figure 4.8**. The ordinate energy values in **Figure 4.8** are ΔG°_{ad}, ΔH°_{ad} and $T\Delta S^\circ_{ad}$.

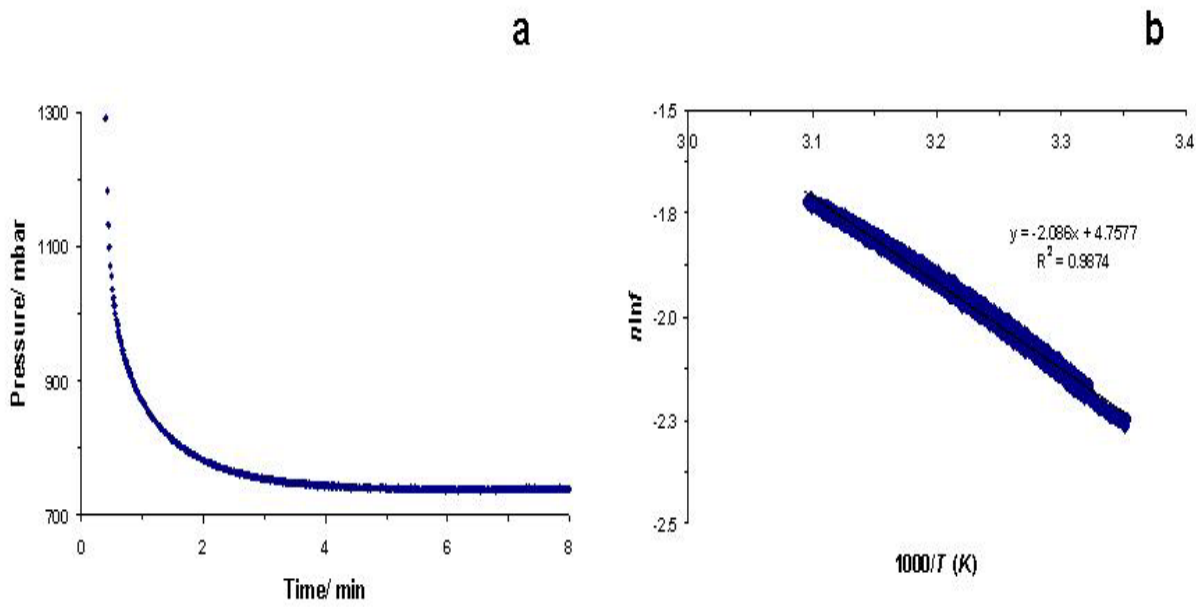

Figure 4.7. (**a**) A plot of the pressure drop during the sorption reaction indicating that equilibrium has been reached after ~6 min. (**b**) The heating and cooling curve of the system ramped from 25 to 50°C and back down to 25°C.

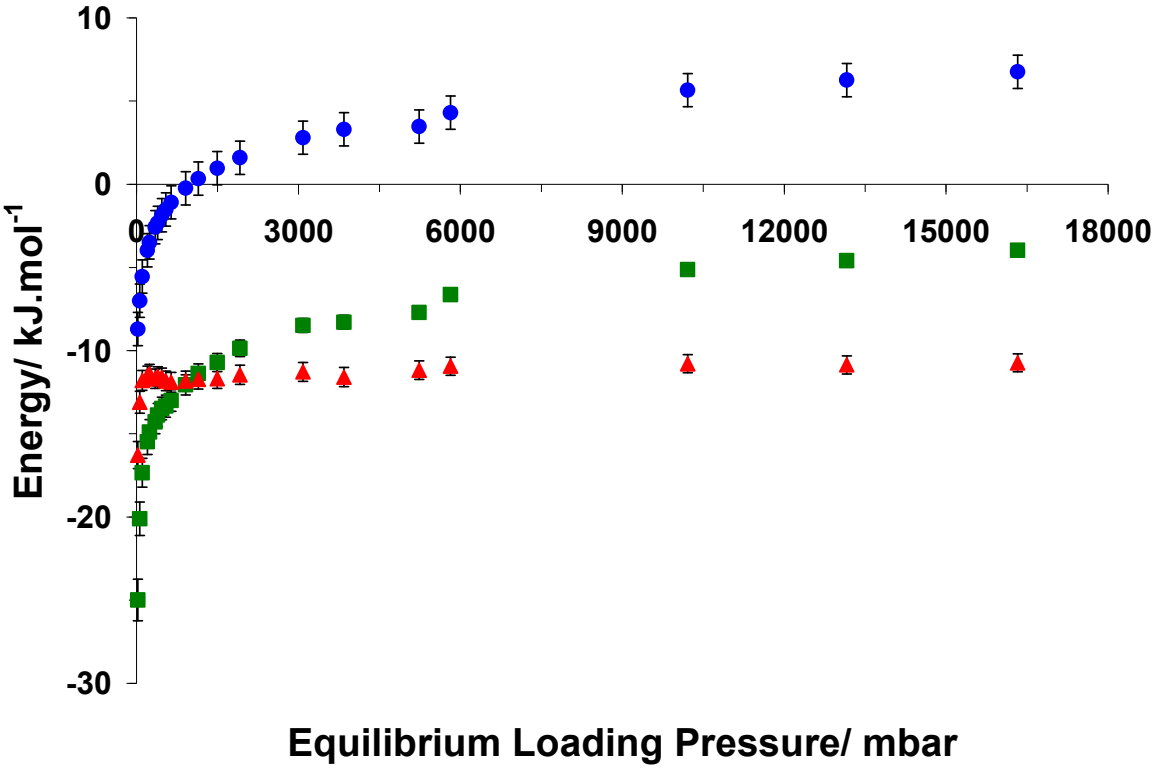

Figure 4.8. Entropic and enthalpic contributions to $\Delta G°_{ad}$ where $\Delta G°_{ad} = \Delta H°_{ad} - T\Delta S°_{ad}$. ● is $\Delta G°_{ad}$; ▲is $T\Delta S°_{ad}$ and ■ is $\Delta H°_{ad}$.

The inherent error in the values of $\Delta H°_{ad}$, and $\Delta S°_{ad}$ at a particular equilibrium loading pressure can be obtained by a regression analysis on the slope and intercept values of the plot

of $n\ln P$ *vs* $1000/T$. The error in $\Delta G°_{ad}$, however, can only be estimated since the experiment must be repeated at exactly the same equilibrium loading pressure for a true value of the error to be calculated. Owing to the nature of the volumetric SIT device used, exact repetition of equilibrium loading pressures is not easily feasible.

The chosen temperature ramp rate is an important aspect deserving careful consideration, since the sample must remain under equilibrium conditions at all times. Different host compounds will achieve equilibrium after different times, owing to their physico-chemical properties such as pore size and affinity for the guest molecule. The effect of various ramp rates on the error of the calculated thermodynamic parameters was investigated in order to select a ramp rate that is reasonably fast but also yields sensible results. The experiments were performed on the host system that requires the longest time periods to reach equilibrium, namely *p-tert*-butylcalix[4]arene. The investigation was performed under an equilibrium pressure of 58 mbar at 25°C. The results of this study are shown in **Table 4.2**. The thermodynamic parameters $\Delta H°_{ad}$ and $\Delta S°_{ad}$ were determined for the system at different ramp rates, and the average values and standard deviations for all the measured values are given in **Table 4.3**. It can clearly be seen that the standard deviation in the calculated values is very small. It was thus decided to use a ramp rate of 0.20 °C.min^{-1} throughout the remainder of this study as it yields an acceptable compromise between the time taken to perform one experiment and the accuracy of the resulting data.

Table 4.2. A comparison of different ramp rates on the error for values of $\Delta H°_{ad}$ and $\Delta S°_{ad}$.

Ramp Rate (°C.min^{-1})	$\Delta H°_{ad}$ (kJ.mol^{-1})	$\Delta S°_{ad}$ (kJ.K^{-1}mol^{-1})	Time/ hrs
0.05	-20.336	-0.0448	16.7
0.10	-19.420	-0.0420	8.3
0.15	-19.350	-0.0412	5.6
0.20	-18.405	-0.0386	4.2

Table 4.3. The average values and standard deviations for $\Delta H°_{ad}$, and $\Delta S°_{ad}$ using four different ramp rates.

	Average	**Standard Deviation σ**
$\Delta H°_{ad}$ (kJ.mol^{-1})	-19.378	0.7886
$\Delta S°_{ad}$ (kJ.K^{-1}.mol^{-1})	-0.0416	0.0026

Table 4.4. The average value of $\Delta H°_{ad}$, and $\Delta S°_{ad}$ obtained from the average of the values determined using the different ramp rates in **Table 4.3**.

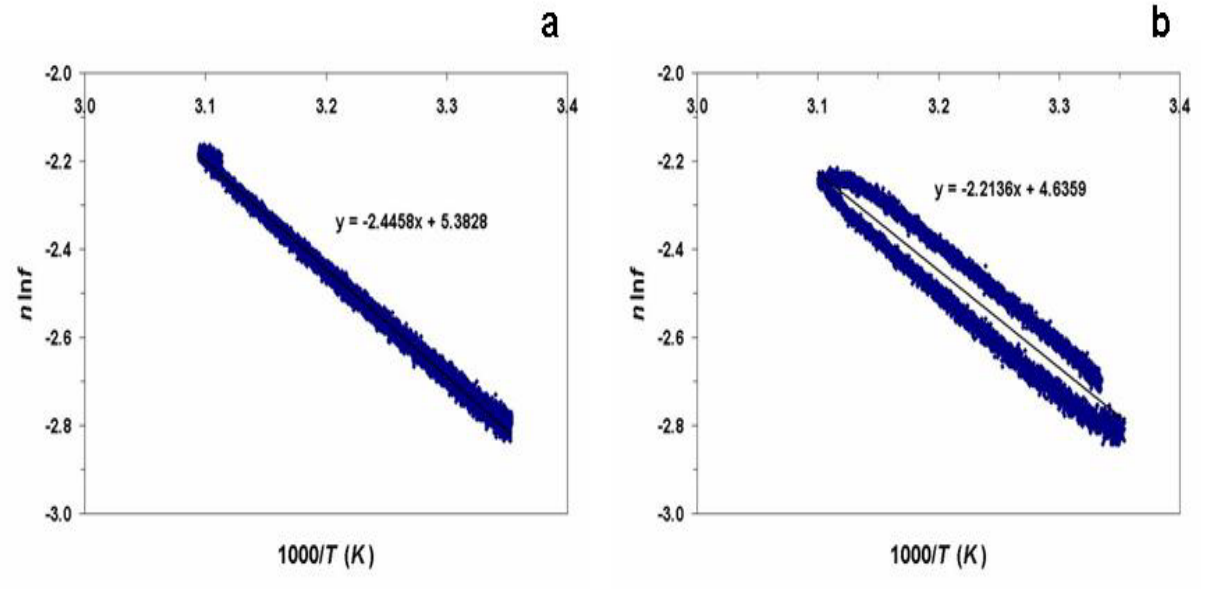

Figure 4.9. The difference between temperature ramp rates. (**a**) Shows a ramp rate of 0.05°C.min^{-1}, with the heating and cooling curves almost superimposed. (**b**) Shows a ramp rate of 0.20 °C.min^{-1} where the heating and cooling curve do not overlay one another.

The curves in **Figure 4.9** show the effect of the ramp rate on the heating and cooling curves. If true equilibrium is maintained at the desired ramp rate, the heating and cooling curves would be superimposable. If not, then true equilibrium lies between the heating and cooling curves. The study shows that, despite not achieving true equilibrium when using a faster ramp rate as shown in **Figure 4.9.b**, the thermodynamic parameters inferred from the data resulting from both ramp rates remain within acceptable standard deviations of one another.

4.3. Advantages & Disadvantages of the Volumetric SIT device.

The main advantage of using the described technique to determine the thermodynamic parameters $\Delta G°_{ad}$, $\Delta H°_{ad}$, and $\Delta S°_{ad}$ is that it eliminates the necessity of calculating the degree of coverage, θ. It is thus suitable for use on *transiently* porous and *conventionally* porous compounds alike. The method yields reliable results with reasonable standard deviations for the calculated thermodynamic parameters. The ready availability of affordable high precision pressure transducers, thermocouples and Swagelok® components allows the construction of the apparatus at a relatively low cost. The method is simple with regard to operational procedures when compared to other techniques described in the literature.

Furthermore, this method offers the unique advantage of monitoring the dependence of $\Delta H°_{ad}$ on temperature by potentially revealing any deviation from linearity in the plot of $n\ln f$ vs $1000/T$ shown in **Figure 4.7.b** for both the heating and cooling curves. Any such deviation would most likely imply a temperature-dependent phase transition in the solid-state. It is imperative to know the exact phase and nature of a solid, its unique sorption capacity and other associated physical properties in order to correctly understand and describe the processes governing sorption. The method described above is particularly useful in this regard because a sudden temperature-dependent change in the sorptive properties of the host would manifest itself as an inflection in the plot of $n\ln f$ vs $1000/T$.

The primary disadvantage of this method is that the guest-host ratio must be known in order to correctly calculate values for $\Delta G°_{ad}$, $\Delta H°_{ad}$ and $\Delta S°_{ad}$. This is generally inferred from crystallographic studies or from prior volumetric sorption studies investigating the guest-host ratio as a function of equilibrium loading pressure. The maximum temperature that experiments can be performed at is rather low, as the Wika® pressure transducers have a temperature compensated linear range from 0 to 80°C. The compound's inherent dependence or independence of $\Delta H°_{ad}$ on temperature can thus only be monitored within a certain limited temperature range. Further, prior assessment of a suitable temperature ramp rate must also be performed, making the total experimental time rather substantial.

4.4. Results and Discussion

Six different supramolecular systems were studied to investigate the versatility of the device described in **Sections 4.1-4.3**. These consisted of compounds **1a**, **2a**, **3a**, **4a**, **5** and **6**, which

were introduced in **Chapter 3 Section 3.7**. All studies were performed using carbon dioxide as the guest molecule. PXRD patterns were recorded of all samples prior to the experiments to confirm that the correct phase was being used. The PXRD patterns can be found in the **Addenda**. The initial sorption experiments were all performed at 25°C. Standard deviations of ordinate values for sorption experiments were calculated by taking only the error on the volume determination into account. The thermodynamic parameters $\Delta G°_{ad}$, $\Delta H°_{ad}$ and $\Delta S°_{ad}$ were calculated with standard deviations for the values of $\Delta H°_{ad}$ and $\Delta S°_{ad}$ obtained from regression analyses of the linear fits of $n\ln f$ vs $1000/T$. It has been mentioned in **Chapter 2** that physisorption is necessarily exothermic and therefore evolves heat. When considering **Equation 4.18**,

$$\Delta G°_{ad} = \Delta H°_{ad} - T\Delta S°_{ad} \qquad \textbf{(4.18)}$$

the change in enthalpy, $\Delta H°_{ad}$, must be negative since the change in $\Delta S°_{ad}$ is negative owing to the sorbed molecules being in a more ordered state in the host framework than in the supernatant gas phase [56]. The $\Delta H°_{ad}$ value at zero equilibrium loading pressure gives an indication of the affinity that a host system has for a guest and can be related to various interaction energies [56]. Some of the most important interactions involved include dispersion and short range repulsion, polarisation and electrostatic energies [56]. In the case of carbon dioxide as the guest molecule, Barrer [158] reports that quadrupolar interactions make an important contribution to the total value for $\Delta H°_{ad}$.

4.4.1. Gossypol

The results of the volumetric sorption experiments compare well with unpublished results of le Roex [161]. The guest-host ratio approaches 1:1 at ~10 bar and remains 1:1 within calculated error for increasingly higher equilibrium loading pressures. This is expected considering the pore of the host framework has a diameter of ~6 Å [140].

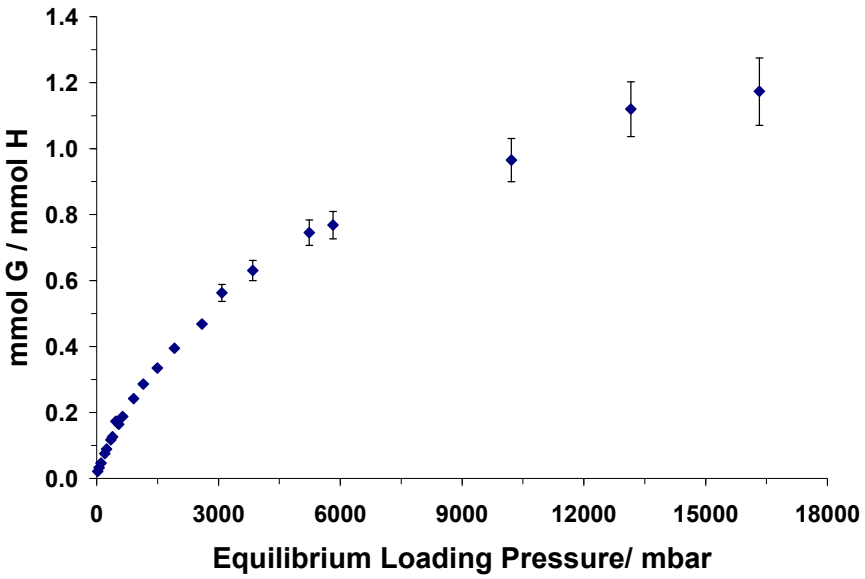

Figure 4.10. Guest-host ratios of gossypol shown as a function of equilibrium loading pressure (mbar) for sorption reactions at 25°C.

A ratio of 1:1 was used for the thermodynamic experiments which necessitates a known or inferred guest-host ratio. The results of the thermodynamic studies, shown in **Figure 4.10**, indicate that for equilibrium loading pressures under the standard pressure of 1.0 bar, the $\Delta G°_{ad}$ values are negative and that, for all pressures above standard pressure, the $\Delta G°_{ad}$ values are positive. This implies that the sorption reaction is spontaneous when the guest equilibrium loading pressure is below 1 bar and non-spontaneous when above 1 bar. It thus follows that the desorption reaction is non-spontaneous, for guest equilibrium loading pressures below 1 bar and that it is spontaneous above 1 bar. Spontaneous sorption by the host up to standard pressure can be thought of as a diffusion effect, where the guest is moving along a concentration gradient from a region of high concentration to a region of low concentration (the host). Above standard pressure the desorption reaction becomes spontaneous. This is to be expected as, in this case, the sorption is of a physical nature and there is no covalent bond formation or cleavage during the sorption process. Consequently, the desorption reaction can *also* be seen as a diffusion effect, where the guest is diffusing out of the host from a region of high concentration to a region of low concentration outside of the host. Kinetic studies discussed in detail in **Chapter 5** confirm that the sorption follows a kinetic model based on three dimensional diffusion.

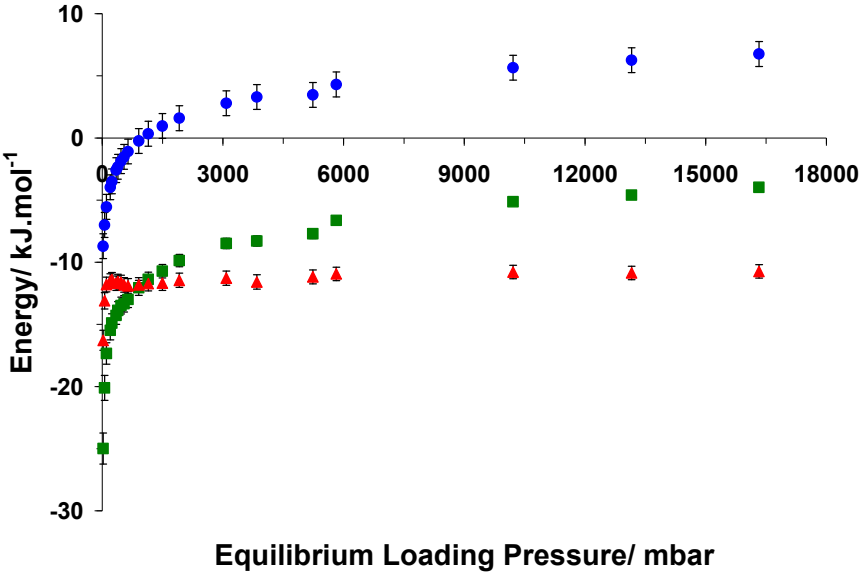

Figure 4.11. Thermodynamic parameters for sorption of carbon dioxide by gossypol, **1**, plotted as a function of equilibrium loading pressure (mbar at 25 °C) where ● is $\Delta G°_{ad}$; ▲is $T\Delta S°_{ad}$ and ■ is $\Delta H°_{ad}$.

The value of $\Delta H°_{ad}$ at zero equilibrium loading pressure can be determined from extrapolation of the graph in **Figure 4.11** and was determined to be *ca* -25 kJ.mol^{-1}. This value falls neatly within the range of -20 to -27 kJ.mol^{-1}, which is considered typical of other conventionally porous organic materials [12] such as carbon nanotubes and activated carbons [162]. Gossypol, carbon nanotubes and activated carbons therefore all display similar affinities for carbon dioxide. As the equilibrium loading pressure increases, the isosteric heat of adsorption becomes correspondingly more positive, contributing to increasingly unfavourable energetics of the reaction. This relationship between $\Delta H°_{ad}$ and equilibrium loading pressure is common among *conventionally* porous zeolites, which have inherently heterogeneous surfaces [12, 57]. The repulsive sorbate-sorbate interactions that increase with increased equilibrium loading pressure [57] are considered to be the primary factors contributing to increasingly unfavourable conditions.

Except for the first two low pressure data points, the entropic contribution to $\Delta G°_{ad}$, which is embodied in the $T\Delta S°_{ad}$ term, remains virtually constant. The value of $\Delta S°_{ad}$ falls within the range -20 to -100 J.K^{-1}.mol^{-1} that has been reported for the sorption of carbon dioxide by activated carbons [162].

It is interesting to note that the enthalpic contribution to $\Delta G°_{ad}$ dominates for all pressures under the standard pressure of 1 bar, but that the entropic contribution to $\Delta G°_{ad}$ dominates for all pressures above 1 bar. This can be rationalised by considering the desorption reaction being spontaneous at pressures exceeding 1 bar and that desorption is believed to be a non-activated diffusion process (**Chapter 5**).

It was assumed that no gas-induced structural phase changes occurred within the host framework whilst conducting the series of experiments. This assumption is questionable in the case of gossypol as implied by the PXRD diffractograms in **Figure 4.12**. It can be seen that the PXRD diffractogram of the sample prior to conducting the experiments fits the predicted diffractogram generated from the crystal structure with reference code BEMLOU12 [163] in the CSD [135]. The diffractogram of the sample taken after *all* the experiments were completed, however, does *not* match the predicted diffractogram, suggesting that a structural gas-induced phase change has probably taken place. This highlights the importance of knowing which phase of the material is being investigated. The observation requires future work employing powder diffraction experiments under controlled pressure to investigate the nature of the possible phase change.

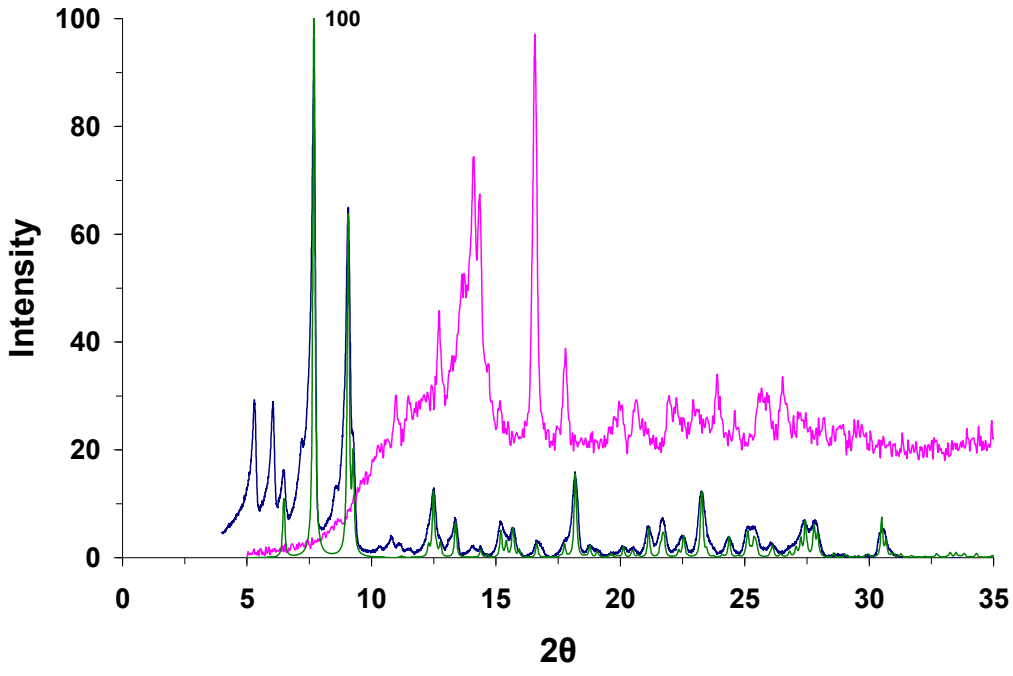

Figure 4.12. PXRD diffractograms of the gossypol sample before (–) and after (–) the sorption and thermodynamic experiments overlaid with the predicted (–) PXRD diffractogram.

4.4.2. *p-tert*-Butylcalix[4]arene

As described in **Chapter 3**, **2a** is one of the most actively investigated transiently porous compounds in the literature. As part of our ongoing efforts to understand the mechanisms governing the gas sorption for this compound, we conducted sorption and thermodynamic experiments. The experimental results are shown in **Figure 4.13**.

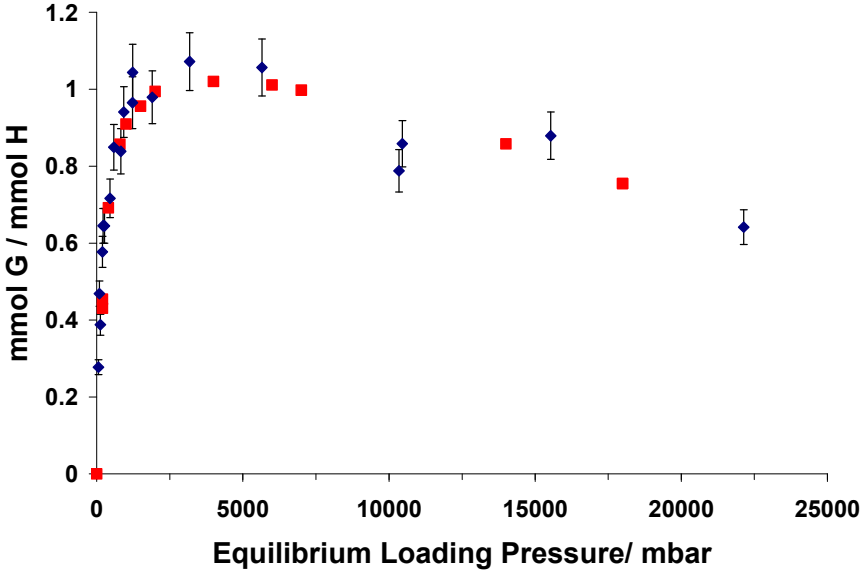

Figure 4.13. Volumetric (♦) and gravimetric (■) sorption results are overlaid to indicate the gas-induced phase that occurs for **2a**. Guest-host ratio is plotted against equilibrium loading pressure (mbar at 25 °C).

There are several points of interest to note in **Figure 4.13**. It can be seen that **2a** approaches a guest-host ratio of 1:1 at ~4 bar and that the guest-host ratio starts to decrease at ~8 bar. This is curious since, firstly, the cavity formed by the bilayer packing arrangement **2a** is large enough to accommodate two carbon dioxide molecules, which would result in a guest-host ratio of 2:1, but this ratio is never observed. This observation corresponds to the results of previous studies [12], but the reason for this observation remains unclear. Secondly, after ~8 bar the guest-host ratio decreases significantly as a function of equilibrium loading pressure. This phenomenon suggests a gas induced phase transition is taking place at higher equilibrium loading pressures, which forces the guest molecules out of the transformed host framework. To verify this observation the experiments were performed using both gravimetric and volumetric sorption apparatus. The results for both techniques, as seen in **Figure 4.13**, confirm that the guest-host ratio is decreasing. Gas induced phase transitions have been reported for this compound by Atwood [145], but the exact nature of the transition

observed in these reported results remains unclear. It is suggested that future work should investigate the phase purity of the sample as a function of increasing equilibrium loading pressure by making use of *in situ* PXRD studies under selective gas pressures and temperatures. Since it is well documented that two polymorphs of the apohost exist (kinetic product **2a** and thermodynamic product **2b**), the results of the suggested *in situ* PXRD experiments might elucidate the possible nature of the phase change.

The results of the thermodynamic studies are shown in **Figure 4.14**. It is noted that the $\Delta G°_{ad}$ values are negative under standard pressure, suggesting that **2a** spontaneously sorbs gas at pressures under 1 bar. The $\Delta G°_{ad}$ values are positive above standard pressure, suggesting that here the energetics of the system favour spontaneous desorption rather than sorption. This phenomenon is to be expected for reasons previously discussed. The $\Delta G°_{ad}$ values calculated under standard pressure compare well with those of typical zeolites in sorption reactions involving carbon dioxide at the same low loading pressures [164]. The energy contributions of the $\Delta H°_{ad}$ and the $T\Delta S°_{ad}$ terms are of similar importance to the $\Delta G°_{ad}$ values for all pressures under standard pressure. For all pressures above standard pressure, the entropy contribution (*i.e.* the $T\Delta S°_{ad}$ term) dominates the energetics of the reaction. This is expected as the desorption reaction is spontaneous and is thought to follow diffusion mechanisms. Hence, the entropy contribution is expected to dominate as the gas desorbs and becomes increasingly disordered.

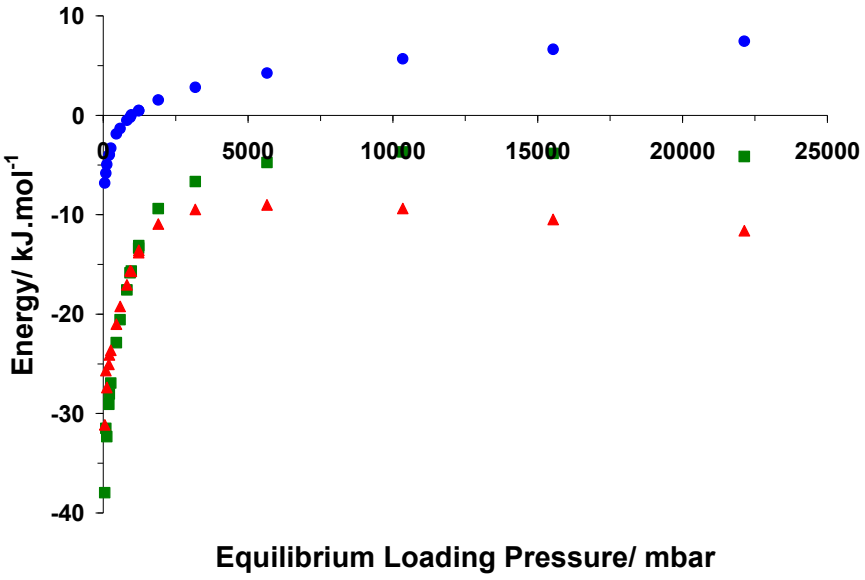

Figure 4.14. Thermodynamic parameters for the sorption of carbon dioxide by **2a** at increasing equilibrium loading pressures (mbar at 25 °). Thermodynamic parameters $\Delta G°_{ad}$ (●), $T\Delta S°_{ad}$ (▲) and $\Delta H°_{ad}$.(■).

The trend of $\Delta H°_{ad}$ values increasing as a function of equilibrium loading pressure is commonly seen in porous materials and implies that the compound has a heterogeneous surface [57], which is indeed the case here. This increase in the value of $\Delta H°_{ad}$ is primarily due to increased guest-guest and host-guest repulsive interactions as the host framework becomes more saturated with guest [57]. In the case of conventionally porous zeolites this increase in $\Delta H°_{ad}$ with increasing equilibrium loading pressure is thought primarily to be the result of increased sorbate-sorbate repulsive forces as the discrete channels fill with guest molecules [57]. It is known that **2a** plays host to only one carbon dioxide molecule per double cup of offset calix[4]arenes, and it is thought that the distance between carbon dioxide molecules is too great to have a dramatic affect on the magnitude of the repulsive forces arising from sorbate-sorbate interactions alone. The initial increase in $\Delta H°_{ad}$ at low equilibrium loading pressures is thus considered to be a surface phenomenon, mainly due to sorbate-sorbate interactions at the surface. The increase in $\Delta H°_{ad}$ at higher pressure is thus most likely the result of increasing repulsive forces caused by sorbate-sorbent interactions. The value of $\Delta H°_{ad}$ at zero equilibrium loading pressure can be estimated by extrapolation and corresponds to *ca* -38 kJ.mol^{-1}. This value is within the same range as observed for known ion-exchange zeolites [12], which typically exhibit $\Delta H°_{ad}$ values ranging from -30 to -60 kJ.mol^{-1}. This is a very curious observation, as the active sites of sorption within ion-exchange zeolites contain metals that are expected to experience greater attractive interactions with carbon dioxide than the purely organic sorption sites of **2a**. This is thought to occur because more efficient binding sites exist in **2a** in the form of the calix[4]arene dimeric capsule that hosts the guest molecule. This encapsulation increases the binding affinity of the guest. Silicates and purely organic porous materials, such as activated carbons, are known to have $\Delta H°_{ad}$ values at zero equilibrium loading pressure of between -20 to -27 kJ.mol^{-1} for sorption reactions with carbon dioxide, which is much lower in magnitude than what is observed for **2a**.

4.4.3. Cu_2(1,3-bis(imidazol-1-ylmethyl)-2,4,6-trimethylbenzene)$_2Cl_4$ [Cu_2(BITMB)$_2Cl_4$]

As discussed in **Chapter 3**, a guest-host ratio of 1:1 is expected in the case of carbon dioxide. Sorption results confirm this assumption which was made on the basis of prior crystallographic studies, with a guest-host ratio of 1:1 being achieved at ~5 bar. Our results

compare favourably to previous sorption studies performed on **3a**. The graph in **Figure 4.15** shows that the host-guest ratio remains 1:1 within a reasonable margin of error for equilibrium loading pressures between 5 and 22 bar. It appears that no phase change, which might affect the host-guest ratio, takes place.

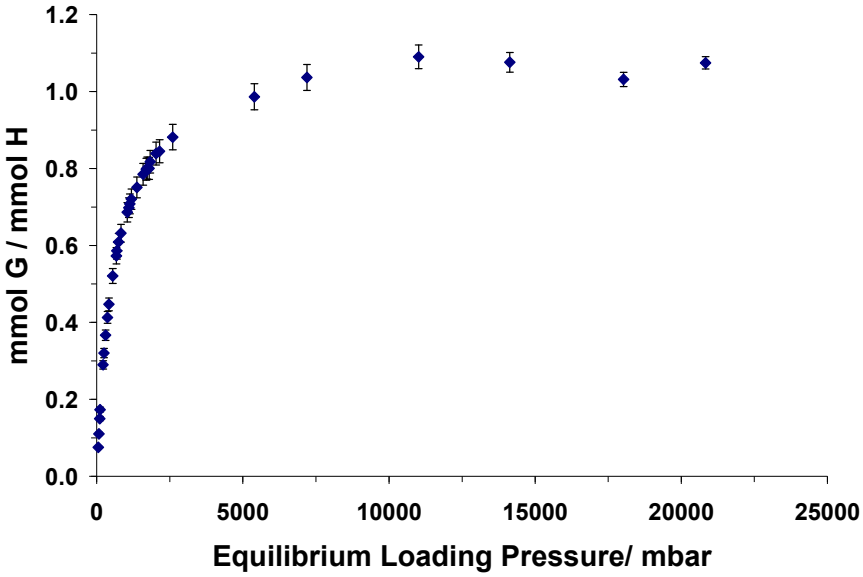

Figure 4.15. Volumetric sorption results for $[Cu_2(BITMB)_2Cl_4]$ (**3a**) where the guest-host ratio is plotted as a function of equilibrium loading pressure (mbar at 25 °C). Full occupancy is achieved at ~5 bar.

Figure 4.15 shows the results of more recent experiments which were conducted as part of this study. At equilibrium loading pressures ranging between 0 and 217 mbar, it can be seen that the $\Delta H°_{ad}$ and the $T\Delta S°_{ad}$ terms become more negative to reach a minimum at ~217 mbar before increasing again with increased equilibrium loading pressure. The zero equilibrium loading pressure value for $\Delta H°_{ad}$ was determined, by extrapolation, to be *ca* -23 $kJ.mol^{-1}$, which corresponds to values typical of carbon dioxide sorption by activated carbons and also agrees well with the value determined during previous studies [12]. The trend of decreasing $\Delta H°_{ad}$ with loading pressure reaches a minimum value of -24 $kJ.mol^{-1}$ at 217 mbar, which corresponds to a guest-host ratio of 0.3:1 or a guest site-occupancy of 30%. This is counter-intuitive, as one might expect $\Delta H°_{ad}$ to decrease with increasing loading pressure due to the increase in sorbate-sorbate repulsive interactions arising from fewer active sites of sorption being available to guest molecules within the host framework. It is suggested that sorbent-sorbate interactions act cooperatively to account for the increasing affinity between host and guest with loading pressure until a maximum affinity is reached at 217 mbar. The thermodynamic experiments yielded results that previous studies [12] had failed to produce

with regard to trends in thermodynamic parameters as a function of equilibrium loading pressure. This is because previous studies were not performed at equilibrium loading pressures lower than ~500 mbar.

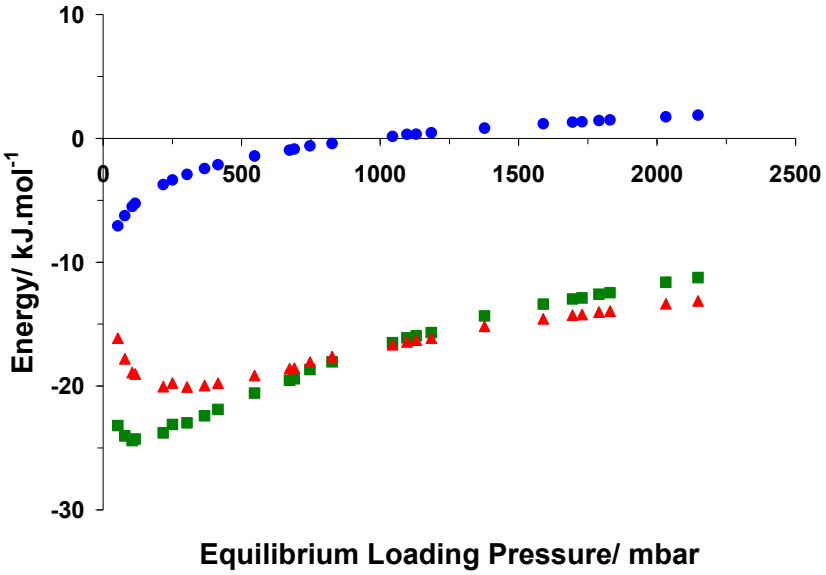

Figure 4.16. Thermodynamic parameters of sorption results for the metallacycle BITMB (**3**). Thermodynamic parameters ΔG°_{ad} (●), $T\Delta S^{\circ}_{ad}$ (▲) and ΔH°_{ad}.(■).

4.4.4. Cd_2(4,4-bis(2-methylimidazol-1-ylmethyl)biphenyl)$_2Cl_4$ [Cd_2(B2MB)$_2Cl_4$]

Sorption experiments employing carbon dioxide were performed using the locally-constructed volumetric device described in **Section 4.1**, as well as a commercially available gravimetric sorption analyser. The results of both studies are shown in **Figure 4.17,** where it can be seen that the results from the two techniques are in reasonable agreement. As discussed in **Section 3.7**, a guest-host ratio of 2:1 is inferred from previous crystallographic studies performed by Jacobs [53]. This ratio is not reached throughout the chosen experimental pressure ranges. The guest-host ratio, however, is still increasing at an equilibrium loading pressure of 20 bar. After an initial rapid guest uptake, the guest-guest repulsive interactions within the active sorption sites give rise to energetically unfavourable conditions, thus hindering further guest uptake to reach a maximum guest-host ratio.

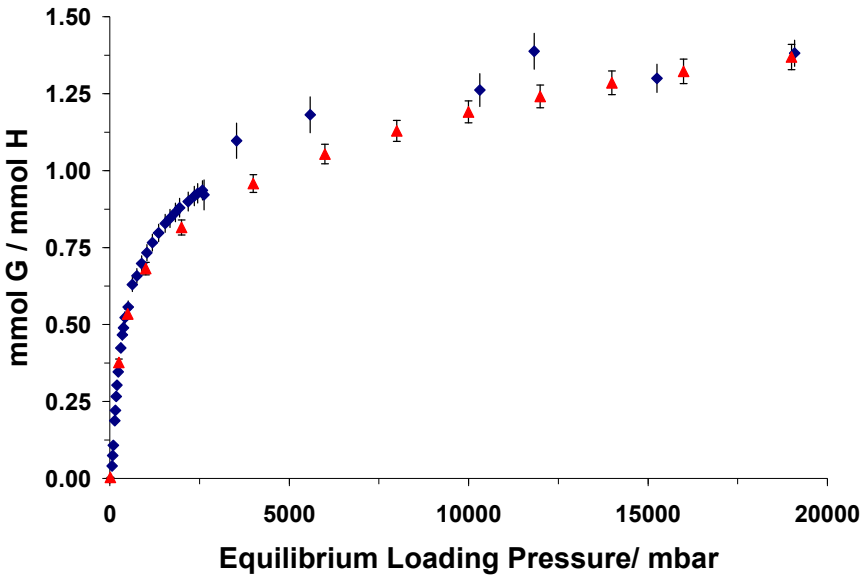

Figure 4.17. Volumetric and gravimetric sorption results of $[Cd_2(B2MB)_2Cl_4]$ (**4a**). The guest-host ratio is plotted against the equilibrium loading pressure (mbar at 25 °C).

The results of the thermodynamic studies performed on the metallacycle **4a** are shown in **Figure 4.18**. The $\Delta H°_{ad}$ and $T\Delta S°_{ad}$ values show the same trend seen in metallacycle **3a**, where the values decrease with increasing loading pressure to reach a minimum before continuing the expected trend to increase as a function of equilibrium loading pressure. This trend is thought to be the result of cooperative sorbate-sorbent interactions. A zero equilibrium loading pressure value of $\Delta H°_{ad}$ was determined by extrapolation to be *ca* -25 kJ.mol^{-1}. At 235 mbar maximum $\Delta H°_{ad}$ and $T\Delta S°_{ad}$ values were measured to be -47 and -40 kJ.mol^{-1}, respectively. The maximum $\Delta H°_{ad}$ value falls within the -30 to -60 kJ.mol^{-1} range of typical zeolites [12, 57]. One of the primary interactions contributing to the zero equilibrium loading pressure value of $\Delta H°_{ad}$ is thought to be the interaction between the carbon dioxide guest and the chloride anions of the host framework, as observed in the crystallographic studies conducted by Jacobs [53].

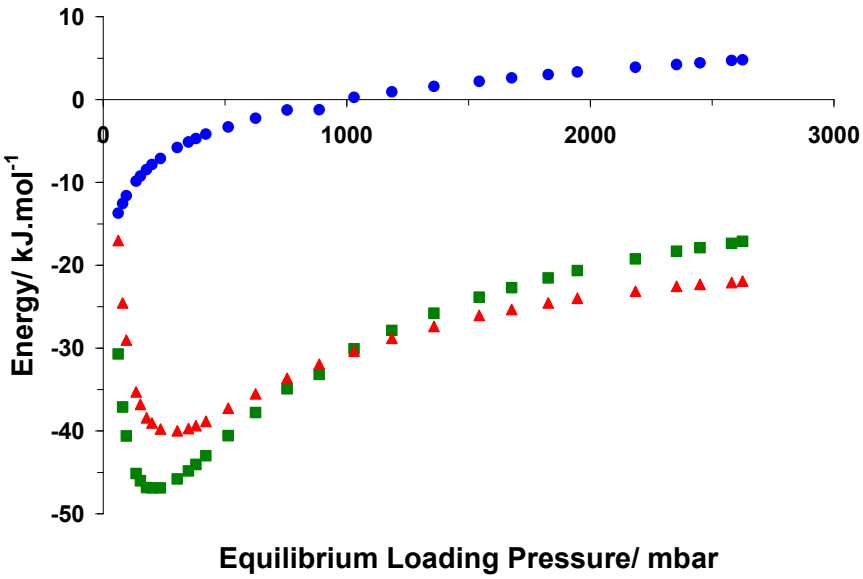

Figure 4.18. Thermodynamic parameters of sorption results for the metallacycle $Cd_2(B2MB)_2Cl_4$ (**4a**). Thermodynamic parameters $\Delta G°_{ad}$ (●), $T\Delta S°_{ad}$ (▲) and $\Delta H°_{ad}$ (■).

After 235 mbar the $\Delta H°_{ad}$ values increase, becoming more positive, as a function of increasing equilibrium loading pressure. The trend between 235 and 2625 mbar, as shown in **Figure 4.18**, is typical of a host comprised of a heterogeneous surface, where sorbate-sorbate repulsive interactions increase as a function of increased equilibrium loading pressure [57].

The $\Delta G°_{ad}$ values are found to be indicative of a spontaneous sorption reaction for all equilibrium loading pressures under the standard pressure of 1 bar and indicate the spontaneous desorption reaction for all loading pressures above 1 bar. This is to be expected for systems involving physisorption, where the uptake of guest does not involve breaking or forming covalent bonds, but rather is thought of in terms of diffusion along a concentration gradient. The results show that, below standard pressure, the standard enthalpy of adsorption $\Delta H°_{ad}$ is the greatest contributing factor to the standard Gibbs free energy $\Delta G°_{ad}$. Where the equilibrium loading pressure exceeds 1 bar the entropic term embodied in the $T\Delta S°_{ad}$ term becomes the greatest contributor to $\Delta G°_{ad}$. When comparing **Figures 4.17** and **4.18** it can be seen that, as the guest-host ratio approaches 2:1, $\Delta G°_{ad}$, $\Delta H°_{ad}$ and $T\Delta S°_{ad}$ approach maximum values. This is expected since as at full guest occupancy, a maximum number of sorbate-sorbate and sorbate-sorbent interactions will result in a maximum value for $\Delta H°_{ad}$ and a corresponding maximum entropy term which will result in $\Delta G°_{ad}$ for the sorption reaction

being most unfavourable. Consequently, the desorption reaction at higher loading pressures will become ever more energetically favourable.

Of the six host compounds investigated as part of this study, metallacycle **4a** yielded the lowest values for the thermodynamic parameters $\Delta H°_{ad}$ and $T\Delta S°_{ad}$.

4.4.5. Molecular Sieve 4A

Sorption results for the commercially available molecular sieve 4A show that the guest-host ratio increases to a value of 0.75:1 at 23 bar equilibrium loading pressure. The irregularities in the curve seen in **Figure 4.19** result from true equilibrium not being fully established at the time when the measurement was taken. Although several hours elapsed before taking the pressure readings, the large pore diameter of the discrete channels of this *conventionally* porous material prevents true equilibrium from being readily established at low pressures, since the gas is able to freely traverse the volume of the pore. The chemical nature of the zeolite causes atmospheric water to easily be sorbed into the aluminosilicate framework, thus affecting the host's sorption capacity. Our guest-host ratio correlates well to that determined by Siriwardane [165] who studied carbon dioxide sorption at room temperature at a equilibrium loading pressure of ~20 bar correlates well. This indicates that the method described in this work yields accurate results that can readily be compared to literature data.

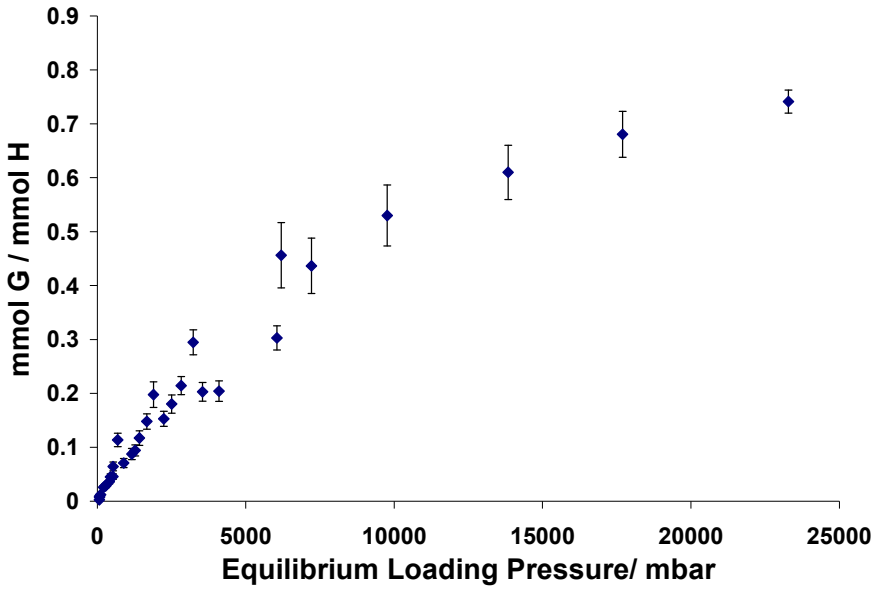

Figure 4.19. Volumetric sorption results for (**5**). The guest-host ratio is plotted against increasing equilibrium loading pressures (mbar at 25 °C).

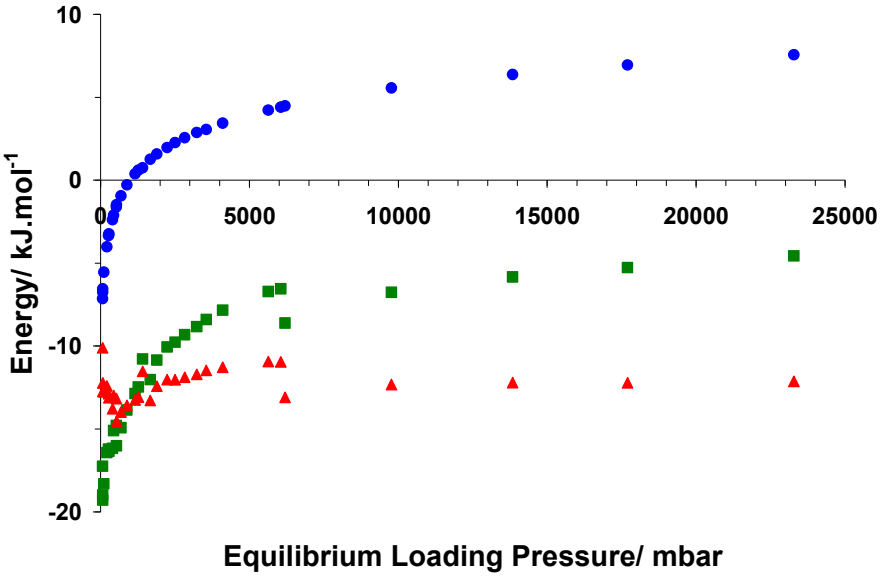

Figure 4.20. Thermodynamic parameters calculated at different equilibrium loading pressures for (**5**). Thermodynamic parameters $\Delta G°_{ad}$ (●), $T\Delta S°_{ad}$ (▲) and $\Delta H°_{ad}$.(■).

The results of the thermodynamic experiments, shown in **Figure 4.20**, yield a $\Delta H°_{ad}$ value at zero equilibrium loading pressure of *ca* -20 kJ.mol^{-1}, as determined by extrapolation. This value is not what is expected of a typical zeolite which generally has $\Delta H°_{ad}$ values at zero loading pressure between -30 and -60 kJ.mol^{-1}. The value reported here is significantly less than that reported by Anderson [166], who reported a value of approximately -33 kJ.mol^{-1}. This discrepancy is thought to arise from two main factors, namely error on the pressure readings at low pressure [16] and differences in sample preparation. Anderson used a different supplier and after substantial treatment the experimental sample was dried in air at 350°C for 36 hours, after which is was evacuated at 450°C for 12 hours. Our sample preparation consisted of crushing the molecular sieve 4A pellets, oven drying them at 120°C for 24 hours followed by overnight evacuation. Since molecular sieve 4A is a known desiccant [167] and is hygroscopic, sample preparation is crucial to ensure a guest-free host.

4.4.6. Tris(*o*-phenylenedioxy)cyclotriphosphazene (TPP)

This *conventionally* porous organic host has a very large pore diameter of ~4.6Å [157]. Consequently, the experimental results show a guest-host ratio approaching 0.25:1 at 12 bar equilibrium loading pressure, as seen in **Figure 4.21**. The sorption results do not correlate with studies performed previously by Sozzani [157]. Although Sozzani reports a guest-host ratio of ~0.4 [157], which compares reasonably to our results of 0.25, they reach this ratio at a

pressure of ~700 mbar. Their crystal structure [157], however, reports no electron density within the channel. This is quite unusual as they do not mention performing the single-crystal X-ray diffraction experiments at reduced pressures. Since a maximum guest-host ratio was reported below standard atmospheric pressures by Sozzani, it is curious that their crystal structure is reported as devoid of electrons inside the channel. This matter requires further investigation in future.

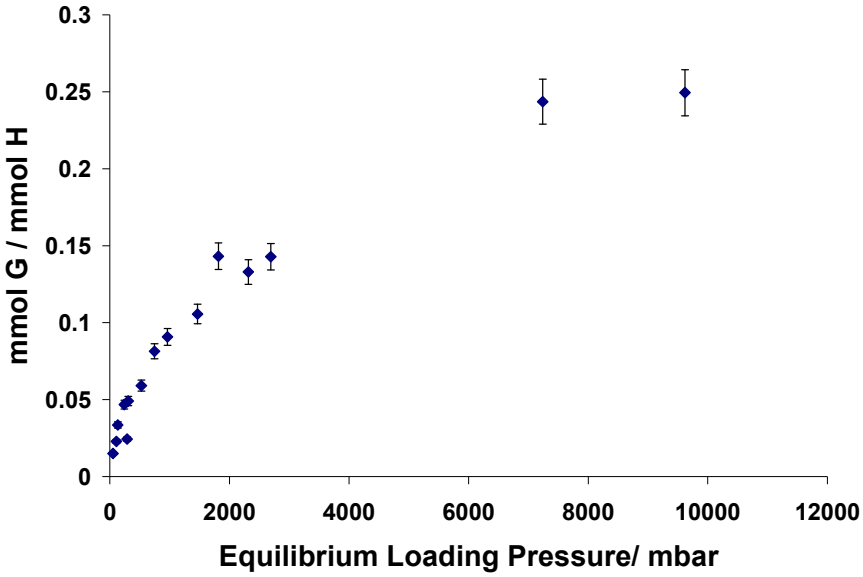

Figure 4.21. Volumetric sorption results for (**6**). The guest-host ratio is plotted as a function of equilibrium loading pressure (mbar at 25 °C).

The results of the thermodynamic studies indicate, that **6** has the lowest magnitudes for $\Delta H°_{ad}$ and $T\Delta S°_{ad}$ of all the host compounds investigated as part of this study. By extrapolation of the graph shown in **Figure 4.22**, a zero equilibrium loading pressure value for $\Delta H°_{ad}$ was determined to be *ca* -17 kJ.mol^{-1}, which falls within the range of other known porous organic hosts such as activated carbon [12]. This, *conventionally* porous organic host, therefore displays a similar affinity for carbon dioxide as other known organic hosts. The calculated values for $\Delta S°_{ad}$ fall within a range of -20 to -100 J.K^{-1}.mol^{-1} shown for activated carbons [162].

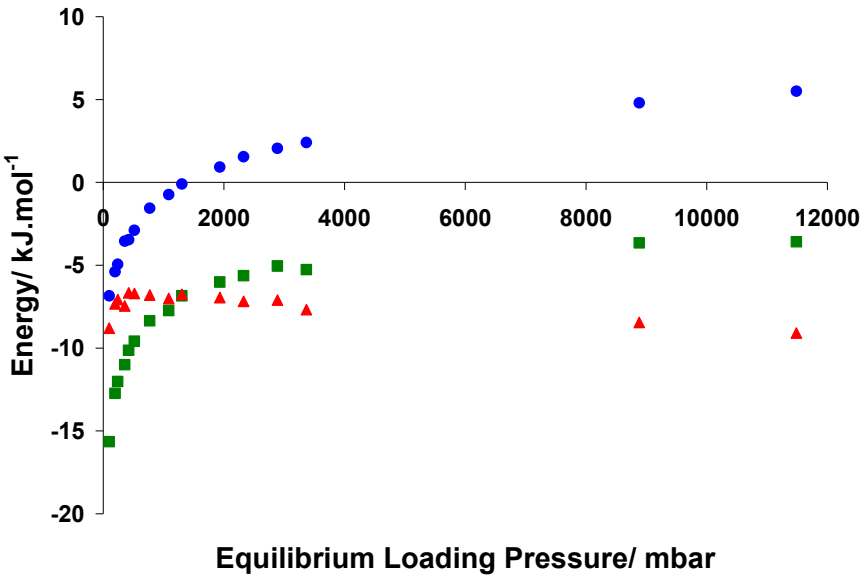

Figure 4.22. Thermodynamic parameters of (6) showing the greatest contribution to ΔG°_{AD} being entropic. Thermodynamic parameters ΔG°_{ad} (●), $T\Delta S^{\circ}_{ad}$ (▲) and ΔH°_{ad}.(■).

4.5. Conclusion

A volumetric isosteric aparatus for the determination of the thermodynamic parameters ΔG°_{ad}, ΔH°_{ad} and ΔS°_{ad} was constructed and tested for its versatility. The results elucidated certain physico-chemical characteristics of each individual compound which assisted in the description of the underlying processes inherent to the sorption reactions that were studied. It has been reported [29] that measurements of thermodynamic parameters using different techniques vary between 10 – 20 %. The inherent error of the method used in this study falls well within this margin of discrepancy. It must be noted that not all possible contributions to error were taken into account. The advantages and disadvantages were discussed, highlighting that this device can be used for the study of both *conventionally* and *transiently* porous compounds. When used in conjunction with other modern analytical techniques and computational modelling the volumetric SIT method can be used to investigate the underlying processes governing solid-gas sorption reactions.

All compounds displayed ΔG°_{ad} values for spontaneous sorption at equilibrium loading pressures under standard pressure. The ΔG°_{ad} values for these spontaneous sorption reactions are similar to those associated with physisorption where no covalent bond breaking or forming occurs during the reaction [168]. Physisorption can be viewed as primarily a surface phenomenon where guest molecules move along a concentration gradient to the host surface

area where guest concentration is initially low. The results thus point to diffusion being the dominant process governing the uptake of guest molecules within the host frameworks that were studied. ΔG°_{ad} values for equilibrium loading pressures exceeding standard pressure were found to be spontaneous for the desorption reaction. This supports the hypothesis that diffusion is the dominant process governing the solid-gas reactions that were studied. At equilibrium pressures higher than standard pressure the gas within the host framework spontaneously follows a concentration gradient and diffuses out of the host. In pressure ranges of spontaneous sorption (<1 bar) the $\Delta H°_{ad}$ contribution to $\Delta G°_{ad}$ (following **Equation 4.12**, $\Delta G°_{ad} = \Delta H°_{ad} - T\Delta S°_{ad}$) dominates over $T\Delta S°_{ad}$ in causing a negative value for $\Delta G°_{ad}$. As explained in Chapter 2, physisorption is necessarily exothermic and it is thus not surprising that the enthalpic term is the chief contributing factor to the energetics of the spontaneous sorption reaction. For pressures exceeding 1 bar it is observed that the entropic term, $T\Delta S°_{ad}$, becomes the dominating contributor to the positive $\Delta G°_{ad}$ values. This phenomenon is sensible when viewing the desorption process as diffusion along a concentration gradient, which is what is expected for physi-desorption, as gas molecules gain entropy by moving out of the host framework.

The results for the two metallacycles, **3a** and **4a**, display a turning point minimum in $\Delta H°_{ad}$ and $\Delta S°_{ad}$ values. It is thought that cooperative mechanisms between the host and guest produce conditions that are most energetically favourable for the sorption reaction to take place.

It has been shown that the technique is versatile and can be used on *conventionally* and *transiently* porous compounds without having to calculate the degree of coverage, θ, thus making it a particularly useful method. It must be noted that the technique is better suited for the study of *transiently* porous compounds as, having to infer a guest-host ratio for *conventionally* porous systems from crystallographic studies can be problematic without prior sorption experiments being performed. Physico-chemical properties such as sorption capacities, rates of sorption and the energetics of sorption will become ever more important when striving to design "*smart*" materials in the future.

CHAPTER 5. Methodology Development for Determining Kinetic Parameters of Solid-Gas Sorption Reactions.

Gaining insight into the kinetics of a reaction elucidates a great deal about the possible mechanisms associated with the process. As mentioned in **Section 2.5.2**, three chief techniques are currently in use to determine kinetic parameters for a solid-gas sorption reaction. The aim of the work described in this chapter was to develop a simple and direct method to calculate the activation energy (E_a) for a solid-gas sorption reaction. The kinetics of solid-gas reactions will be of great importance when considering the economic viability of a particular host-guest system, as a host material will have to display optimal sorption capacities, suitable lifetimes and controllable delivery rates [169] to be suited for a particular purpose.

The volumetric SIT device discussed in **Section 4.1**, was modified for the determination of kinetic parameters. The design (**Section 5.1**), theory (**Section 5.2**) and use (**Section 5.3**) of this novel instrument are discussed, highlighting some advantages and disadvantages. Possible future work and method development of the technique is also discussed in **Section 5.4**.

5.1. Instrument Description

The main obstacle in designing a volumetric instrument to determine kinetic parameters for sorption experiments is that one requires a constant pressure throughout the sorption experiment. This can be seen by considering the Arrhenius equation, **Equation 5.1**:

$$k = Ae^{\frac{-E_a}{RT}} \qquad \textbf{(5.1)}$$

where k is the rate constant of the reaction, A is the pre-exponential factor, R is the gas constant, T is absolute temperature and E_a is the activation energy.

By linearization of **Equation 5.2** the pressure dependence becomes evident:

$$\ln k = \frac{1}{T}\left[\frac{-E_a}{R}\right] + \ln A \qquad \textbf{(5.2)}$$

can be expressed as y = mx + c where y = ln$k$, x = 1/T

$$m = \left[\frac{\delta \ln k}{\delta\left(\frac{1}{T}\right)}\right]_{pressure} = \left[\frac{-E_a}{R}\right]_{pressure} \text{ and } c = \ln A$$

Thus, plotting ln$k$ vs 1/T should yield a linear graph with a gradient of $-E_a/R$ so that the value of E_a can readily be determined. The general principle of the volumetric approach to studying sorption processes is that gas uptake is followed by monitoring a drop in pressure as the gas in the sample chamber becomes depleted. Thus, the pressure of the gas is not kept constant during the sorption process. The notion of determining kinetic parameters for solid-gas sorption reactions using a volumetric system thus becomes seemingly implausible: how does one measure gas sorption by keeping the pressure constant in a volumetric device? We have overcome this problem by installing a high precision gas regulator between the gas reservoir chamber (V_A) and the valve V_2 which separates the gas reservoir from the sample chamber (V_B), as shown schematically in **Figure 5.1**. The gas regulator can be set to a desired pressure that is maintained at a constant volume in the sample chamber (V_B) during the sorption process. The device is also thermostated in an insulated cupboard.

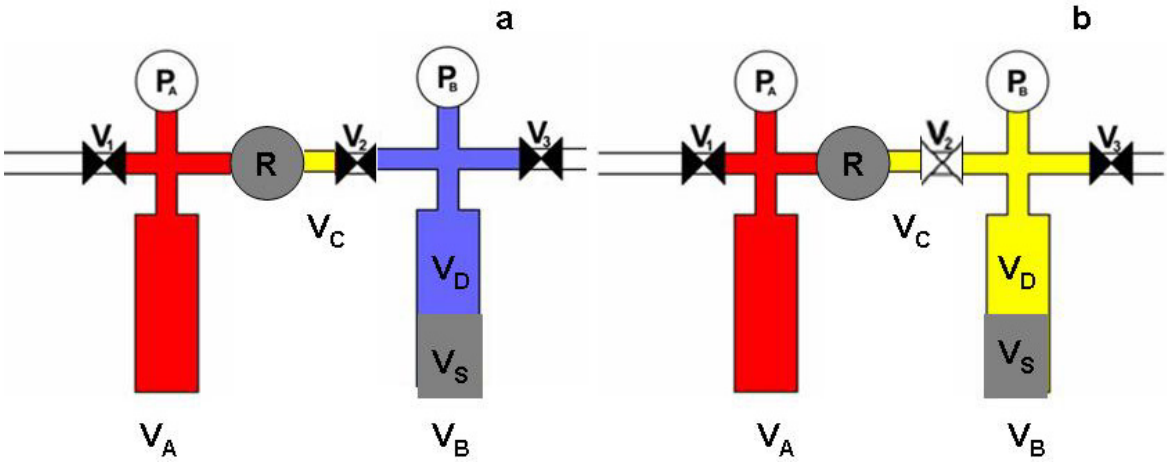

Figure 5.1. A schematic diagram of the constructed apparatus. (**a**) The sample chamber is under vacuum (blue) with V_2 closed and the gas reservoir, V_A, under an arbitrary pressure (red). The regulator, R, regulates the pressure in V_C to a specific pressure (yellow), which is lower than the pressure in the gas reservoir V_A. (**b**) Shows the situation when V_2 is opened. The pressure in V_B and V_C is now regulated to the set pressure of the regulator (yellow).

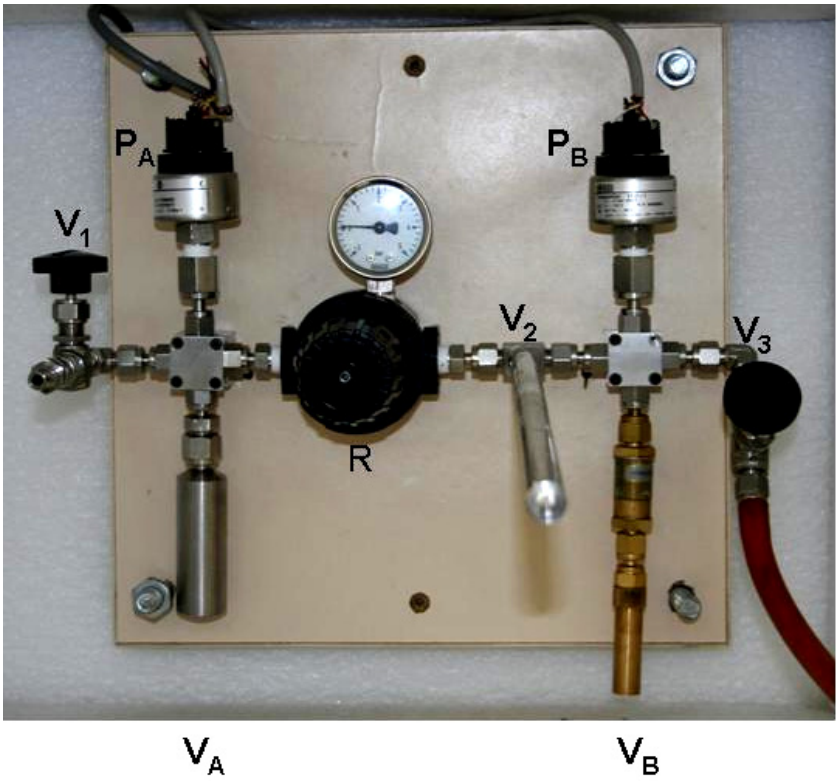

Figure 5.2. A photograph of the constructed apparatus. V_A and V_B are the gas reservoir and sample chamber volumes, respectively. P_A and P_B are pressure transducers. V_1, V_2 and V_3 are valves. The regulated pressure can be read off the analogue pressure gauge attached to the high precision Wilkerson® pressure regulator, labelled R.

Typically, the entire system with the sample in place is evacuated before closing all valves. The regulator is also closed. The reservoir chamber is then filled with gas. The regulator is adjusted slowly to the desired pressure at which the sorption reaction is to take place. The gas is then allowed to stabilize at room temperature. The sample chamber is then set to a desired temperature. Upon opening V_2, the pressure in the sample chamber changes suddenly from vacuum to the desired regulated pressure. A porous sample would then start to sorb gas. The pressure regulator keeps the pressure in the sample chamber constant by feeding it gas from the reservoir. Thus, by monitoring the pressure drop in P_A one can record a sorption experiment at constant pressure in order to determine the kinetic parameters of the reaction.

The choice of gas regulator is important for the successful determination of the kinetic parameters of a sorption reaction. A high precision regulator that could effectively regulate the pressure in the sample chamber to a constant pressure had to be chosen. A Wilkerson®

P16-C2-000 type regulator was used, as it showed the greatest capacity to ensure a constant pressure for several hours as indicated by the curve in **Figure 5.4**.

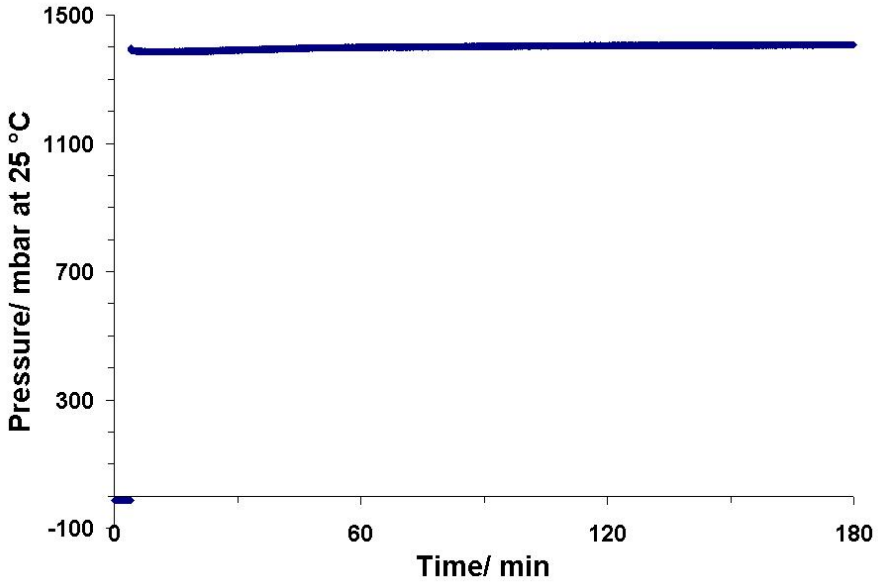

Figure 5.3. The pressure in P_B regulated at 1400 mbar by the Wilkerson P16-C2-000 gas regulator. The sample chamber V_B contains compound **2**. In the first 12 min the sample is under vacuum. As V2 is opened, the pressure in the sample chamber is regulated at 1400 ± 14 mbar for the remainder of the experiment.

The described method is highly dependent on the stability and precision of the gas regulator that maintains the constant pressure in the sample chamber. It is thus of paramount importance to ensure proper operation of the gas regulator during all experimental procedures. It was determined that the regulator maintains a constant pressure in the sample chamber with a mean error of 1.00% over a period of up to 3 hours, as shown in **Figure 5.3**. This was deemed sufficient for our experimental purposes.

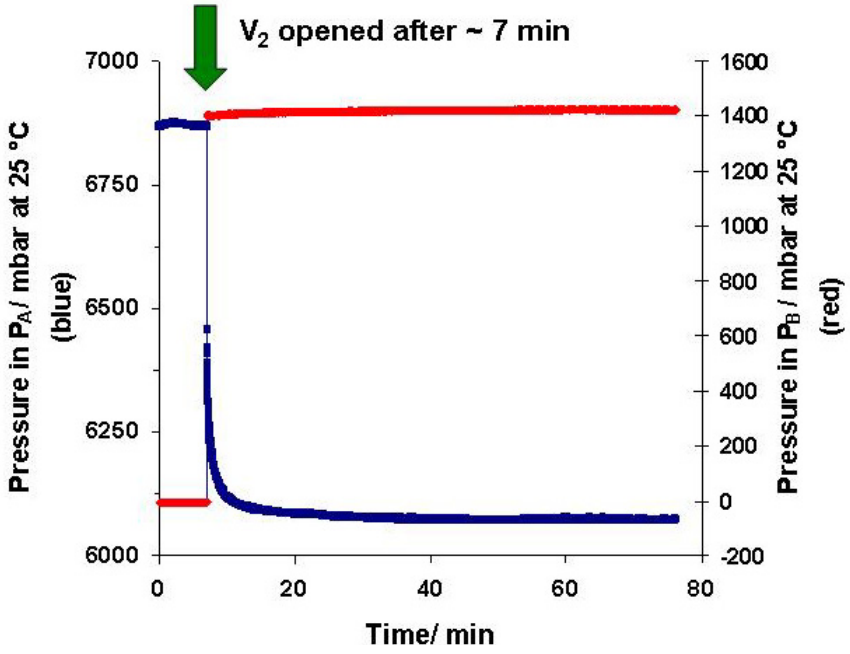

Figure 5.4. A typical experiment where the pressure drop in P_A due to the sample sorbing gas is recorded (blue), while the pressure in P_B is kept at a constant regulated value (red).

The curves in **Figure 5.4** show how the pressures of V_A and V_D are monitored. During the first 7 min the sample chamber (red) is under vacuum and the reservoir chamber is at ~6800 mbar. At ~7 min, indicated by the arrow, V_2 is opened. Now the pressure in V_D is accurately regulated to ~1400 ± 14 mbar until the reaction is complete. As the porous sample sorbs gas, the pressure in V_A drops (shown in blue).

5.2. A Typical Experiment: Theory & Practice

Since it is now possible to indirectly measure the sorption rate at a constant pressure using a volumetric approach, the notion of obtaining kinetic parameters for solid-gas sorption reactions becomes feasible.

Using the Arrhenius equation, **Equation 5.1**, E_a and A of a sorption reaction can therefore be determined by performing a series of sorption experiments at different temperatures. The instrument described in **Section 5.1.** was used to monitor a solid-gas sorption reactions at selected temperatures and pressures until equilibrium had been reached in each case. The isosteric gas sorption curve can be used to plot the extent of the reaction (α) from which k can be determined empirically. **Figure 5.5** shows the raw results of a typical solid-gas isosteric sorption experiment performed with the sample under a specific controlled pressure and temperature.

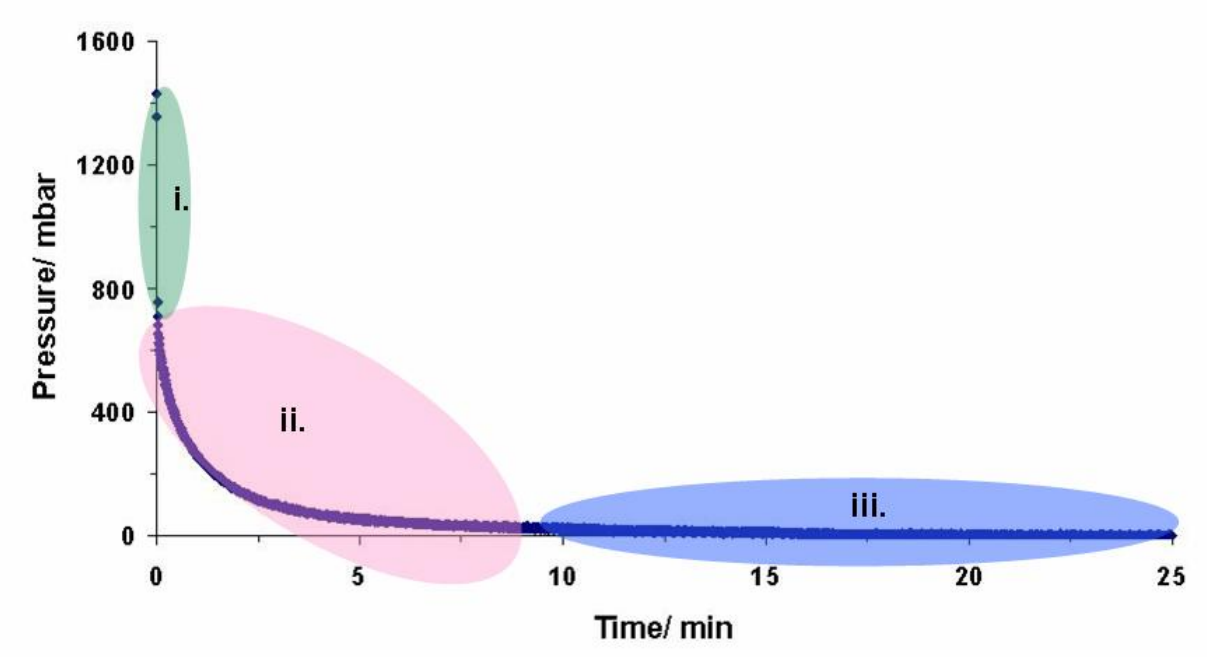

Figure 5.5. A result of a typical volumetric solid-gas sorption experiment before processing to obtain a conventional α-time curve.

The sorption experiment can be divided into three sections:

i. The initial sudden drop in pressure occurs when V_2, **Figure 5.1.b**, is opened to expose the sample to the desired gas pressure (shaded green).

ii. The period during which most of the gas sorption takes place (*e.g.* the area of the graph in **Figure 5.5** between 0 and 10 min) (shaded pink).

iii. The conclusion of the sorption reaction is the period when there is little change in pressure with time, signifying that the system is reaching equilibrium conditions. This can be seen to occur in **Figure 5.5** between time 10 and 25 min (shaded blue).

By processing the data typified in **Figure 5.5**, the extent of the reaction α, can be monitored with time at constant pressure and temperature. The data are replotted and rescaled to between $0 < \alpha < 1$, where $\alpha = 0$ is the start of the reaction and $\alpha = 1$ represents a solid-gas equilibrium state, or the end of the reaction. Typical α-time plots thus generated are shown schematically in **Figure 5.6.**

Blank control experiments were performed prior to the kinetic studies to determine the "*dead volume*", V_D, inside the sample chamber by using a non-porous compound (*e.g.* NaCl) of equal volume to the sample under study. Since the sorption that takes place in V_B is indirectly

monitored by P_A, it is imperative to compensate for the initial pressure drop due to filling of the "*dead volume*" V_D in the sample chamber.

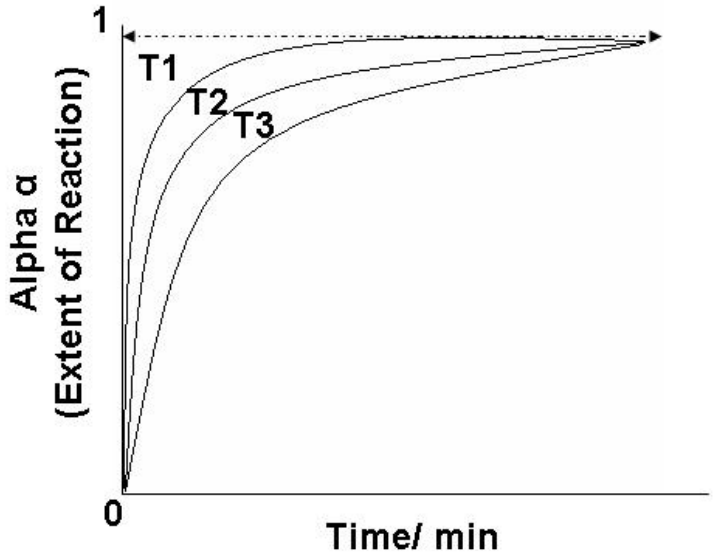

Figure 5.6. An α-time plot of three reactions performed at different temperatures, T1, T2 and T3, where T1>T2>T3. The temperature dependence on the rate of the reaction is evident.

The curves in **Figure 5.6** shows α-time plots of sorption reactions recorded at a series of temperatures but at the same pressure. It can clearly be seen that the rate of reaction, *k*, is temperature-dependent and that that the rate increases as a function of temperature, implying typical Arrhenius-type behaviour. Consider **Equation 5.3**,

$$f(\alpha) = kt \qquad \textbf{(5.3)}$$

where *k* is the rate constant for the reaction and *t* is time.

A number of models have been proposed [170] to account for the shapes of α-time curves, depending on the mechanisms of gas uptake. These models can all be expressed as equations taking the general linear form of **Equation 5.3** (see **Table 5.1**). A general approach to selecting the best model involves plotting the α-time data using each of these models in turn. Usually, the model that yields the best linear fit to the data is presented to indicate the most likely mechanism of the sorption process.

Table 5.1. Different kinetic models [170].

		Kinetic model	$f(\alpha) = kt$
Sigmoid α-time curves		B1 Prout-Tomkins	$\ln[\alpha/(1-\alpha)]$
		A2 Avrami-Erofeev	$[-\ln(1-\alpha)]^{1/2}$
		A3 Avrami-Erofeev	$[-\ln(1-\alpha)]^{1/3}$
		A4 Avrami-Erofeev	$[-\ln(1-\alpha)]^{1/4}$
Acceleratory α-time curves		P1 power law	$\alpha\ 1/n$
		E1 exponential law	$\ln \alpha$
Deceleratory α-time curves	Based on Geometric Models	R2 contracting area	$1-(1-\alpha)^{1/2}$
		R3 contracting volume	$1-(1-\alpha)^{1/3}$
	Based on Diffusion Models	D1 one-dimensional	α^2
		D2 two-dimensional	$(1-\alpha)\ln(1-\alpha) + \alpha$
		D3 three-dimensional	$[1-(1-\alpha)^{1/3}]^2$
		D4 Ginstling-Brounshtein	$(1-2\alpha/3)-(1-\alpha)^{2/3}$
	Based on "order of the reaction"	F1first order	$-\ln(1-\alpha)$
		F2 second order	$1/(1-\alpha)$
		F3 third order	$[1/(1-\alpha)]^2$

The α-time data for all the compounds studied as part of this work were best represented by the "D3" three dimensional diffusion model as discussed in **Section 5.3**.

Diffusion of atoms in crystal lattices can occur *via* many possible mechanisms, including the *exchange*, *ring* and *interstitial* mechanisms, to mention but a few [171]. It is thought that every atom or molecule that diffuses through the host lattice, does so by making a series of "*jumps*" between energetically favoured lattice sites [171]. Each proposed mechanism of diffusion involves a different explanation of how the "*jumps*" between lattice sites take place [171]. In the case of host-guest systems, the so called "*interstitial diffusion mechanism*" is thought to take place [171, 172]. The theory behind the *interstitial mechanism* regards the host lattice framework as being rigid, ignoring the inherent thermal motion of the host lattice as well as additional possible mechanisms such as the exchange and ring mechanisms [171]. The theory states that diffusion takes place by moving the atom or molecule from one interstitial site of minimum energy through a maximum energy point to an adjacent interstitial site of minimum energy as shown in **Figure 5.7.a**.

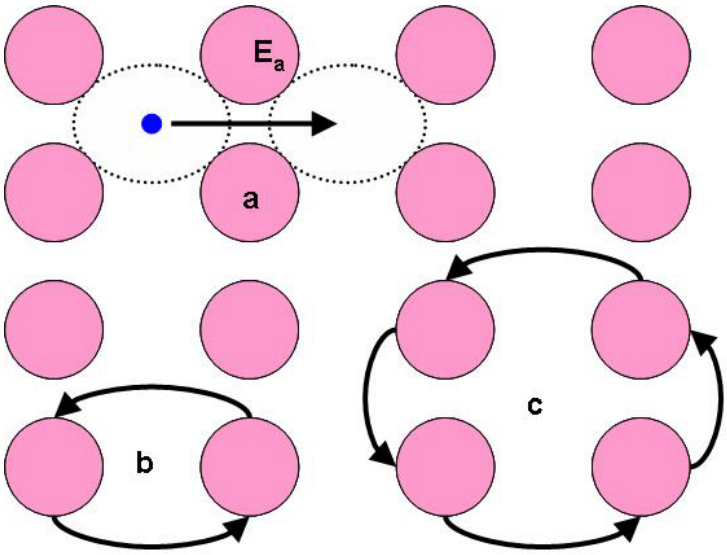

Figure 5.7 The interstitial mechanism showing the diffusion of the guest (●) from one interstitial space to an adjacent interstitial space in the host lattice (●) is shown in (**a**). The exchange mechanism is shown in (**b**) where two atoms in the host lattice exchange positions. The ring mechanism is shown in (**c**) where a ring of atoms moves in a concerted manner [171].

The guest atom or molecule must therefore have enough energy to move between adjacent interstitial sites and to distort the host lattice if this is necessary for such movement [172]. The *interstitial* mechanism of diffusion requires considerably less energy than the *exchange* or *ring* mechanisms [171].

For diffusion to occur, a *driving force* or diffusion potential must be present, and this must be of significant magnitude to make the process energetically feasible [172]. Generally, the flow of molecules occurs from regions of high chemical potential to regions of low chemical potential is termed *flux* [160, 172]. When diffusion occurs across a concentration gradient, and in a single phase, at constant temperature, the diffusion potential or *driving force* is equal to the negative gradient of the chemical potential [160, 172] as shown in **Equation 5.4**.

$$F = -\frac{d\mu}{dx} \qquad \textbf{(5.4)}$$

where F is the driving force and x is the distance that the molecules travel.

For a van der Waals gas, we know from **Equation 4.14** that the chemical potential can be described as follows:

$$\mu_i = \mu_i^0 + RT \ln\left(\frac{f}{P^0}\right) \qquad \textbf{(5.5)}$$

Thus, the *driving force* for diffusion is directly related to the pressure of the guest diffusing into the host lattice during the course of a sorption reaction.

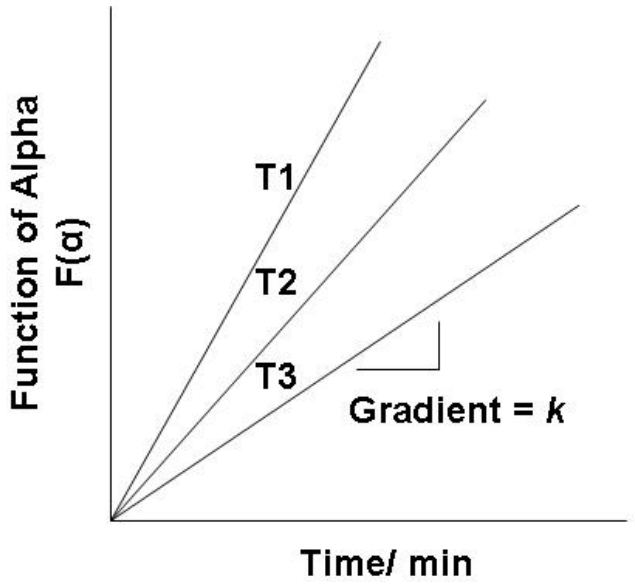

Figure 5.8. A schematic plot showing three reactions performed at three different temperatures (T1 > T2 > T3), yield different gradients in a plot of F(α) as a function of time. The different gradients thus show the temperature dependence of the rate constant *k*.

The Arrhenius-type behaviour showing an increase in the value of *k* as a function of temperature is shown schematically in **Figure 5.8**. Following **Equation 5.2**, one can now determine E_a and A for the reaction by plotting ln$k$ as a function of $1/T$ (K) as shown in **Figure 5.9**. In cases where *k* is inversely proportional to temperature, the behaviour is viewed as being anti-Arrhenius.

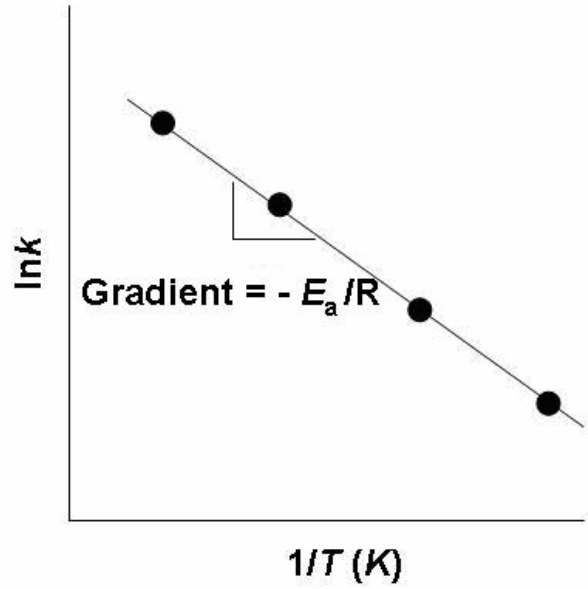

Figure 5.9. An Arrhenius-plot, where the gradient can be used to determine the activation energy.

From the experimental data is it possible to ascertain whether the physico-chemical properties of the solid-gas interaction give rise to Arrhenius or anti-Arrhenius behaviour. A kinetic model can be fitted to the sorption data to elucidate further information regarding the underlying mechanisms of the reaction and the E_a of the reaction. The primary advantages of our novel experimental approach are that the apparatus is inexpensive to manufacture and it is relatively simple to operate when compared with commercially available methods. The primary disadvantage is that the correct phase of the solid host compound must be ensured; this will be highlighted when discussing results obtained using this method in **Section 5.3**. That the thermocouple monitoring the temperature is not in direct contact with the sample is also a disadvantage, as the exact temperature of the sample is uncertain.

5.3. Results and Discussion

It has been reported in the literature that porous systems often show an increased guest uptake with a decrease in temperature [3, 173]. The results of the present study confirm this phenomenon and show that the rate of reaction, *k*, is inversely proportional to the temperature. This is contrary to what is generally observed for reactions in solution where an increase in temperature increases the energy available to the system, and thus necessarily increases the probability of reactant molecules interacting with one another to form the reaction product. When considering solid-gas sorption reactions, one needs to consider the effect of temperature on the host framework. Where the porous host system consists mainly of organic moieties, increased temperatures will cause increased thermal motion of the host atoms. In cases of transiently porous systems and conventionally porous materials with a small pore sizes, this increased thermal motion will sterically obstruct guest transport, thus hindering not only the amount of guest uptake, but also the rate of guest uptake. Consequently, the inverse relationship between *k* and temperature is to be expected.

An important part of this study was to investigate whether our instrument yields reproducible results. It was found that sample preparation is of significant importance to ensure reproducibility. Thus, for all experiments the sample was evacuated for exactly 10 hours, using the same vacuum pump throughout. When the sample was exposed to a specific temperature, this was done for an exact length of time to ensure the same conditions prevailed for all repeat experiments. The gas regulator was also set to one desired pressure for all the experiments performed on a particular sample.

5.3.1. $[Cu_2(BITMB)_2Cl_4]$

Compound **3a** was used extensively to show reproducibility in the data obtained using the constructed device. For experiments performed on **3a**, the regulator was set to 1000 mbar and the sample exposure time to specific temperatures was 12 min. Any given experiment at a certain temperature and pressure was repeated to ensure the precision of the recorded data. **Figure 5.9** shows four experiments all performed at -72°C and it can clearly be seen that the curves appear to be almost identical in all four cases, clearly showing the reproducibility of the data.

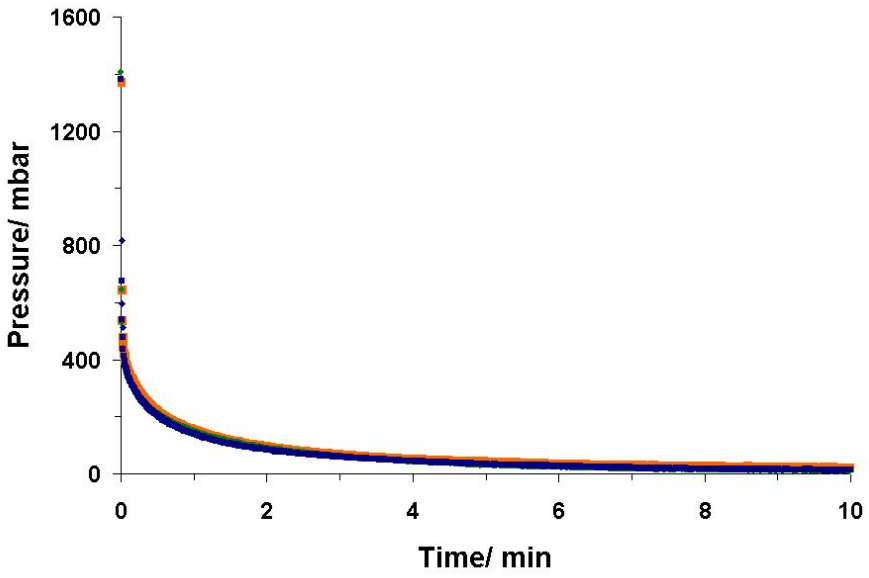

Figure 5.9. Sorption of carbon dioxide by compound **3a** where the sample is at -72 C. The experiment was repeated 4 times where ■ is experiment (i), ● is (ii), ▲ is (iii) and ■ is (iv). It is evident that the experimental technique is reproducible.

However, repeat experiments performed at the same temperature did yield slightly different values for *k* after the pressure *vs* time graphs were converted to α-time plots as shown in **Figure 5.10**. These different values for *k* were used to calculate a standard deviation for the final values of E_a.

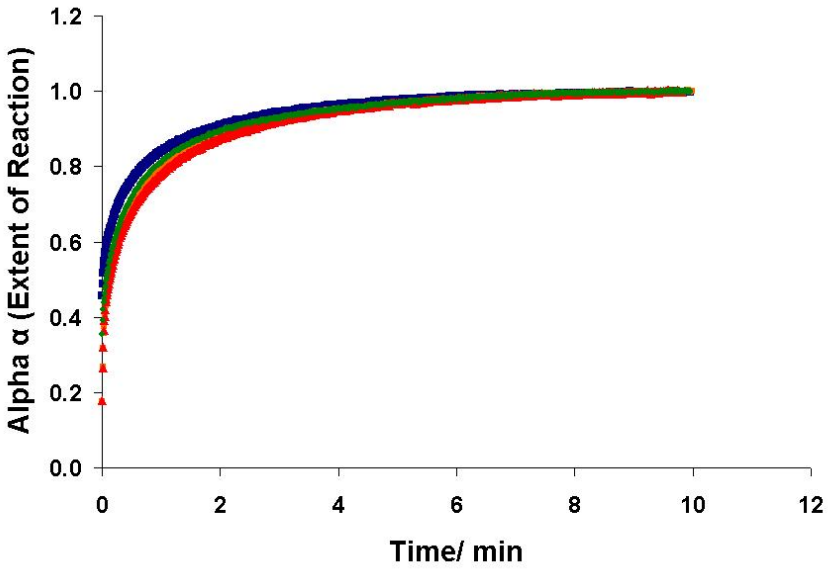

Figure 5.10. Alpha-time curves showing four sorption experiments involving **3a** and carbon dioxide at a regulated gas pressure of 1000 mbar.

Once it was clear that the method is reproducible within acceptable margins, multiple experiments at five different temperatures were conducted in order to investigate the effect of temperature on k, and to determine E_a for the sorption reaction. **Figure 5.11** shows α-time curves of the reaction at different temperatures. It is observed that the reaction takes longer as the temperature increases (*i.e.* anti-Arrhenius behaviour). It is thus expected that the values for k will decrease with increasing temperature. This is indeed so, except in the case of the two lowest temperatures, -72°C and -43°C, which overlay one another and yield similar k values.

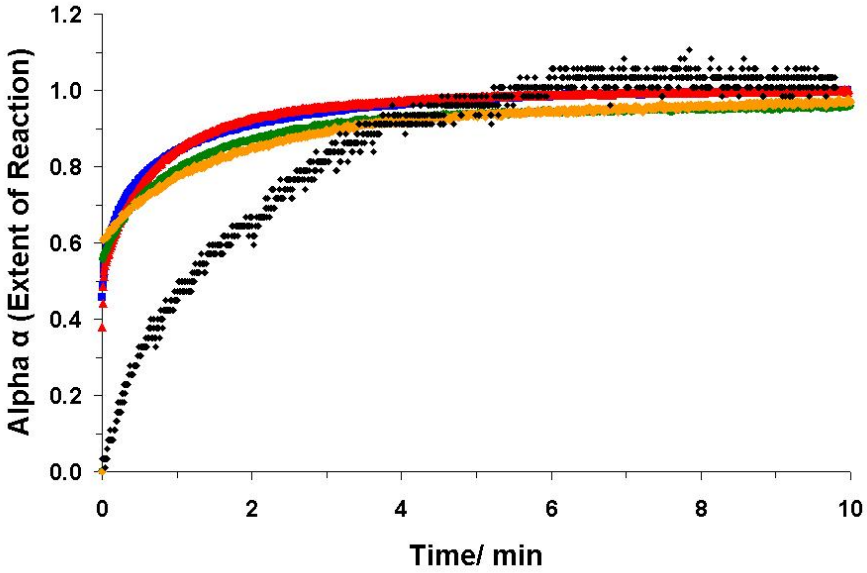

Figure 5.11. Alpha-time curves for the sorption reaction of **3a** with carbon dioxide for a series of increasing temperatures. The rate of reaction decreases with increasing temperature. ■ is at -43 °C; ▲ is at -15 °C; ● is at 0 °C; ■ is at 24 °C and ♦ is at 50 °C.

Figure 5.12.a shows the α-time plot for the sorption reaction of **3a** with carbon dioxide for a specific temperature. The data were fitted to different kinetic models, $f(\alpha)$, some of which are shown in **Figure 5.12.b – 5.12.d**) in order to determine the value of k for the reaction. The three dimensional diffusion kinetic model "D3" (see **Table 5.1**) best describes the data from the experiment as a linear function. This suggests that the mechanism of guest uptake is governed by diffusion. Indeed, it was observed that the data for *all* the experiments at *all* the studied temperatures could best be described by the "D3" kinetic model. Since sorption occurs at all experimental temperatures studied, it can be concluded that the chemical potential of the gas provides enough energy for diffusion to occur at all these temperatures.

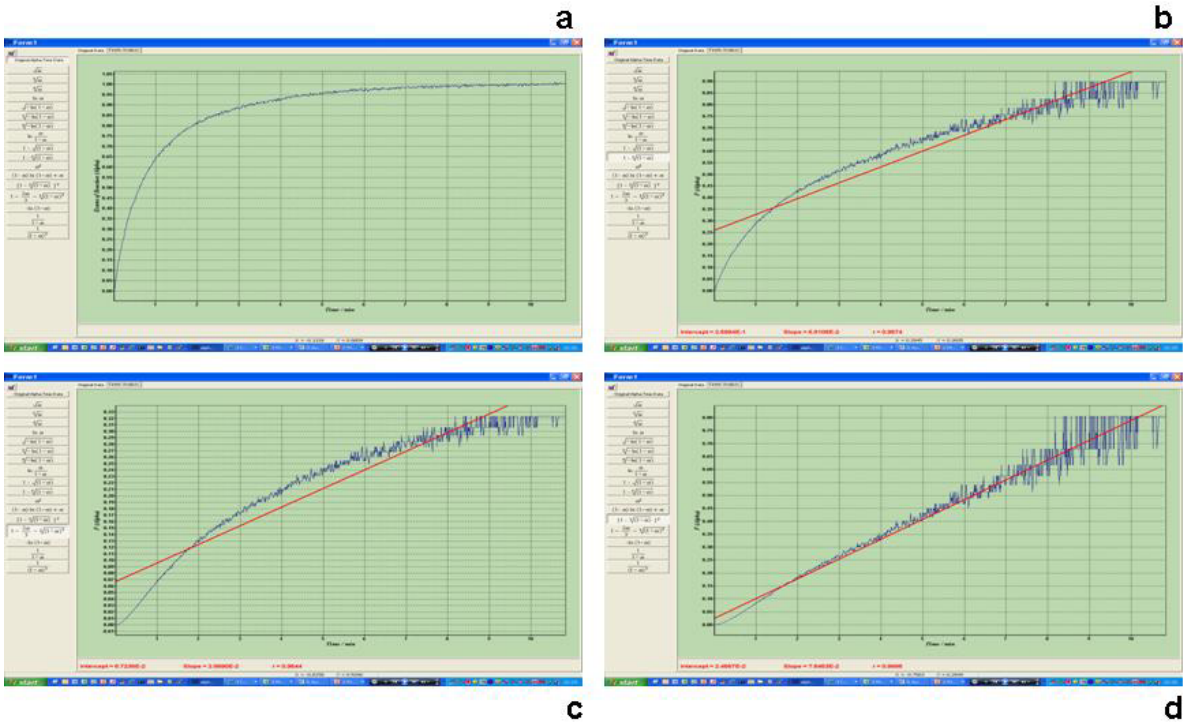

Figure 5.12. **(a)** shows the α-time plot for the sorption reaction of **3a** with carbon dioxide at -43 °C. **(b)** – **(d)** show different kinetic models used to describe the data from **(a)**. The model in **(d)**, the three dimensional diffusion model "D3", best describes the data as a linear function.

From the $f(\alpha)$ *vs* time curves, the reaction rates, k, for the experiments performed at different temperatures could be determined. The values for k of a similar magnitude, and the resulting graph of $\ln k$ *vs* $1/T$ yields an almost horizontal trend, as shown in **Figure 5.13**. This result implies that the activation energy, E_a, is approximately 0 kJ.mol^{-1} for **3a** sorbing carbon dioxide.

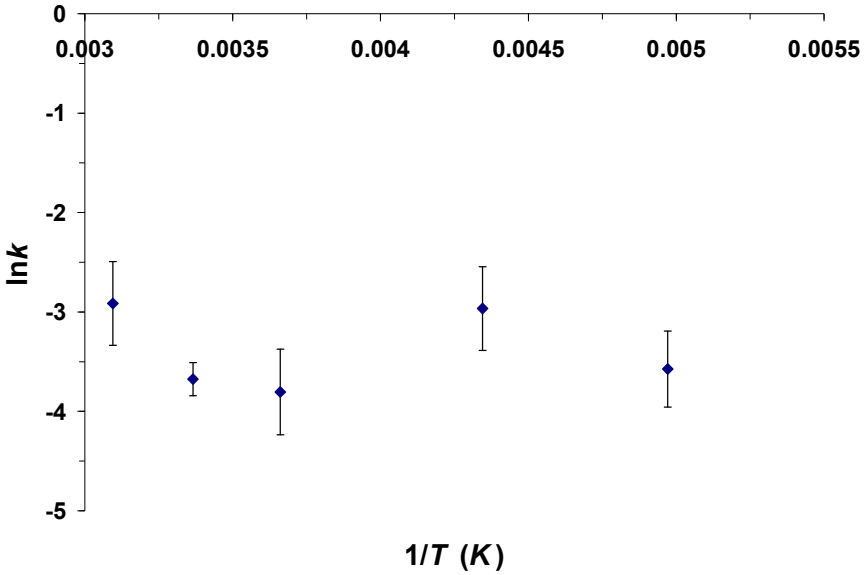

Figure 5.13. An Arrhenius-plot indicating the non-activated nature of the reaction when **3a** sorps carbon dioxide gas.

The graph in **Figure 5.14** shows that the amount of guest sorbed by the host framework decreases with increasing temperature, as is commonly observed for porous systems [3, 173]. This result supports the conjecture that the increased thermal motion of the organic moieties comprising the host framework decreases the amount of guest uptake.

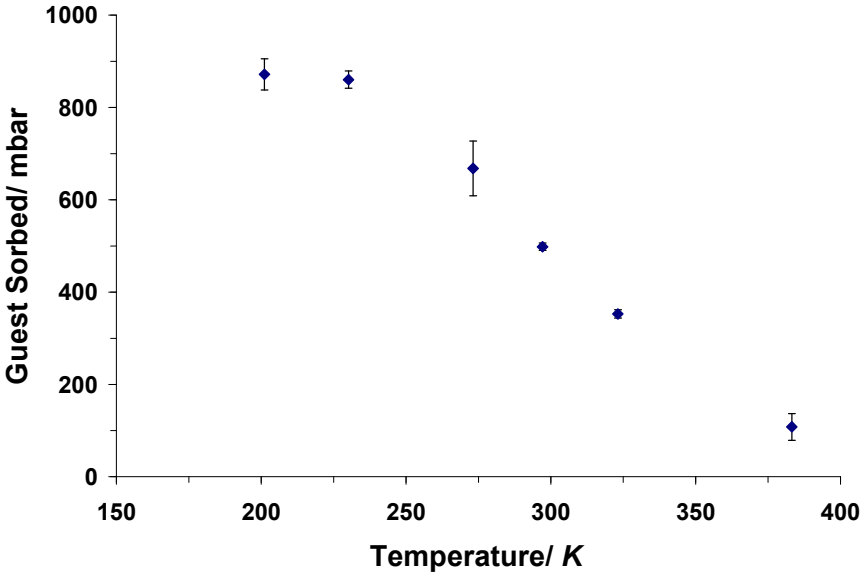

Figure 5.14. The amount of guest sorbed (mbar) shown as a function of temperature. The sorption capacity of the host framework increases with decreasing temperature.

The results for the sorption of carbon dioxide by compound **3a**, suggests that the mechanism of sorption is a non-activated diffusion process. The formation of transient pores within the host lattice are thus thought to be inherent to the system and are not due to the presence of guest molecules. The thermal motion of the atoms within the host framework is thought to cause the formation of the transient windows.

5.3.2. Gossypol

All sorption reactions with this organic polyphenol were performed at a regulated gas pressure of 1400 mbar and at a series of different temperatures. The exposure time of the sample chamber to a specific temperature prior to the start of an experiment was arbitrarily chosen to be exactly 12 min to ensure reproducibility of the sample preparation. From the α-time curves in **Figure 5.15** it can clearly be seen that the rate of reaction increases with decreasing temperature.

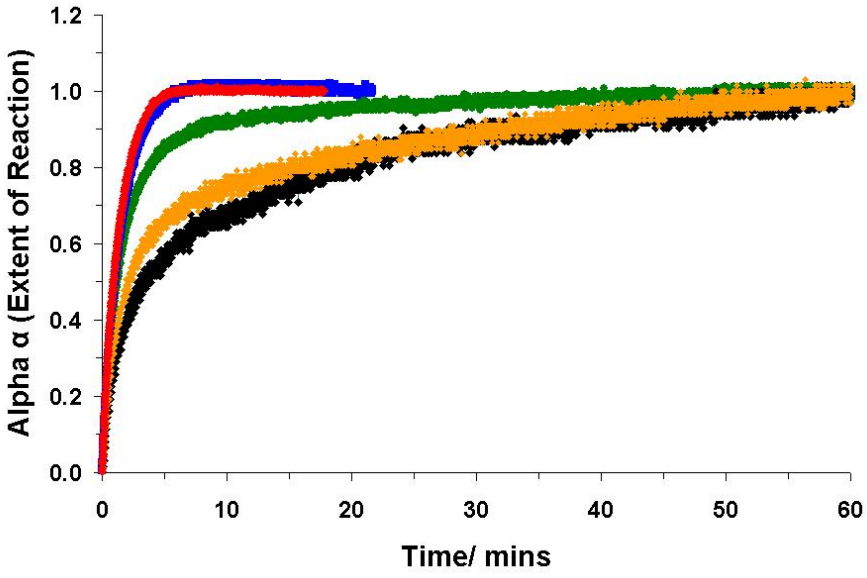

Figure 5.15. α-time plots of sorption reactions of **1a** with carbon dioxide at various temperatures. The temperature-dependence on the reaction rate can be seen. ■ is at -43 °C; ▲ is at -15 °C; ● is at 0 °C; ■ is at 15 °C and ♦ is at 24 °C.

The kinetic model that best describes the data from the sorption experiments is the deceleratory α-time function based on "D3" three dimensional diffusion (**Table 5.1**). It is interesting to note that all the materials studied fit the same kinetic model despite being very different from one another. Since sorption is experimentally observed in all the experiments, it can be concluded that the gas molecules have an inherent chemical potential which causes the

driving force for the diffusion to be large enough thus allowing the sorption reaction to readily take place. The graph seen in **Figure 5.16** shows a positive gradient in the graph of ln*k* *vs* 1/*T*. This would suggest that the activation energy, E_a, is negative. Conventionally, a negative E_a is not considered possible. However the graph in **Figure 5.16** indicates that energy needs to be removed from the system in order to increase the rate of guest sorption.

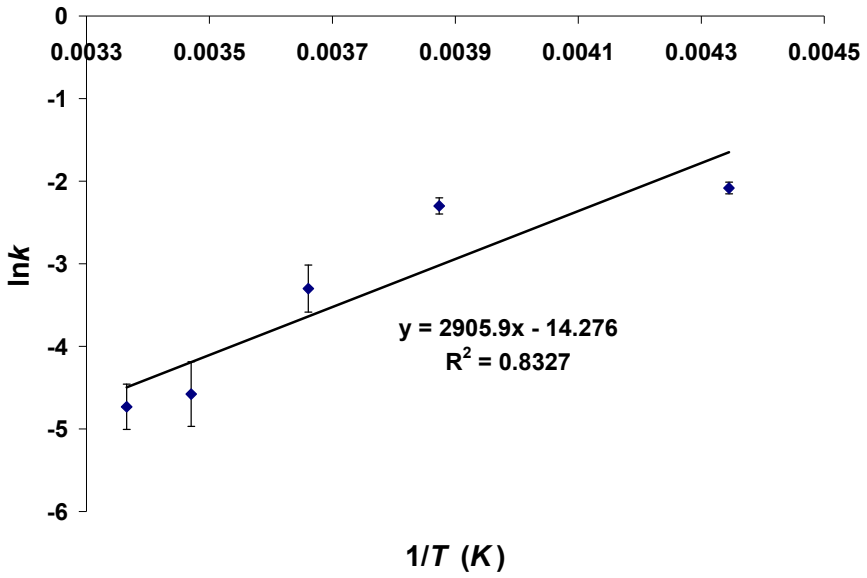

Figure 5.16. An Arrhenius-plot of **1a** showing the anti-Arrhenius behaviour of **1a** for the sorption of carbon dioxide gas.

The observed anti-Arrhenius temperature-dependence of *k* yields a positive gradient, as seen in the curve of **Figure 5.16**. This phenomenon can be attributed to increased thermal motion of the host framework with increasing temperatures thus sterically obstructing guest molecules from passing through the pores of the host framework. Of all the compounds investigated in this study, **1a** shows the most pronounced anti-Arrhenius behaviour.

5.3.3. *p-tert*-butylcalix[4]arene

This organic transiently porous compound, **2a**, showed a marked temperature dependent difference in the rate of reaction, *k*, between the sorption reaction performed at -43°C and the remaining temperatures, as seen in **Figure 5.17**. For the remainder of the studied temperatures there is little temperature dependence on the values of *k*. Consequently, it was expected that the Arrhenius-plot would approximate a gradient of zero, save for the impact of the rate constant determined for the reaction at -43°C. The sorption data was again best

described by the "D3" model of three dimensional diffusion. This suggests that the concentration dependence is the primary factor governing the sorption of guest by the host.

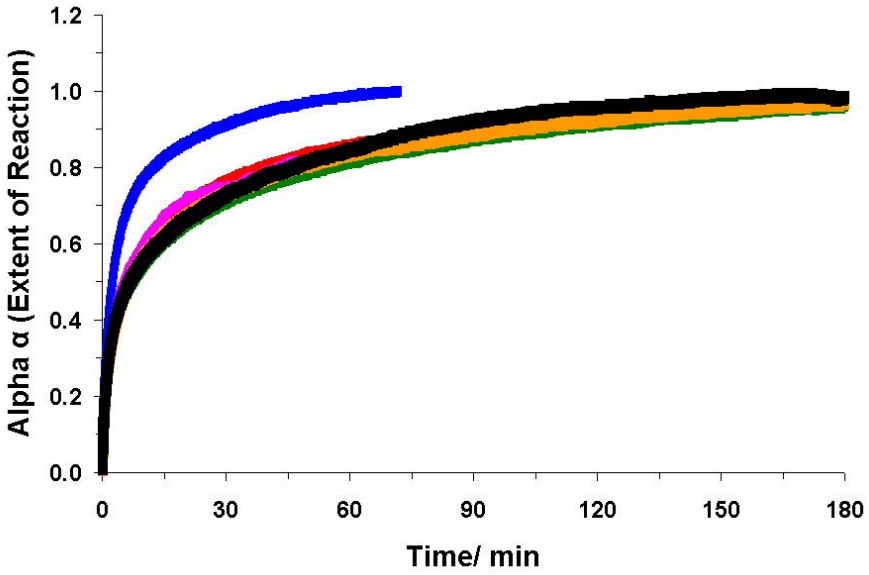

Figure 5.17. α-time plots of sorption reactions between **2a** and carbon dioxide performed at various temperatures. ■ is at -43 °C; ▲ is at -15 °C; ● is at 0 °C; ■ is at 15 °C; ♦ is at 24 °C and ■ is 35 °C.

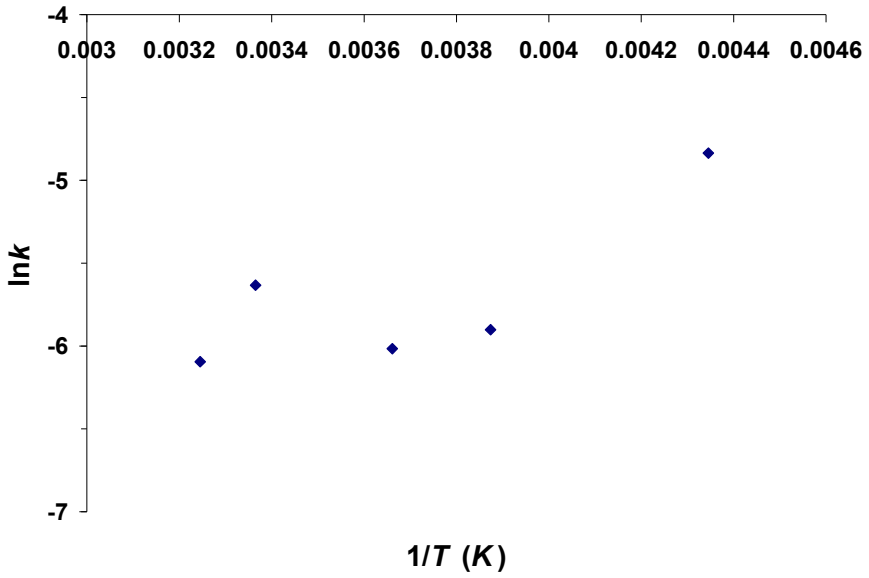

Figure 5.18. The Arrhenius-plot for the sorption reaction of **2a** with carbon dioxide showing negligible activation energy.

From the data point of the graph in **Figure 5.18** it can be seen that the *k* value determined at -43°C is considerably different to the remainder of the *k* values determined at higher

temperatures. The trend of the graph indicates a positive gradient which results in a negative E_a. This again shows that energy needs to be removed from the system to increase the rate of reaction.

5.4.3. $[Cd_2(B2MB)_2Cl_4]$

This *transiently* porous metallacycle, **4a**, shows only a slight dependence of the rate of reaction on the temperature according to **Figure 5.19**. As there is a very slight temperature-dependence on the rate of reaction *k*, a very low activation energy is expected.

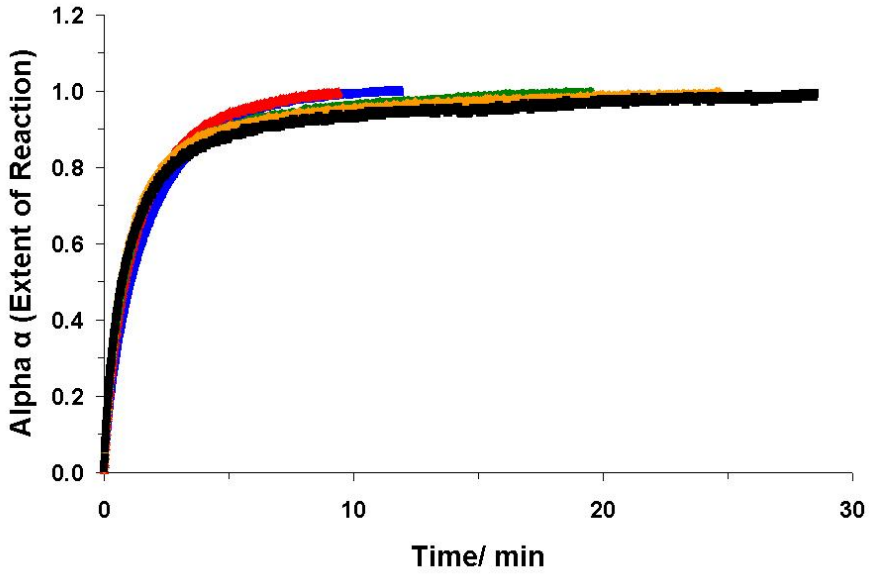

Figure 5.19. α-time plots of **4a** undergoing sorption reactions with carbon dioxide at various temperatures. There is only a very slight temperature-dependence on the rate of sorption. ■ is at -43 °C; ▲ is at -15 °C; ● is at 0 °C; ■ is at 24 °C and ♦ is at 50 °C.

The positive gradient in the curve in **Figure 5.20** again confirms that the energy of the system needs to be decreased in order to facilitate the increase of gas uptake by the host framework. This finding again suggests that the formation of *transient* pores within the host is not caused by the presence of guest molecules, but rather that the host framework inherently deforms as a result of temperature-dependent atomic displacement, resulting in the formation of *transient* pores within the crystalline lattice. The uptake of gas by this compound thus does not appear to be an activated process.

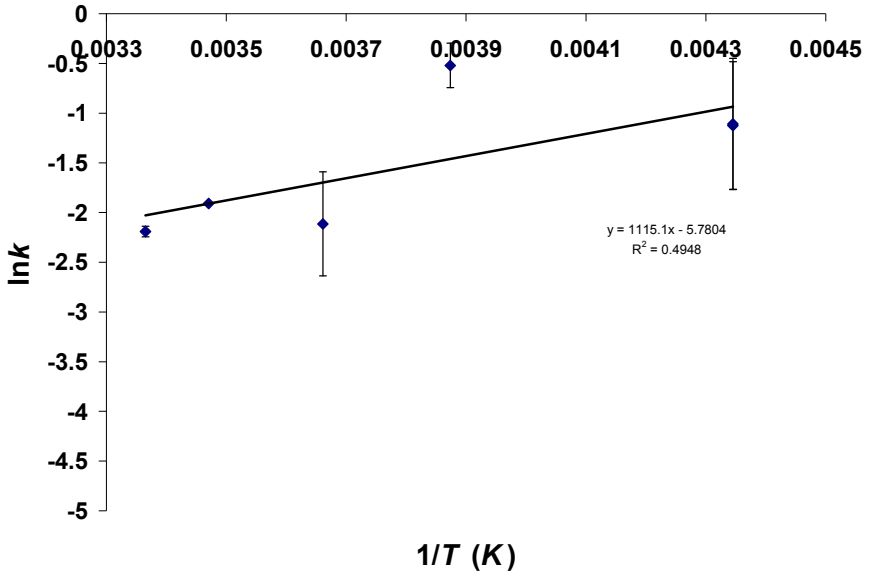

Figure 5.20. The Arrhenius-plot of **4a**, indicating that the sorption of carbon dioxide is a non-activated process.

The metallacycle **4a** yields similar α-time curves for reactions performed at different temperatures and exhibits the least amount of temperature dependence on the reaction rate when compared to the other compounds investigated as part of this study.

5.4. Conclusion

An instrument was designed and constructed to enable the accurate determination of the kinetic parameters of solid-gas sorption reactions. The reproducibility of the method was tested. The technique was found to be a viable and credible alternative to the existing commercial instruments available. The advantages regarding its simplicity and cost-effective construction further makes this method an attractive alternative to existing commercial methods. Results of measurements using four different porous compounds undergoing sorption reactions with carbon dioxide are presented. Data were fitted to a kinetic model and in all cases, the sorption reactions were best described by the "D3" [170] three dimensional diffusion kinetic model. This suggests that the sorption processes in these systems are primarily governed by diffusion. Diffusion will only take place if there is sufficient energy to allow the movement of the guest molecules through the host framework. Anti-Arrhenius behaviour was observed for all the compounds where the rate of reaction k is inversely proportional to the temperature. Consequently, energy needs to be removed from the system to facilitate a higher rates of sorption.

It is recommended that these experiments be repeated using commercial instruments in order to compare the results from the different methods. It must be stressed that this technique, when used in conjunction with other analytical tools such as crystallographic, thermoanalytical, computational and solid-state NMR methods, has the potential to suggest possible mechanisms of solid-gas reactions. Understanding the kinetics of solid-gas sorption reactions will become ever more important when designing "*smart*" materials aimed at specific applications.

The design of the instrument can be substantially modified to hopefully yield more accurate results along with the capability of use over a much greater temperature range. In order to perform experiments where the temperature control is more accurate, and where the temperature range is greater, it is suggested that the device be thermostated in a silicon oil bath. This will allow the gas and the sample to be at the same temperature, and owing to the heat capacity of the oil, sudden temperature fluctuations will be less likely to occur. It is also suggested that the thermocouple be positioned with its tip in direct contact with the sample. This would enable an accurate determination of whether the sample is truly at the desired temperature. It would also allow *in situ* monitoring of the sample temperature throughout the course of the reaction. Furthermore, there is an inherent thermal effect when gas enters a void volume due to the expansion it experiences. By accurately measuring the sample temperature one would be able to take into account the temperature decrease due to the expansion of the gas and compensate for this. It is further suggested that an electronomechanical gas regulator and solenoid valves be used in order to limit operational error.

Additional experiments should aim at investigating the affect of a series of regulated gas pressures on the values of k, E_a and A and on the kinetic model that best fits the experimental data. It would be interesting to investigate whether the type of mechanism associated with a particular solid-gas sorption reaction is pressure-dependent. The size and electrostatic contributions of the gas molecule on the kinetic parameters and their affect on the mathematical model should be investigated for the same host compound. Owing to their similar size, but inverse electrostatic topology, experiments using carbon dioxide and acetylene should be performed. By performing experiments using similar host compounds (*e.g.* isostructural compounds) and different gases, an investigation could be launched to determine whether similar frameworks display similar kinetics.

The effect of particle size of the host should also be investigated. Particle size is important when considering kinetic parameters as it will influence the rate of reaction. In this study, the particle size distribution was arbitrary but is assumed to remain constant for repeated experiments using the same sample. The rate constants are thus peculiar to the compound with a particular sample size distribution. It has been assumed that the values obtained for E_a are independent of particle size distribution, as they should be in principle, but this assumption should be investigated. The possible degradation of the sample over time is an additional concern when considering repeat experiments as highlighted in **Section 4.4.1**. It is suggested that a particle size sieve be used to obtain multiple samples of differing particle size. The kinetics of the sorption reaction are affected by the particle size, thus repeatability on a specific compound, with a particular particle size should be possible. The particle-size distribution may reasonably be expected to have a dramatic affect on the kinetics, but should not affect the value obtained for the activation energy (*i.e.* the activation energy should be a constant for a particular host-guest system). Future experiments should be conducted in order to establish whether the experimentally determined activation energy is indeed independent of particle-size distribution. If this is not the case, then the most likely explanation is that the experimental process is flawed. This unfortunately poses a substantial challenge to the synthetic chemist, as the production of the desired compounds is often laborious and does not give high yields. It is thus suggested that the system be tested on an inexpensive commercially available porous compound, where the effect of particle size on the kinetic parameters can be investigated feasibly.

CHAPTER 6. Carbon Dioxide Gas-Transport in *p-tert*-Butylcalix[4]arene.

Applications of porous solids include the effective storage of gas [169] for use in energy technologies, biology, medicine and environmental science [169]. The successful synthesis of gas storage materials that display sufficient sorption capacities, appropriate lifetimes, phase purity and tuneable sorption and desorption rates is still a substantial challenge [169]. As mentioned above, a sound understanding of the thermodynamics and kinetics of the system is needed, in conjunction with structural information, to postulate a transport and storage mechanism for the material in question. With porosity, as defined by Barbour [58], being displayed in conventionally non-porous materials it becomes obvious that an investigation into the physical and chemical processes intrinsic to the system, or imposed upon it, need to be considered. This study aims to postulate a transport and storage mechanism for the most studied transiently porous crystal system, *p-tert*-butylcalix[4]arene, **2**, [45-48, 74, 148, 149, 174, 175]. Computational molecular force field, standard crystallographic, and solid state CP-MAS NMR techniques were employed to gain insight into the mechanism of gas sorption by the crystalline host framework.

Computational investigations employing Cerius^2 3.8 [129] were performed to establish the most reasonable energetic pathway for gas transport and storage within the crystalline host framework.

6.1. Postulating a Possible Path for Gas Movement

Owing to the bilayer arrangement of **2a**, conventional pores are notably absent. A space filling diagram in **Figure 6.1** illustrates that the voids in **2a** are not linked, thus one would not expect it to be porous in the conventional sense of the term. It is thus a very curious phenomenon for **2a** to display any porosity whatsoever.

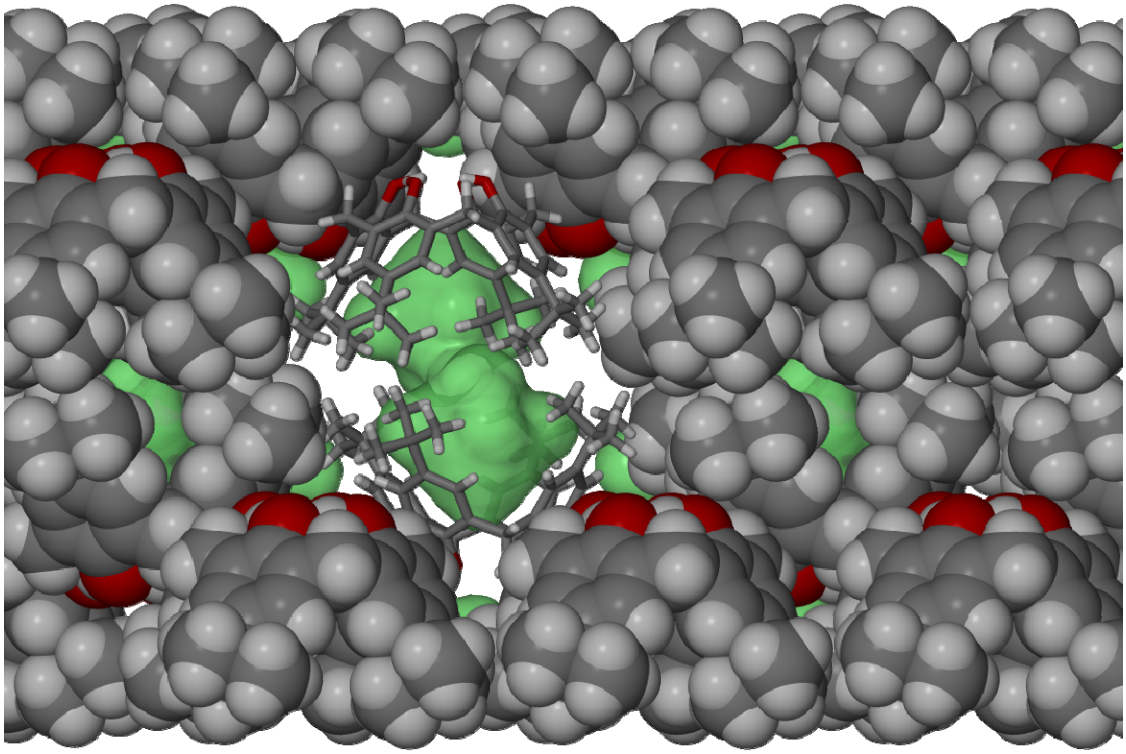

Figure 6.1. A space filling diagram with one pair of calix[4]arene molecules shown in capped stick representation to illustrate the inaccessibility of the void spaces (mapped in green), viewed along [001]. That porosity in **2a** is observed is a remarkable phenomenon.

Barbour and Atwood have shown that only one of the *tert*-butyl groups of **2a** is disordered at −100°C, and that all four *tert*-butyl groups are disordered at 20°C [12, 149], as shown in **Figure 6.2**. Therefore, they postulated that free rotation of the disordered *tert*-butyl moieties of the upper rims of the molecules facilitates diffusion of the gas into, and through, the crystal [99]. Single-crystal X-ray diffraction data suggest that the rotation of the *tert*-butyl moieties about the C(ar)−C(sp^3) bond facilitates gas uptake, more than does movement of the hydroxyl and aromatic regions, which are generally regarded as being far more rigid in the solid state. The nature of the observed disorder is important when postulating a mechanism for sorption.

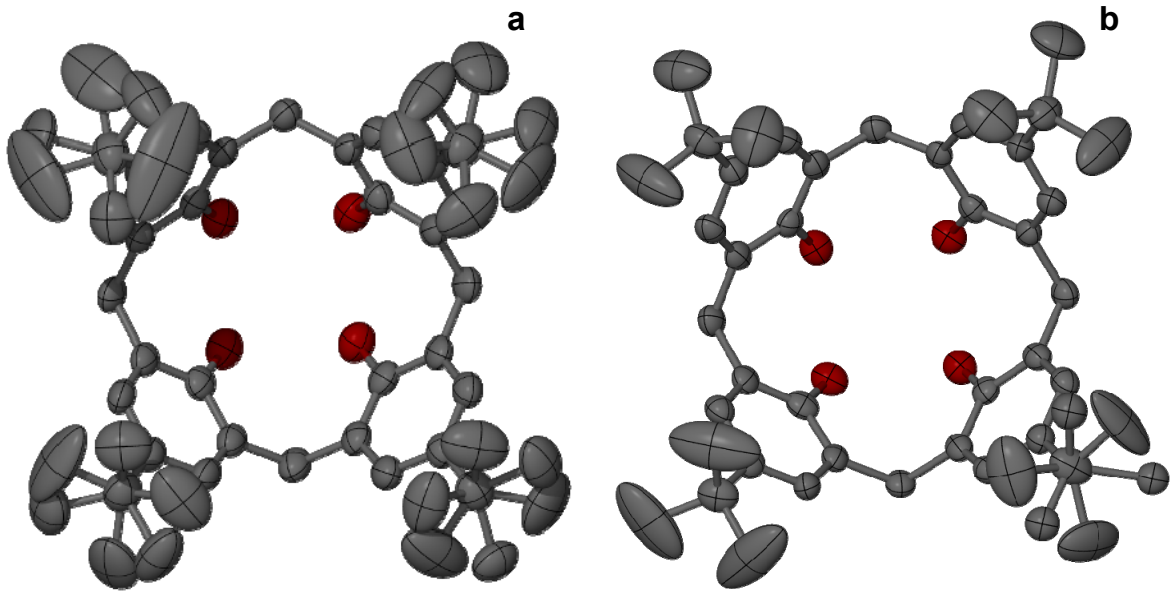

Figure 6.2. The crystal structure of **2a** compared at two different temperatures, (**a**) 20°C and (**b**) −100°C, showing the disorder within the *tert*-butyl moieties. In (**a**) all four *tert*-butyl moieties are disordered and in (**b**) only one *tert*-butyl group is disordered. This suggests that the amount free rotation of the *tert*-butyl moiety about the C(ar)–C(sp^3) bond may play an important role in facilitating gas uptake. Less rotation at lower temperatures will allow easier access for guest molecules. Increased rotation will hinder the path of guests through the host lattice.

Diffraction data suggests that all the *tert*-butyl groups are disordered over two positions that differ by *ca* 60° rotation about the C(ar)–C(sp^3) bond at room temperature [149]. The thermal ellipsoids of the room temperature structure, shown in **Figure 6.2**, imply that the disorder is probably of both a static and a dynamic nature [99]. It is believed that the static disorder exists because of the two distinct equilibrium positions that differ by *ca* 60° from one another. However, the dynamic disorder most likely exists because of extensive vibrations about these two sets of equilibrium positions (*i.e.* the displacement ellipsoids are too large to only indicate static disorder). The thermal motion of neighbouring *tert*-butyl groups is thought to act cooperatively and to thus create transient pores that facilitate the transport of gas molecules into the void space. In **Chapter 5** it is shown that the gas uptake can best be described using a kinetic model of three dimensional diffusion, and that the guest sorption is a non-activated process. It is therefore important to note that we suggest that the rotation about the C(ar)−C(sp^3) bond in **2a** only *facilitates* gas uptake, and not that it *causes* gas uptake.

Molecular dynamics simulations at room temperature using Cerius^2 3.8 [129] suggested that free rotation of the *tert*-butyl moieties about the C(ar)−C(sp^3) bond, in conjunction with a clam-like opening and closing of the calixarene (with the highest degree of angular distortion about the C(ar)−C(sp^3)−C(ar) angles) allows sufficient host deformation to successfully facilitate gas uptake into the system. These distortions are indicated in **Figure 6.3**.

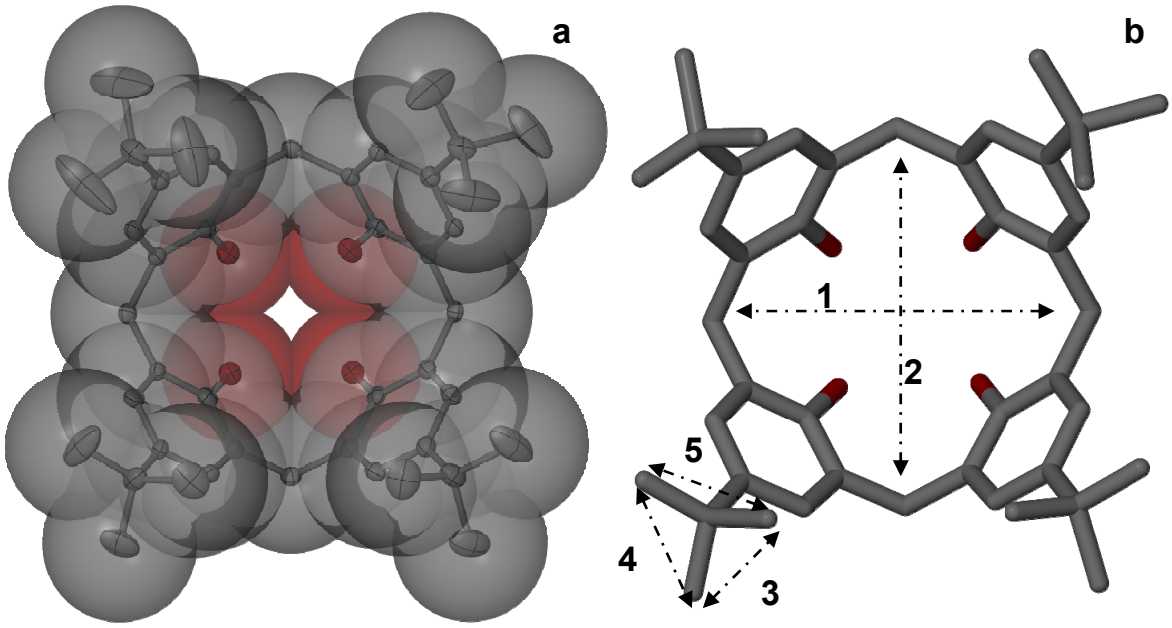

Figure 6.3. In (**a**) a calix[4]arene cup is shown with displacement thermal ellipsoids overlaid by van der Waals radii to give an indication of space filling. In (**b**) the bond deformations (labelled 1-5) observed during room temperature molecular dynamics simulations are shown. The maximum amount of deformation caused by the C(ar)–C(sp^3)–C(ar) angular distortion in **1** and **2** was 0.884 Å. The maximum amount of rotation around the C(ar)–C(sp^3) bond (causing lengthening or shortening of the distances **3-5**) was found to be 0.274 Å.

The program MSROLL [136-138] was used to identify and map guest-accessible voids (*i.e.* those large enough to accommodate carbon dioxide), either within the calixarene cups, or in the interstitial spaces between adjacent host molecules. From these data a possible guest trajectory could was postulated. The chemically reasonable path suggested for gas transport through the crystal is shown in **Figure 6.4** and is subdivided into three discrete steps viewed along [001].

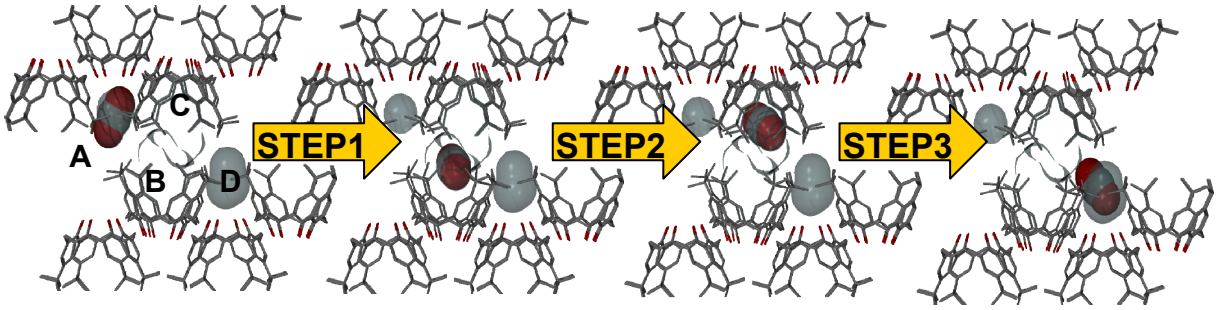

Figure 6.4. Postulated trajectory of gas transport taking place approximately along [100] within **2a**, viewed along [001]. Step 1: Carbon dioxide moves from the interstitial space (**A**) of the top bilayer to a calixarene cup (**B**) of the bottom bilayer; Step 2: Carbon dioxide moves from (**B**) in the bottom bilayer to the cup in the other half of the void space in the top bilayer (**C**); Step 3: Carbon dioxide moves from (**C**) to the interstitial space in the bottom layer (**D**).

6.2. Choice of force field

In order to perform the various molecular force field calculations, a suitable force field needed to be chosen. A force field that best describes the structure as it occurs in Nature would be the best model to use in order to accurately describe the experimental phenomena. The coordinates from the room temperature X-ray crystal structure were imported into Cerius^2 3.8 [129], the disorder removed, and then optimised using a multitude of available force fields, whilst constraining the unit cell dimensions to those of the crystal structure. The different minimised structures were compared to the X-ray structure; the force field that yielded an equilibrium structure most similar to the X-ray structure was then deemed the best suited to performing further calculations. The force field that compared most favourably to the single-crystal structure of **2a** was found to be the PCFF 300 1.01 [176-179] force field, which was then used throughout the remainder of this study.

6.3. Building the crystal lattice

The size of the crystal lattice needed to be carefully considered before building a model for the ensuing molecular force field calculations. The structure needed to be small enough to limit computational expenditure to an acceptable minimum, but large enough to be able to incorporate an entire periodic unit of the postulated trajectory that the gas molecule is thought to follow through the crystal lattice.

The PCFF 300 1.01 [176-179] minimised structure was used to build a 3 × 1 × 3 periodic crystalline super-lattice of **2a**, with the unit cell dimensions and space group constrained to that of the experimentally determined crystal structure. The model was then converted into a non-periodic superstructure. The entire 3 × 1 × 3 system was made into a rigid non-mobile structure save for two offset calix[4]arene cups forming a capsule like non-rigid mobile structure.

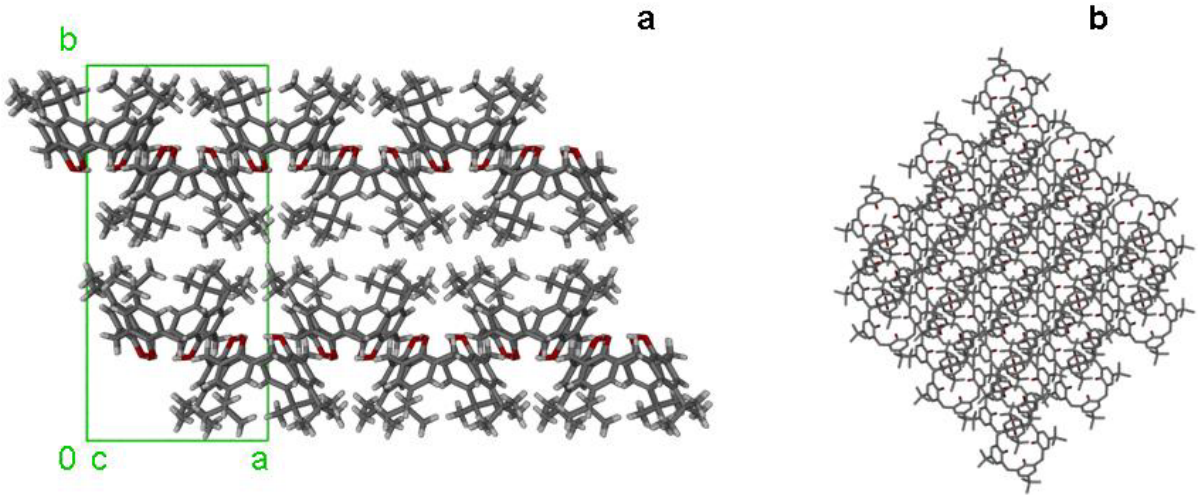

Figure 6.5. (**a**) Shows the 3 × 1 × 3 model used for the computational modelling, viewed along [001] and (**b**) shows the model viewed along [010]. It was necessary to choose a large enough model to ensure that the gas would remain inside the host, but simultaneously being small enough to allow reasonable computational time.

6.4. Incorporation of the guest in the host structure

A carbon dioxide molecule was constructed in Cerius^2 3.8 [129] and the structure minimised with the PCFF 300 1.01 [176-179] force field. The 3 × 1 × 3 periodic crystalline super-lattice was changed to a non-periodic super-structure and the carbon dioxide was imported into the super-structure. MSROLL [136-138] was used to determine a sensible position within the calix[4]arene cup to place the gas molecule. Once the gas molecule was imported, the entire system was minimised, thus establishing an *in silico* host-guest equilibrium structure. The computational calculations confirmed the MSROLL prediction that the central point between the *tert*-butyl carbons was indeed the most energetically favoured position for the carbon dioxide molecule: the optimised carbon dioxide inside the cup was at an angle of ~10° relative to the plane formed by the phenyl *para* carbon atoms, as shown in **Figure 6.6**.

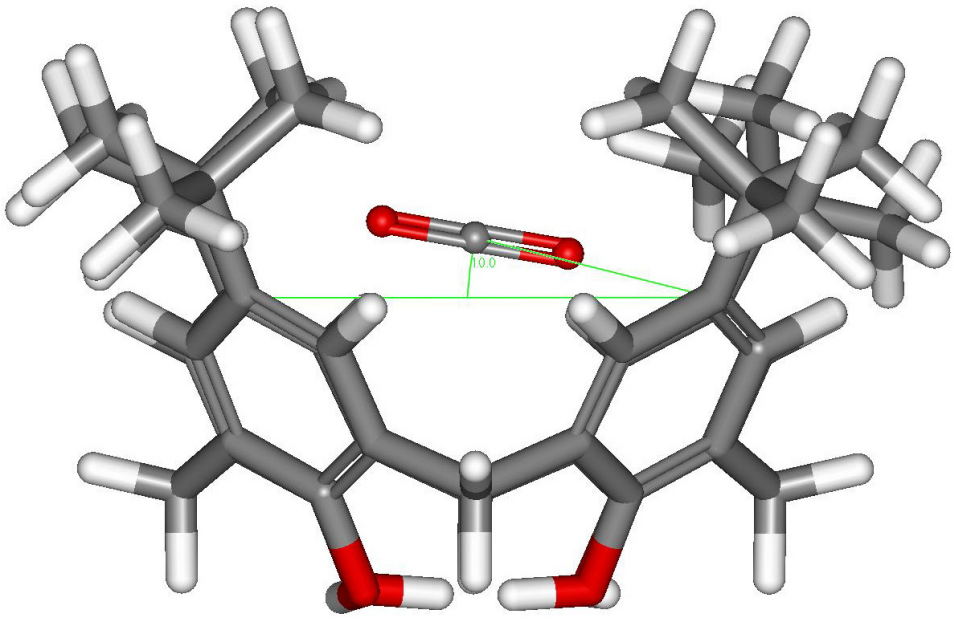

Figure 6.6. The minimum energy location of the linear carbon dioxide molecule inside the calix[4]arene cup was found to form an angle of 10° relative to the plane formed by the phenyl *para* carbon atoms. The distance from the centre of the molecule defined by a centroid between opposite sp^3-hybridised methylene bridging carbon atoms was found to be 3.088 Å following the computational simulations.

6.5. Executing the Calculation

In each step the carbon dioxide molecule was taken to a starting position and a dummy atom was positioned at the end of the intended trajectory. A second dummy atom was positioned along the same trajectory but at a distance four times further than that of the first dummy atom from the carbon dioxide. This was specifically chosen to limit the occurrence of artefacts in the resulting data. The distance to the first dummy atom was recorded and was programmed into a script describing the movement of the carbon dioxide along the chosen trajectory to its end position (that of the first dummy atom). The first dummy atom was subsequently deleted from the model. A force constant restraint of 500 Nm^{-1} was set on the distance between the remaining dummy atom and the carbon dioxide. The magnitude of the force constant restraint was of particular importance, as it influenced the degree of flexibility with which the gas molecule could deviate from its forced trajectory through the model system to its end position.

The simulation was facilitated by a script that defined a trajectory between the carbon atom of the carbon dioxide and the second placed dummy atom. The carbon dioxide would be moved

in a step-wise manner toward to the dummy atom until a preset distance had been reached. After each step a minimisation would be performed and the coordinates and energy value then recorded. A molecular dynamics simulation then commenced, followed by another energy minimisation recording the atomic coordinates and the energy value. The carbon dioxide was then moved one step further along the set trajectory and the cycle repeated until the set distance had been traversed.

The step size was found to be of particular importance and was chosen on the basis of comparing computational efficiency to realistic coordinates of the gas molecule after minimisation. In a sterically crowded region lying in the trajectory pathway a large step size could "*force*" the molecule into a chemically unreasonable position, where the minimised energy value would be higher than if a smaller step size was used. Consequently, when moving the molecule through sterically obstructed areas, a step size of 0.02 Å was used, and in less sterically obstructed areas, 0.05 Å.

The force constant restraint on the trajectory and the molecular dynamics simulation performed at each step is necessary to ensure that the *in silico* model best represents the conditions of the proposed model of sorption in Nature. Consider a string connecting the carbon dioxide to the dummy atom: the force constant restraint can be likened to the tautness of the string between the atoms that define the trajectory. The force constant restraint allows for marginal deviations away from an exactly linear trajectory to enable the molecule to find the path of least energy resistance. This is feasible as the carbon dioxide will, in Nature, follow the path of least energy resistance and not necessarily a straight line. The molecular dynamics simulation allows the re-evaluation of the spatial orientation of the carbon dioxide at each step along the trajectory in order to best represent the most probable position and orientation of the gas in Nature. The recorded energy values from minimisations performed before and after the molecular dynamics simulation at each step were used to plot a graph of energy *vs* reaction coordinate, as seen in **Figure 6.8**. The energy barrier associated with each step can be read off the curve to ascertain whether the proposed gas transport trajectory is indeed possible or not.

```
LOAD THIS IMAGE FILE              FILES/LOAD                          "../STEP1sub1CO2.msi"
LOAD THIS FORCE FIELD             FORCE-FIELD/LOAD_FORCE_FIELD ./../Cerius2-Resources/FORCE-FIELD/pcff_300_1.01"
                                  MECHANICS/METHOD                    "SMART MINIMIZER"
                                  MECHANICS/CONV_LEVEL                "HIGH CONVERGENCE"
                                  MECHANICS/MAX_ITERATIONS            5000
TYPE OF MOLECULAR DYNAMICS        DYNAMICS/METHOD                     "CONSTANT NVT"
                                  DYNAMICS/REQUIRED_TEMPERATURE 298.0000
                                  DYNAMICS/INFORMATION_LEVEL          BRIEF
                                  DYNAMICS/WRITE_TRAJECTORY           NO
PRESET DISTANCE FOR STEP                  set Dist 36.868
NUMBER OF STEPS TO RUN                    set Steps 100
STEP SIZE IN Å                            set StepSize 0.02
CREATE A FILE TO WRITE RESULTS TO         set fOut [open STEP1sub1CO2.summary w]
                                          for {set i 0} {$i <= $Steps} {incr i} {
                                          set R [expr $Dist-$StepSize*$i]
                                  FORCE-FIELD/TYPING_SCOPE            ALL
                                  FORCE-FIELD/CALCULATE_TYPING
                                  FORCE-FIELD/TYPING_SCOPE
                                  SELECTED
SELECTS DUMMY ATOM                SELECT/ATOM RESTART                 Atom(3823)
MAKE DUMMY FORCE FIELD TYPE X     FORCE-FIELD/ATOM_TYPE_PALETTE       X
                                  FORCE-FIELD/SET_TYPING
                                  RESTRAINTS/DIS_USE_MOD              NO
                                  FORCE-FIELD/ALLOW_UNDEFINED         YES
                                  RESTRAINTS/DELETE_ALL
                                  RESTRAINTS/DIS_EQ $R
DISTANCE RESTRAINT 500 kN         RESTRAINTS/DIS_FORCE                500
DEFINES THE RESTRAINT BETWEEN
TWO ATOMS                         RESTRAINTS/DISTANCE ATOMS           Atom(3831) Atom(3823)
                                  RESTRAINTS/RES_PANEL 0
                                  FORCE-FIELD/SETUP_EXPRESSION
                                  MECHANICS/AUTOSET_VARY_CELL         NO
MINIMISE MODEL                    MECHANICS/MINIMIZE
RECORD ENERGY VALUE                       set E1 [FORCE-FIELD/GET TOTAL_ENERGY]
NVT DYNAMICS CHOSEN               DYNAMICS/METHOD                     "CONSTANT NVT"
                                  DYNAMICS/RUN_TIME                   250
                                  DYNAMICS/RUN_SIMULATION
                                  #MODEL/SET_CURRENT                  Model(STEP1sub1CO2.msi)
MINIMISE AFTER DYNAMICS RUN       MECHANICS/MINIMIZE
RECORD ENERGY VALUE                       set E2 [FORCE-FIELD/GET TOTAL_ENERGY]
DATA OUTPUT FORMAT                        puts $fOut [format "R = %12.3f  E1 =  %12.3f E2 =  %12.3f " $R $E1 $E2 ]
DATA OUTPUT FORMAT                        puts [format "Distance = %12.3f  Energy =  %12.3f %12.3f" $R $E1 $E2]
SAVES OUTPUT TO FILE              FILES/SAVE  "./STEP1sub1CO2.msi_$R.msi"
                                          }
STOPS SCRIPT                              close $fOut
```

Figure 6.7. An example of a script used in modelling a gas transport trajectory in **2a**.

6.6. Results and Discussion

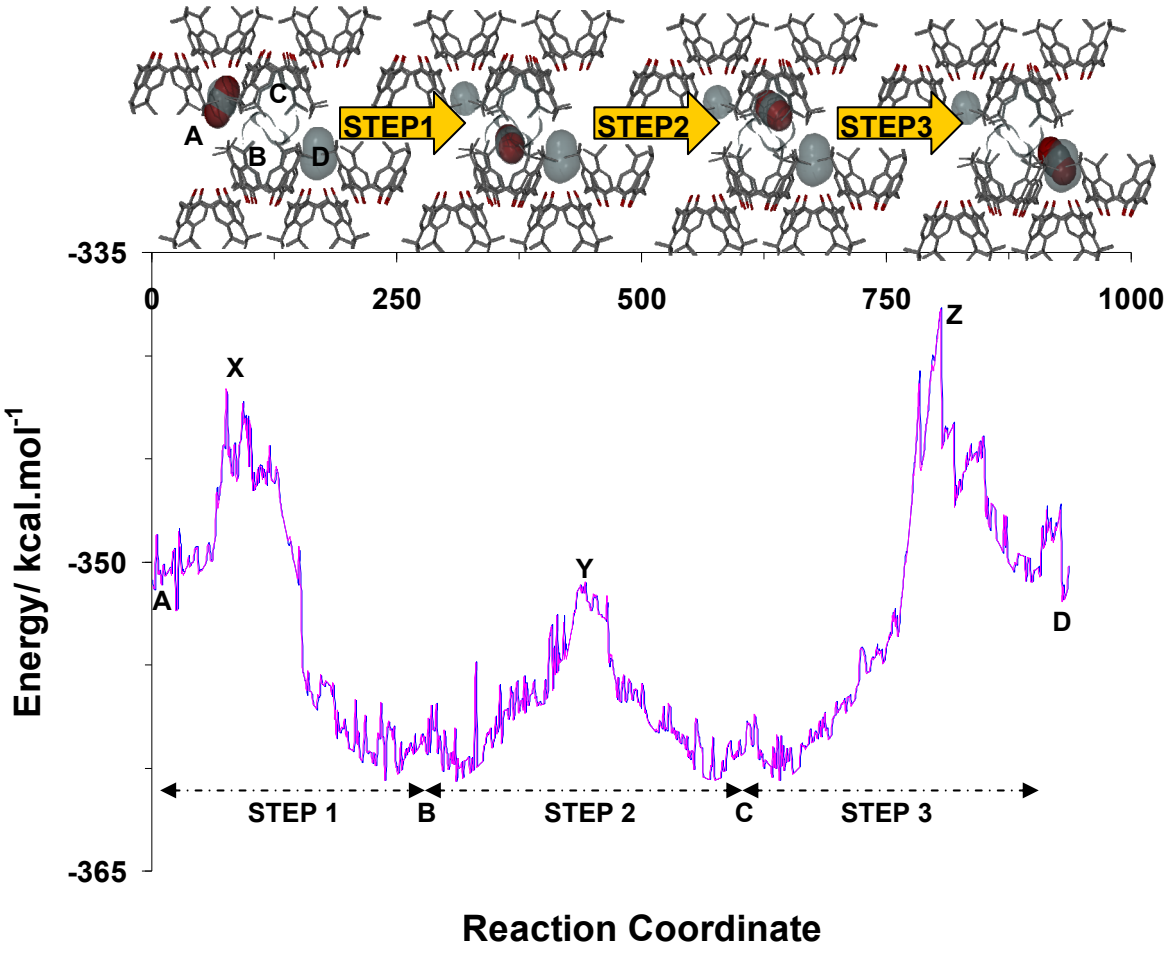

Figure 6.8. Energy *vs* reaction coordinate for the postulated gas transport trajectory in **2a**. The blue (-) represents the energy of the minimised structure prior to molecular dynamics, and the pink (-) represents the energy of the minimised structure after molecular dynamics.

Step 1 starts with the carbon dioxide molecule in the upper layer's interstitial surface and corresponds to a local energy minimum of -350.41 kcal.mol^{-1} seen in **Figure 6.8** as position **A**. As the carbon dioxide moves along the trajectory it encounters a region which is sterically obstructed by rotating *tert*-butyl moieties. The weak repulsive forces associated with C−C, C−H and O−H interactions cause a local energy maximum of -341.74 kcal.mol^{-1} indicated as position **X**. This corresponds to an energy barrier of 8.67 kcal.mol^{-1}, which is to be overcome at room temperature during a sorption process. The inherent, clam-like motion of the host and the rotational motion of the *tert*-butyl moieties facilitates the passage of the guest molecule into the calix[4]arene cup in the lower layer, where it is less sterically crowded, reaching a local minimum energy of -360.48 kcal.mol^{-1} near position **B** and orientated at an angle of

~10° to the horizontal. The carbon dioxide molecule is now relatively far away from the host structure, so repulsion is minimised while the π···O interactions between the host phenyl groups and the guest oxygen atoms facilitate the stabilisation of the host-guest system.

Step 2 starts with the carbon dioxide in a local energy minimum inside the calix[4]arene cup in the lower layer near position **B**. The carbon dioxide now moves along the chosen trajectory into the other half of the void in the upper layer. As it comes into closer proximity to the rotating host *tert*-butyl groups it passes through an energy barrier of 9.52 kcal.mol^{-1} at **Y** until it reaches the local minimum (-359.98 kcal.mol^{-1}) inside the calix[4]arene cup of the upper layer, **C**, again at an angle of ~10° to the horizontal. Again, this energy barrier is of a chemically reasonable size to expect this process to occur spontaneously in Nature. Since the physical properties of the chemical environments describing **B** and **C** are virtually identical, it is expected that the energy values of **B** and **C** should be the same. This is indeed observed, with a difference of 0.5 kcal.mol^{-1} between the two minima.

Step 3 is designed to move the carbon dioxide between points that are crystallographically equivalent to those of Step 1, but instead of the molecule moving from the interstitial surface to the calix[4]arene cup, it now moves from inside the calix[4]arene, **B**, to an interstitial space, **D**. One would expect the energy profile of Step 3 to be the same as Step 1. The shape is indeed similar but with slightly different energy values. This can easily be rationalised: the calix[4]arene capsule is modelled as non-rigid and is allowed to move while the rest of the model is rigid. The trajectory between crystallographically equivalent points in Steps 1 and 3 can be viewed as a string defining a path along which the carbon dioxide moves. This string is not completely taut but has a degree of flexibility, as defined by a force constant. This allows the carbon dioxide to slightly deviate off the defined trajectory so that it can find its lowest energy position at every step along the trajectory. The minimised starting structures of Steps 1 3 will be intrinsically different with regard to the exact positions and orientations of the host atoms. Since these atoms interact with the guest carbon dioxide, slightly different energy profiles will be obtained for the two steps. The difference is, however, marginal and the overall shapes of the two energy profiles are similar.

From the graph in **Figure 6.8** it can be concluded that the postulated trajectory for the movement of carbon dioxide along the [001] direction of **2a** is a chemically reasonable choice

and could occur in Nature. Of course, the proposed transport trajectory along [001] is not the only pathway for gas transport through the crystal, but is perhaps the most obvious choice.

Using the Boltzmann distribution, the percentage relative probabilities of finding a carbon dioxide molecule in one of the two minimum positions can be determined using the energy values from the generated graph.

$$\frac{n_i}{N} = \frac{e^{-\varepsilon_i / kT}}{z} \qquad \textbf{(6.1)}$$

where n_i is the number of guest molecules in the energy state ε_i, N is the total number of guest molecules in the system, k is the Boltzmann constant and z is the molecular partition function.

Using the data summarised by **Figure 6.8**, it can be seen that the minimum energy positions within the calix[4]arene cup, **B1** and **B2**, are the most favoured positions, with carbon dioxide having a 99.99% probability of residing there. The minimum energy positions in the interstitial sites, **A1** and **A2**, are less favoured with carbon dioxide having a 0.01% probability of residing in these positions.

The results from the computational study led to the postulation of the transport trajectory being tested experimentally, using solid-state CP-MAS NMR, volumetric sorption and single crystal X-ray diffraction under constant controlled gas pressure. It is of interest to investigate the factors that facilitate the movement of gas molecules through the crystal lattice *in situ*,and to correlate these with what has been calculated.

In order to investigate the nature of the disorder of the *tert*-butyl moieties, solid-state CP-MAS NMR studies were performed at varying temperatures. If the disorder is dynamic, more methyl peaks are expected when the temperature is lowered from room temperature to -100°C, whereas if the disorder is static there should be no change in the complexity of spectra. The solid ^{13}C CP-MAS spectrum of **2a** under at 273K is shown in **Figure 6.10**. The ^{13}C CP-MAS spectra in **Figures 6.11** and **6.12** show the aromatic and methyl chemical shift regions at different experimental temperatures. Concomitant polymorphism, a previously undescribed phenomenon for the sublimed low-density β_0 apohost, was inferred from the

spectra, making it difficult to accurately assign the peaks. Preparing a pure sample of the β_0 phase of **2a** has proven to be difficult since both, the kinetic, **2a**, and thermodynamic, **2b**, polymorphs form during the same sublimation experiment, as seen in **Figure 6.9**. However, the methyl chemical shift region of the CP-MAS NMR spectra showed an increase in complexity as the temperature was lowered suggesting, although inconclusively, that the disorder may be dynamic in nature. Thus, a question requiring further investigation arose: would the proposed mechanism of transport and storage "*switch off*" at a certain temperature, causing the cessation of gas uptake and providing a means for permanent gas storage? Owing to an unstable solid-state probe head, investigations below 173K could not be carried out.

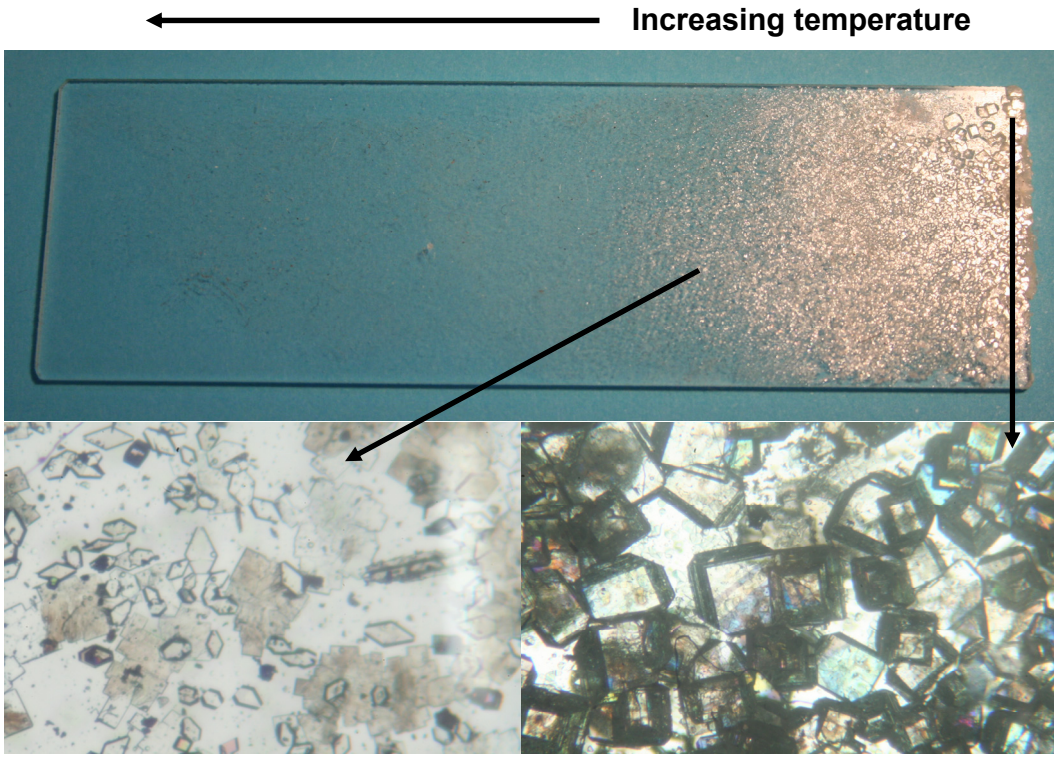

Figure 6.9. Concomitant polymorphism by sublimation at 270°C under vacuum. The kinetic, **2a**, (**a**), and thermodynamic, **2b**, (**b**), products can be distinguished and appear on the same glass microscope slide. The kinetic product is concentrated at one end of the microscope slide at the top of the temperature gradient, and the thermodynamic product at the opposite end of the microscope slide, at the bottom of the temperature gradient.

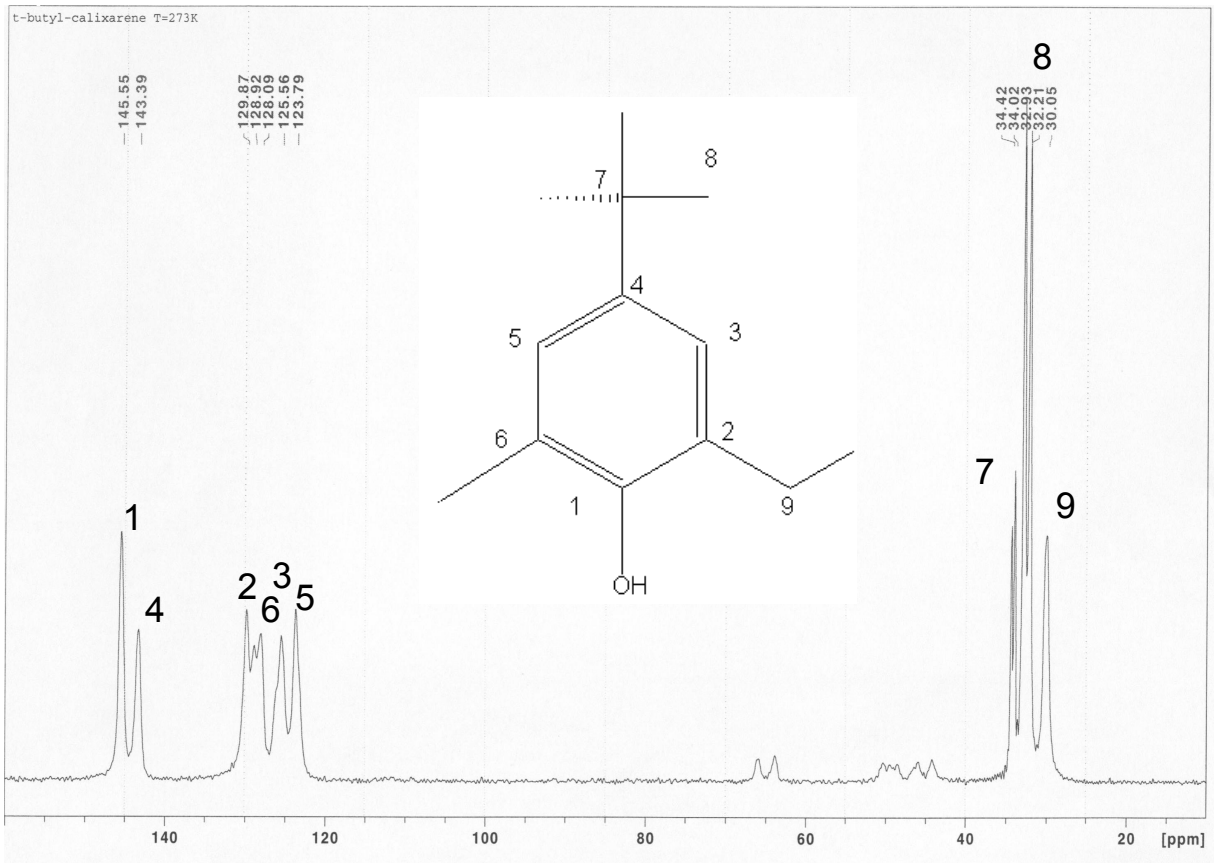

Figure 6.10. ^{13}C CP-MAS NMR spectrum of **2a** performed at 173K. Full assignment of the spectrum was not possible owing to its complex nature. A spectrum of **2a** by Schatz [180] was left unassigned, and it was noted that the complexity decreased considerably in the spectrum of the toluene clathrate formed by **2**. This decrease in complexity was believed to be related to an increase in symmetry from the monoclinic $P2_1/n$ space group of **2a** to the tetragonal $P4/n$ space group of the toluene clathrate. Partial assignment of the main functional groups are in good agreement with ^{13}C CP-MAS spectra of the inclusion compounds formed by **2** [181, 182]. The assignment of our spectrum correlates well with the recent assignment of **2a** by Ripmeester [183]. We propose that the complexity in the ^{13}C CP-MAS NMR spectrum of **2a** is possibly due to polymorphism. This supposition cannot be confirmed without further ^{13}C CP-MAS NMR studies, which is proposed as future work.

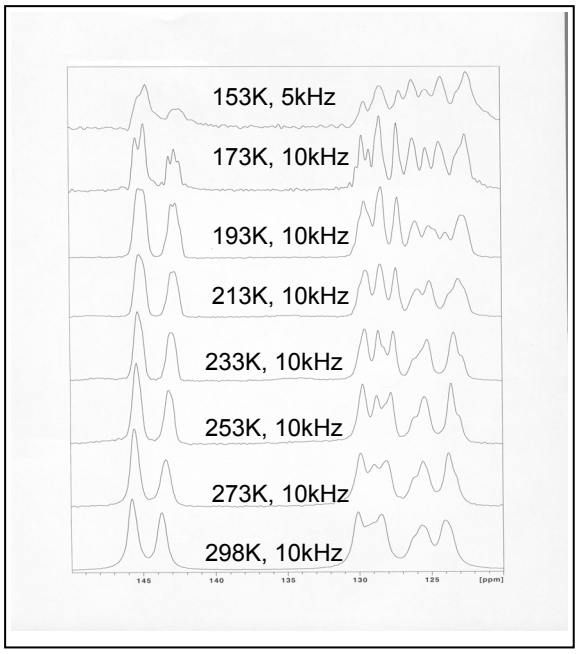

Figure 6.11. Aromatic peaks

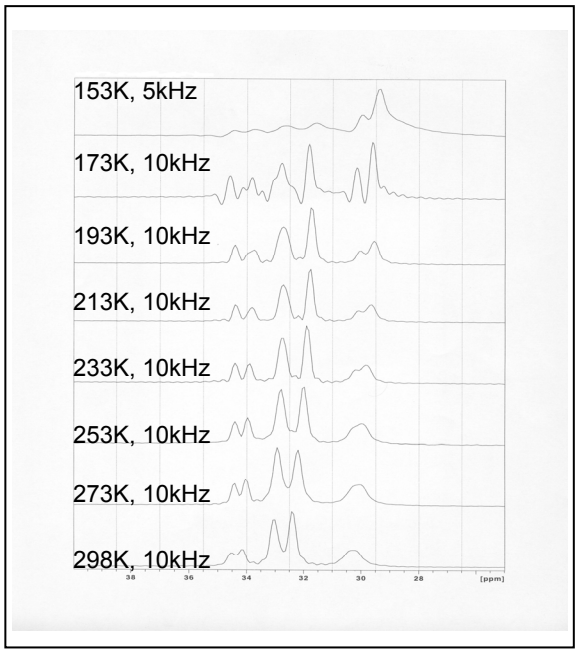

Figure 6.12. Methyl peaks

From structural studies it can be deduced that the void space inherent to **2a** is large enough for a carbon dioxide molecule. Using a "*pressure cell"*, **Figure 6.13**, designed by Barbour [184], single crystal X-ray studies could be carried out with the crystal under a selected pressure. A single crystal of **2a** was glued and sealed inside a gas-tight glass capillary and the system was then evacuated to remove all guest molecules. The system was then pressurised to a desired pressure with a chosen gas and left to equilibrate. It was then sealed and mounted on a single crystal X-ray diffractometer for X-ray diffraction studies.

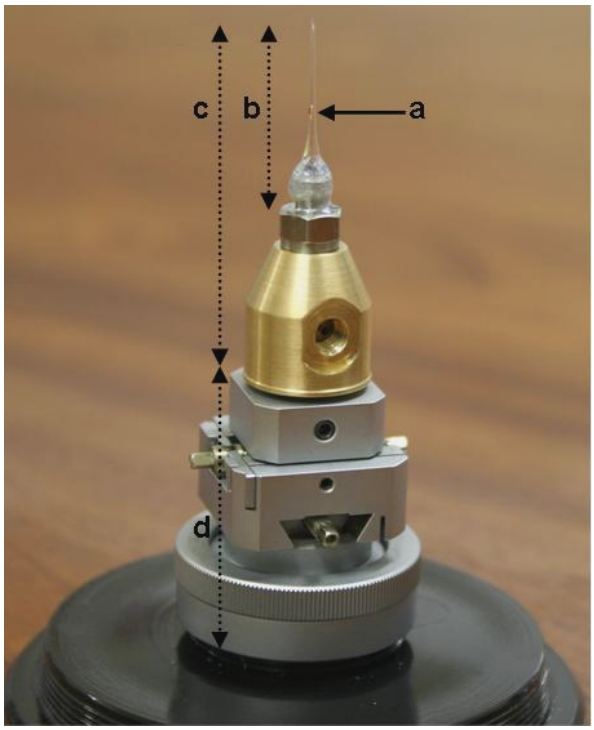

Figure 6.13. The "*pressure cell"* used for *in situ* diffraction studies under controlled gas pressure where (**a**) points to the crystal inside a Lindemann capillary (**b**). The entire "pressure cell" indicated by (**c**) fits into a goniometer head (**d**) for single-crystal X-ray diffraction studies.

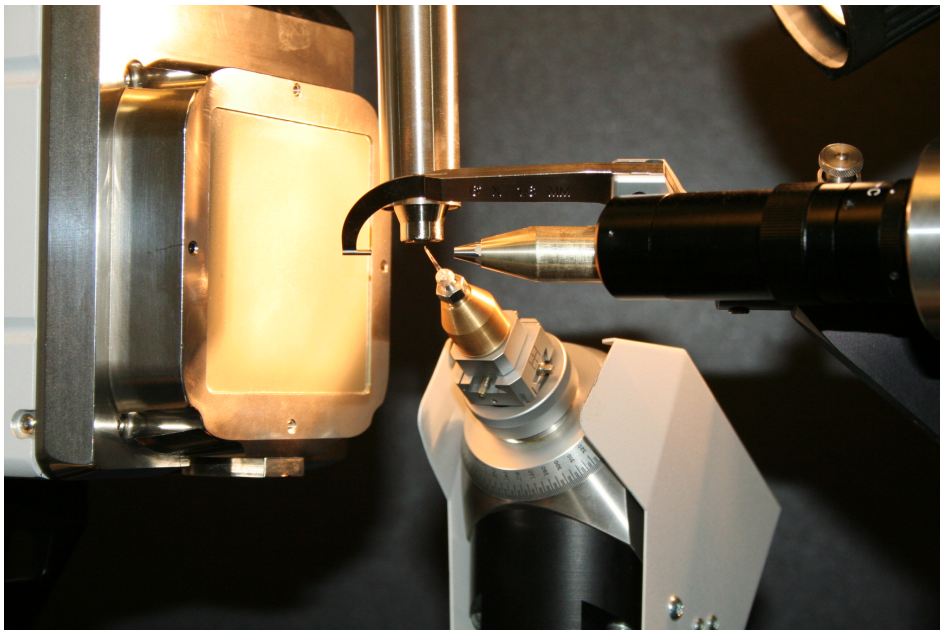

Figure 6.14. The *"pressure cell"* mounted onto the Bruker SMART Apex single-crystal X-ray diffractometer.

The program SQUEEZE [134], originally written to locate disordered solvent in crystal structures, was used to perform difference Fourier electron density mapping to *"count"* the

number of electrons present in the calix[4]arene cup within the Connolly surface. The number of electrons inside the void should correspond to an integer number (or multiple thereof) of electrons in a single molecule of the specific gas inside the *pressure cell* if full occupancy is assumed. A plethora of different gases were studied in an attempt to confirm the nature of the proposed gas transport mechanism. Owing to the nature of the gases, most studies had to be performed at room temperature, drastically affecting the quality of the crystal structures. The poor crystal data are evident in **Table 6.1** and contributed to the poor quality of the SQUEEZE results, as not all the electron density is effectively modelled. Although a sizable electron density due to the guest was detected in all the studies performed (**Table 6.1**), it was not well enough defined enough to model discrete guest molecules with specific atomic coordinates. It is thought that the relatively large calix[4]arene cup surface allows the gas guest molecules to rapidly rotate, causing the average electron density to be localised over too large a volume for a discrete molecule to be modelled. Despite not being able to model gas coordinates it can be concluded that gas sorption always occurs *via* a mechanism incorporating the void inside the offset pair of facing calix[4]arene cups, as electron density was detected for all gases studied within this space.

Table 6.1. Table showing the different investigated gases and their SQUEEZE[134] results.

	Name of gas	Formula	Total number of electrons in gas molecule	Number of electrons in calix[4] cup (SQUEEZE)	Number of electrons in interstitial space (SQUEEZE)	R 1 for structure	Pressure in bar
1	**Acetylene**	C_2H_2	14	8	0	0.0705	3.2
2	**Carbon dioxide**	CO_2	22	10	1	0.1279	4
3	**Carbonyl sulphide**	COS	30	20	0	0.0926	6
4	**Isobutane**	C_4H_{10}	34	33	2	0.3255	3.5
5	**Methane**	CH_4	10	11	1	0.1975	3.5
6	**Nitrogen dioxide**	NO_2	23	30	2	0.2140	3.5
7	**Freon-13**	CF_3Cl	50	5	0	0.0626	3.2

The volumetric and gravimetric sorption results discussed in **Section 4.4.2** indicate a guest-host ratio of 1:1 where the host is defined as the void created by a facing pair of offset calix[4]arene molecules, and the guest as one carbon dioxide molecule. This indicates that the energetics of the system allow only one carbon dioxide molecule inside each the void created by each facing pair of offset calix[4]arene molecules, and that it remains energetically unfavourable for a guest molecule to reside inside the interstitial void. This reinforces the results from the computational modelling of the gas transport. Electron density, albeit small, is sometimes observed in the *in situ* diffraction studies inside the interstitial voids. As discussed in **Section 4.4.2** a gas-induced phase change was observed at approximately 8 bar of carbon dioxide pressure. The nature of this phase change remains unknown but should be investigated in future studies using *in situ* pressure and temperature controlled PXRD experiments.

Crystallographic and computational studies both point to the free rotation of the methyl groups (part of the *tert*-butyl moiety) around the C(ar)−C(sp^3) bond as being an important part of the inherent motion of the crystal that facilitates gas uptake *via* diffusion. By synthesising an analogue of **2a** with one methyl group less, namely **7**, we hoped to investigate the importance of the *tert*-butyl moiety not only for its ability to facilitate gas uptake, but also for its role regarding the unique packing arrangement of the calix[4]arene cups in **2a**, that lead to void spaces available to guest molecules.

Two polymorphs of the empty structure of **7** were found concomitantly by sublimation as described in **Chapter 3**. However, both crystal structures possess no void spaces available for guest uptake. Since it was not possible to separate large enough quantities of the two polymorphs, a powdered sample containing both polymorphs was tested experimentally and failed to exhibit any sorptive properties. This finding confirms that the *tert*-butyl moiety plays a crucial role in the **abcd** bilayer stacking motif of **2** to form the kinetic, low density, *transiently* porous, β_0 phase **2a**.

6.7. Conclusion

A mechanism for gas transport and gas storage was postulated using computational, crystallographic, solid-state CP-MAS NMR and isosteric sorption techniques. The guest-accessible voids were mapped using MSROLL [136] to assist in the postulation of a transport

trajectory. The PCFF 300.01 force field was then used to calculate the minimum energies along the suggested trajectory. Once it was established that the proposed trajectory was indeed energetically, and thus chemically sensible, molecular dynamics studies were employed to establish which physico-chemical means facilitates gas uptake into the crystal system. These results point to the dynamic rotation of *tert*-butyl moieties around the C(ar)−C(sp^3) bond and the clam-like angular deformation of the calix[4]arene at the C(ar)−C(sp^3)−C(ar) angle as the main mechanical movements that facilitate the uptake of guest molecules by the host framework of **2a**. Computational results were used to calculate the Boltzmann distribution and different minimum energy positions along the proposed gas transport trajectory. It was found that 99.99% of the guest should be found inside the calix[4]arene void, as apposed to 0.01% inside the interstitial void. The correctness of this calculation is supported by *in situ* single-crystal X-ray diffraction studies of **2a** under carbon dioxide pressure, where only a negligible amount of electron density was detected in the interstitial void space at room temperature, despite very poor crystal data.

It was hoped that a device for the crystallographic study of single crystals under selected gas pressures could be used to identify the active adsorption sites within the guest accessible voids and, consequently, to formulate transport mechanisms. However, owing to rapid gas reorientation and the size of the calix[4]arene cup, single-crystal diffraction data did not yield reliable atomic coordinates of the gas molecules within the void. Difference electron density maps were employed to ascertain whether the gas under investigation was indeed present within the void. The results were correlated to volumetric sorption data.

Finally, solid-state CP-MAS NMR studies at varying temperatures indicated that the observed disorder of the *tert*-butyl groups is indeed of a dynamic nature. Thus, a question requiring further investigation arose: would the proposed gated mechanism "*switch off*" at a certain temperature, causing cessation of gas uptake, thus providing a means for permanent gas storage?

It was shown by synthesising an analogue of **2a**, namely **7**, that the *tert*-butyl moiety plays a crucial role in the **abcd** bilayer packing motif displayed by **2a** that is responsible for the availability of void spaces for guest uptake into the host framework.

This study highlights the potential of using an array of analytical and theoretical tools to explain mechanisms of gas transport and gas storage. It is, however, suggested that owing to the intrinsic difficulty of obtaining a pure phase of the host compound, **2a**, that another host system should be used in future as a model host system. Despite **2a** being the most studied transiently porous system, it appears that it is far from being ideal as a model compound in the development of new method.

CHAPTER 7. Conclusion

The concepts of host-guest chemistry, porosity and sorption have been introduced against a historical background to provide context to the aims and objectives of this study. The aim of this study was to investigate gas transport mechanisms in porous supramolecular compounds and to develop methodologies suitable for use with both *conventionally* and *transiently* porous supramolecular systems. The primary reason for this is that understanding the underlying mechanisms governing specific physical properties will become ever more important in the challenge to develop property-specific supramolecular materials.

The gas sorption capacities of several supramolecular hosts were investigated using a locally-constructed volumetric sorption apparatus. The validity of the results was checked against a commercially available gravimetric sorption analyser. It was found that the constructed device yielded accurate results within an acceptable margin of error. The sorption processes, not necessarily the same, were investigated from thermodynamic and kinetic perspectives. This was undertaken in order to gain further insight into the energetics of the sorption reaction and the possible mechanisms governing the sorption process.

The thermodynamic parameters of gas sorption experiments with carbon dioxide were determined using a locally-constructed volumetric sorption apparatus. The method described in **Chapter 4** is particularly advantageous, as it can be used on *conventionally* and *transiently* porous systems, owing to the fact that it is not necessary to determine the degree of coverage θ to obtain thermodynamic parameters. The results show that, for the compounds that were studied, sorption reactions are spontaneous up to standard pressure and that the desorption reaction is spontaneous at equilibrium loading pressures greater than standard pressure. The isosteric heat of adsorption, ΔH°_{ad}, at zero equilibrium loading pressure was investigated as a function of equilibrium loading pressure for the studied compounds and compared with literature values of known porous compounds. Compounds **1a**, **2a**, **5** and **6** displayed typical trends where the magnitude of ΔH°_{ad} decreases (*i.e.* the value becomes more positive) with increasing equilibrium loading pressure. This can be attributed to the increasing degree of guest-guest and guest-host interactions as the host becomes saturated with guest. An interesting phenomenon was observed for the metallacycles **3a** and **4a**, where turning point minima for ΔH°_{ad} and ΔS°_{ad} were observed. It is thought that cooperative guest-guest and

host-guest interactions cause this phenomenon. The method also enabled us to monitor the temperature dependence of $\Delta H°_{ad}$ and to detect any temperature-induced structural transformations. Errors in the values of $\Delta G°_{ad}$ could only be estimated, as exact repetition of a certain equilibrium loading pressure is not possible with the current design of the instrument. The disadvantages of using this technique with *conventionally* porous systems are (i) that the guest-host ratio must be known (either being calculated experimentally or inferred from crystallographic studies prior to performing the thermodynamic experiments) and (ii) that the experiments cannot be performed over a wide range of temperatures, as excessive heat will melt the electrical components and drastically affect the linear range of the pressure transducer.

In order to determine the kinetic parameters of solid-gas sorption reactions, a method needed to be developed to perform sorption experiments with the sample under constant pressure. The solution to this problem was to design and construct the instrument described in **Chapter 5**. It was shown that the instrument yields reproducible results within an acceptable margin of error. Data from the sorption experiments with carbon dioxide were fitted to known kinetic models. All carbon dioxide sorption reactions using the range of investigated supramolecular compounds were found to fit the "D3" three dimensional model of diffusion best. This suggests that the chief mechanism governing the sorption of carbon dioxide in the studied host compounds is a diffusion process. All the systems studied showed an inverse relationship between the rate of the reaction k and the temperature. Such anti-Arrhenius behaviour was rationalised by suggesting that the organic moieties comprising the host framework undergo increased thermal motion at higher temperatures, thus sterically obstructing the passage of guest molecules through the host lattice. This is supported by the fact that Arrhenius plots generally yielded positive gradients, indicating that energy needed to be removed from the system to increase the rate of guest uptake. The advantages and limitations of the instrument were discussed in **Chapter 5** and suggestions regarding improvements to the current design were made. Future studies should investigate the effect of the regulated pressure on the kinetic parameters and the mathematical model of the system. The effect of particle size on the kinetic parameters and on the kinetic model should be investigated, on the condition that a suitable host compound can be acquired in large quantities and at relatively low cost.

The aim of **Chapter 6** was to investigate possible gas transport mechanisms in the β_0 phase of *p-tert*-butylcalix[4]arene, **2a**, using the developed methodology and complementary analytical

and computational techniques. By using single-crystal X-ray diffraction, a possible gas transport trajectory through the transiently porous host framework was postulated. Computational simulations were performed to confirm the notion that the rotation of the *tert*-butyl moiety around the C(sp^3)–C(ar) bond and the C(ar)–C(sp^3)–C(ar) angular deformation play important facilitatory roles in creating transient windows for guest passage. Disorder of the *tert*-butyl groups in the crystal structure suggests that this movement is inherent to the crystal and not caused by the presence of guest molecules. Results from kinetic studies confirm this hypothesis, with sorption experiments best fitting a kinetic model based on three dimensional diffusion. The thermodynamic, kinetic and computational results suggest a spontaneous non-activated sorption process. The disadvantages of the host compound were numerous. A curious gas-induced transformation was observed but requires further investigation into the exact cause of the phenomenon. Concomitant polymorphism was also observed and raises questions concerning the phase of the host throughout the experimental procedures. It is suggested that a host system with fewer inherent problems be selected as a suitable model in future studies.

This study describes the development and implementation of analytical techniques for the elucidation of the underlying processes governing solid-gas sorption reactions, and the use of associated experimental results in conjunction with other analytical tools to suggest a mechanism for gas transport through the crystal lattice of the *transiently* porous compound, **2a**.

CHAPTER 8. References

1. R. Matsuda, R. Kitaura, S. Kitagawa, Y. Kubota, R.V. Belosludov, T.C. Kobayashi, H. Sakamoto, T. Chiba, M. Takata, Y. Kawazoe, and Y. Mita, *Nature*, **2005**. 436. 238.

2. X. Zhao, *Science*, **2004**. 306. 1012.

3. O.M. Yaghi, M. O'Keefe, R. Banerjee, A. Phan, B. Wang, C. Knobler, and H. Furukawa, *Science*, **2008**. 319. 939.

4. K. Uemera, S. Kitagawa, M. Kondo, K. Fukei, R. Kitaura, H.-C. Chang, and T. Mizutani, *Chem. Eur. J.*, **2002**. 8. 3587.

5. G.J. Halder, C.J. Kepert, B. Moubaraki, K.S. Murray, and J.D. Cashion, *Science*, **2002**. 298. 1762.

6. J.W. Steed and J.L. Atwood, *Supramolecular Chemistry*. 2 ed. **2000**: John Wiley & Sons, Ltd.

7. J.-M. Lehn, J.W. Steed, and J.L. Atwood, *Supramolecular Chemistry*. 2 ed. **2000**: John Wiley & Sons, Ltd.

8. H.-J. Schneider and A. Yatsimirsky, *Principles and Methods in Supramolecular Chemistry*. **2000**: John Wiley & Sons, Ltd.

9. H. Davy, *Philosophical Transactions of the Royal Society of London*, **1814**. 1. 62.

10. M. Faraday and H. Davy, *On Fluid Chlorine. Philosophical Transactions of the Royal Society of London*, **1823**. 113. 160.

11. A. Werner, *Z. Anorg. Chem*, **1893**. 3. 267.

12. G.O. Lloyd, *Crystal Engineering of Porosity, Master of Science Thesis*, in *Department of Chemistry & Polymer Science*. 2006, University of Stellenbosch: Stellenbosch.

13. P. Ehrlich, *Studies on Immunity*. **1906**: John Wiley & Sons, Ltd.

14. E. Fischer, *Ber. Dtsch. Chem. Ges*, **1894**. 27. 2985.

15. K.L. Wolf, F. Frahm, and H. Harms, *Z. Phys. Chem. Abt. B*, **1937**. 36. 17.

16. K. Rouquerol, J. Rouquerol, and K. Sing, *Adsorption by Powders and Porous Solids Principles, Methodology and Applications*. **1999**, London: Academic Press.

17. B. Crittenden and W.J. Thomas, *Adsorption Technology and Design*. **1998**: Butterworth-Heinemann.

18. J.-M. Lehn, *Angew. Chem. Int. Ed*, **1990**. 27. 1304.

19. G.O. Llloyd, *Crystal Engineering of Porosity, Master of Science Thesis*, in *Department of Chemistry & Polymer Science*. 2006, University of Stellenbosch: Stellenbosch.

20. J.D. Dunitz, *Pure Appl. Chem.*, **1991**. 63. 177.

21. P. Ball, *Nature*, **1996**. 381. 648.

22. J. Maddox, *Nature*, **1988**. 335.

23. A. Gavezzotti, *Acc. Chem. Res.*, **1994**. 27. 309-314.

24. K.T. Holman, A.M. Pivovar, and M.D. Ward, *Science*, **2001**. 294. 1907.

25. D.J. Cram, *Angew. Chem. Int. Ed*, **1988**. 27(188). 1009.

26. J. Monod, J. Wyman, and J.P. Changeux, *J. Mol. Biol.*, **1965**. 12. 88.

27. D. Voet and J.G. Voet, *Biochemistry*. 3 ed. Vol. 1. **2004**: John Wiley & Sons, Inc.

28. D.E.J. Koshland, G.Nemethy, and D. Filmer, *Biochemistry*, **1966**. 1. 365.

29. A.G. Grechin, H.-J. Buschmann, and E. Schollmeyer, *Angew. Chem. Int. Ed*, **2007**. 46(6499).

30. L.R. Nassimbeni, *Acc. Chem. Res.*, **2003**. 36. 631.

31. T. le Roex, *The Physico-Chemical Properties of Organic Inclusion Compounds*, in *Department of Chemistry*. 2004, University of Cape Town: Cape Town.

32. C.H. Giles, *J. Chem. Educ.*, **1962**. 39. 584.

33. C.W. Scheele, *Chemische Abhandlung vor der Luft und dem Feuer*, **1773**.

34. J.W. McBain, *The Sorption of Gases and Vapours by Solids*. **1932**, London: Rutledge & Sons.

35. F. Fontana, *Mem. Mat. Fis. Soc. Ital*, **1777**. 1. 679.

36. H. Kayser, *Wied. Ann. Phys.*, **1881**. 12. 526.

37. H. Kayser, *Wied. Ann. Phys.*, **1881**. 14. 141.

38. C. Tien, *Adsorption Calculations and Modeling, Butterworth-Heinemann Series in Chemical Engineering*. **1994**, USA: Butterworth-Heinemann.

39. M. Suzuki, *Adsorption Engineering, Chemical Engineering Monographs 25*. **1990**: Kondansha Ltd and Elsevier Publishers B.V.

40. S. Brunauer, L.S. Deming, W.E. Deming, and E.J. Teller, *J. Am. Chem. Soc.*, **1940**. 62. 1723.

41. D.M. Ruthven, *Principles of Adsorption and Adsoprtion Processes*. **1984**, USA: John Wiley & Sons, Inc.

42. M.D. Donohue and G.L. Aranovich, *Adv. Colloid Interface Sci.*, **1998**. 76-77. 137.

43. P.K. Thallapally, L. Dobrzanska, R.T. Gingrich, T.B. Wirsig, L.J. Barbour, and J.L. Atwood, *Angew. Chem. Int. Ed*, **2006**. 45. 6506.

44. L. Dobrzanska, G.O. Lloyd, C. Esterhuysen, and L.J. Barbour, *Angew. Chem. Int. Ed*, **2006**. 45. 5856.

45. P.K. Thallapally, G.O. Lloyd, T.B. Wirsig, M.W. Bredenkamp, J.L. Atwood, and L.J. Barbour, *Chem. Commun.*, **2005**. 5272.

46. P.K. Thallapally, T.B. Wirsig, L.J. Barbour, and J.L. Atwood, *Chem. Commun.*, **2005**. 4420.

47. J.L. Atwood, L.J. Barbour, and A. Jerga, *Angew. Chem. Int. Ed.*, **2004**. 43. 2948.

48. J.L. Atwood, L.J. Barbour, A. Jerga, and B.L. Schottel, *Science*, **2002**. 298. 1000.

49. L. Pauling, *The Nature of the Chemical Bond*. Vol. 3. **1960**, Ithaca, New York: Cornell University Press.

50. M. Bowker, *The Basis and Applications of Heterogeneous Catalysis*. Oxford Chemistry Primers, ed. R.G. Compton. **1998**, New York: Oxford University Press.

51. F. London, *Z. Phys.*, **1930**. 63. 245.

52. J.E. Leonard-Jones, *Trans. Farad. Soc.*, **1932**. 28. 333.

53. T. Jacobs, *Design and Construction of Novel Porous Materials*, in *Department of Chemistry & Polymer Science*. 2007, University of Stellenbosch.

54. A. Cronstedt, *Akad. Handl. Stockholm*, **1756**. 18. 120.

55. A. Cronstedt, *Mineral. Stockholm*, **1758**. 102.

56. D.W. Breck, *Zeolites Molecular Sieves*. **1974**, New York: John Wiley & Sons.

57. R.M. Barrer, *Zeolites and Clay Minerals as Sorbents and Molecular Sieves*. **1978**, London: Academics Press Inc.

58. L.J. Barbour, *Chem. Commun.*, **2006**. 1163.

59. *www.bza.org/zeolites.html*. www.bza.org/zeolites.html.

60. D. Garber, *The Cambridge History of Science*. Modern Early Science, ed. K. Park and L. Daston. Vol. 3. **2006**, Cambridge: Cambridge University Press. 25-30.

61. O.M. Yaghi and H. Li, *J. Am. Chem. Soc.*, **1995**. 117. 10401.

62. D.N. Dybtsev, H. Chun, S.N. Yoon, D. Kim, and K. Kim, *J. Am. Chem. Soc.*, **2004**. 126. 32-33.

63. M. Eddaoudi, D.T. Vodak, J. Kim, M. O'Keefe, and O.M. Yaghi, *Science*, **2003**. 300. 1127.

64. A.W. Coleman, S. Jebors, S. Cecillion, P. Perret, D. Garin, D. Marti-Battle, and M. Moulin, *New J. Chem.*, **2008**. 32. 780.

65. A.W. Coleman, S. Jebors, P. Shahgaldian, G.S. Ananchenko, and J.A. Ripmeester, *Chem. Commun.*, **2008**(20). 2291.

66. J.L. Atwood, K.T. Holman, and J.W. Steed, *Chem. Commun.*, **1996**. 1401.

67. M.J. Rosseinsky, X.B. Zhao, B. Xiao, A.J. Fletcher, K.M. Thomas, and D. Bradshaw, *Science*, **2004**. 306. 1012.

68. H.K. Chae, D.Y. Siberio-Perez, J. Kim, Y. Go, M. Eddaoudi, A.J. Matzerger, M. O'Keefe, and O.M. Yaghi, *Nature*, **2004**. 427. 523.

69. in *Chambers's Twentieth Century Dictionary*, W. Geddie, Editor. 1966, W. & R. Chambers, Ltd.: Edinburgh.

70. K. Uemera and S. Kitagawa, *Chem. Soc. Rev.*, **2005**. 34. 109.

71. S. Kitagawa, T. Nakamura, and S.-I. Noro, *Chem. Commun.*, **2006**. 701.

72. S. Kitagawa, R. Kitaura, and S.-I. Noro, *Angew. Chem. Int. Ed*, **2004**. 43. 2334.

73. G.R. Desiraju, M.A. Viswamitra, R. Radhakrishnan, and J. Bandekar, *J. Am. Chem. Soc.*, **1993**. 115. 4868.

74. S.J. Delgarno, P.K. Thallapally, L.J. Barbour, and J.L. Atwood, *Chem. Soc. Rev.*, **2007** 36. 236.

75. J.L. Atwood, L.J. Barbour, and A. Jerga, *Science*, **2002**. 296. 2367.

76. S. Kitagawa, R. Kitaura, K. Seki, and G. Akiyama, *Angew. Chem. Int. Ed*, **2003**. 42. 428.

77. K. Kim, D.N. Dybtsev, and H. Chun, *Angew. Chem. Int. Ed*, **2004**. 43. 5033.

78. S. Kitagawa, T.K. Maji, G. Mostafa, and R. Matsuda, *J. Am. Chem. Soc.*, **2005**. 127. 17152.

79. A.A. Frost and R.G. Pearson, *Kinetics and Mechanism: A Study of Homogenous Chemical Reaction*. 2 ed. **1961**, New York: John Wily & Sons, Inc.

80. B. Stevens, *Chemical Kinetics for General Chemistry Students of Chemistry*. **1970**, U.K.: Chapman & Hall Ltd and Science Paperbacks.

81. www.leonardo-energy.org/drupal/node/2101.

82. Unknown. *Thermodynamics vs. Kinetics*. http://www.columbia.edu/itc/chemistry/chem-c140499/chemgate/module_sn2.pdf.

83. L.J. Barbour, M.R. Caira, and L.R. Nassimbeni, *J Chem. Soc. Perkin Trans. 2*, **1993**. 2321.

84. E. Garrone and C.O. Arean, *Chem. Soc. Rev.*, **2005**. 34. 846.

85. R.M. Barrer and D.A. Ibbitson, *Trans. Farad. Soc.*, **1944**. 4. 195.

86. H.H. Hey, *Miner. Mag.*, **1935**. 24. 99.

87. S. Sircar, A.L. Myers, J.A. Dunne, R. Mariwala, M. Rao, and R.J. Gorte, *Langmuir*, **1996**. 12. 5888.

88. N.A. Katsanos, *J. Chromatogr. A*, **1999**. 845. 103.

89. J.M. Bulow and P. Lorenz, *Fundamentals of Adsorption*, ed. A.I. Liapis. **1987**, U.S.A.: Engineering Foundation, U.S.A. 119-128.

90. J.M. Bulow, A.L. Myers, D. Shen, F. Siperstein, and M. Engelhard, *Adsorption*, **2000**. 6. 275.

91. A. Tian, *Bull. Soc. Chim. Fr.*, **1923**. 33(4). 427.

92. E. Calvet and H. Prat, in *Recent Progres en Microcalorimetrie*. 1958, Dunod: Paris.

93. H. Purnell, *Gas Chromatography*. **1962**, New York: Wiley.

94. A.B. Littlewood, *Gas Chromatography*. **1970**, New York: Academic Press.

95. V.V. Gorbatchuk, *J. Gen. Chem. USSR.*, **1999**. 60. 1069.

96. V.V. Gorbatchuk, *J. Inc. Phen. Macrocycl. Chem.*, **1999**. 35. 309.

97. V.V. Gorbatchuk, A.G. Tsifarkin, I.S. Antipin, B.N. Solomonov, A.I. Konovalov, P. Lhotak, and I. Stibor, *J. Phys. Chem. B*, **2002**. 106. 5845.

98. C.O. Arean, P. Nachtigallova, E. Nachtigall, E. Garrone, and M. Rodriguez-Delgado, *Phys. Chem. Chem. Phys.*, **2007**. 9. 1421.

99. J.L. Atwood, L.J. Barbour, T.B. Wirsig, and P.K. Thallapally, *Chem. Commun.*, **2005**. 51.

100. P.A. Redhead, *Vacuum*, **1962**. 12. 203.

101. R.M. Nix. *An Introduction to Surface Chemistry*. http://www.chem.qmul.ac.uk/surfaces/scc/.

102. S. Morton and C. Walker. *UK Surface Science Forum, Surface Science Techniques - Temperature Programmed Desorption*. http://www.uksaf.org/tech/tpd.html.

103. R.J. Cvetanovic and Y. Amenomiya, *Adv. Catal.*, **1967**. 17. 103.

104. E.T. Nelson and P.L. Walker Jr, *J. Appl. Chem.*, **1961**. 11. 358.

105. R.M. Barrer and B.E.F. Fender, *J. Phys. and Chem. Solids.*, **1961**. 21. 12.

106. H. Rohwer, *The Structure and Properties of the Dihalo (dimethyl) Germanes and Related Compounds*, in *Department of Chemistry & Polymer Science*. 2002, University of Stellenbosch: Stellenbosch.

107. F. Jensen, *Introduction to Computational Chemistry*. **1999**, U.S.A.: John Wiley & Sons, Inc.

108. J. Dillen, *Understanding Chemistry with Theoretical Molecular Models: An Introduction to Some Classical and Quantum Techniques of Molecular Modeling*. **2006**, Stellenbosch: University of Stellenbosch.

109. P.W. Atkins, *Physical Chemistry*. **1978**, Oxford, U.K.: Oxford University Press.

110. H. Dorsett and A. White, *Overview of Molecular Modelling & ab initio Molecular Orbital Methods Suitable for use with Energetic Materials*. **2000**, Salisbury, Australia.: DSTO Aeronautical and Marine Research Laboratory.

111. W. Crous, *The Evaluation of the ONIOM-EE Method for the QM/MM Hybrid Modeling of HF, CO and CO/HF Clusters*, in *Department of Chemistry and Polymer Science*. 2006, Univeristy of Stellenbosch: Stellenbosch.

112. A. Hinchliffe, *Modelling Molecular Structures*. **1996**, Chichester: John Wiley and Sons, Ltd.

113. A. Hinchliffe, *Molecular Modelling for Beginners*. **2003**, USA: John Wiley & Sons, Inc.

114. R.P. Feynman, *The Feynman Lectures on Physics*. Commemorative Edition ed. **1970**: Addison Wesley Longman.

115. A. Leach, *Molecular Modelling: Principles and Applications*. 2nd ed. **2001**: Prentice Hall.

116. S.J. Stuart, R. Zhou, and B.J. Berne, *J. Chem. Phys.*, **1996**. 105(4). 1426.

117. A.B. Richon, *Mathematech*, **1994**. 1. 83.

118. A.B. Richon. *An Introduction to Molecular Modeling*. http://www.netsci.org/Science/Compchem/feature01.html

119. *SMART Data Collection Software, Verson 5.629*: Bruker AXS, Inc. Madison, WI. 2003.
.

120. *SAINT, Data Reduction Software*. Version 6.45 ed: Bruker AXS, Inc. Madison, WI. 2003.

121. Z. Otwinowski and W. Minor, *Denzo & Scalepack, HKL Research, Inc.* 1998.

122. *SADABS, Version 2.05*: Bruker AXS, Inc, Madison, WI. 2003.

123. G.M. Sheldrick, *Acta Cryst. A64*, **2008**. 112.

124. L.J. Barbour, *J. Supramol. Chem.*, **2001**. 1. 189.

125. A.L. Spek, *PLATON, A Multipurpose Crystallographic Tool*. 2007, Utrecht University, Utrecht. The Netherlands.

126. C.R. Reid, I.P. O'Koye, and K.M. Thomas, *Langmuir*, **1998**. 14. 2415.

127. C.R. Reid and K.M. Thomas, *Langmuir*, **199**. 15(3206).

128. A.J. Fletcher and K.M. Thomas, *Langmuir*, **2000**. 16. 6253.

129. *Cerius2 molecular simulation program version 3.8*. 1998, Molecular Simulations Inc.: San Diego, USA.

130. *XPrep, Data Preparation & Reciprocal Space Group Exploration, Version 5.1/NT*. 1997, Bruker Analytical X-Ray Systems.

131. G.M. Sheldrick, *The Shelx-97 Manual, Dept. of Structural Chemistry, Gottingen, Germany.* **1997**.

132. C. Cason, T. Froehlich, N. Kopp, and R. Parker, *POV-Ray for Windows, 3.6*. 2003, Persistence of Vision Raytracer, Pty.Ltd.

133. www.povray.org.

134. P. van der Sluis and A.L. Spek, *Acta. Cryst. A*, **1990**. 46.

135. *Cambridge Structural Database and Cambridge Structural Database System, Version 5.29 (January 2008)*, Cambridge Crystallographic Data Centre, University Chemical Laboratory, Cambridge, England.

136. M.L. Connolly, *J. Mol. Graph.*, **1993**. 11. 139.

137. M.L. Connolly, *Science*, **1983**. 221. 709.

138. M.L. Connolly, *J. Am. Chem. Soc.*, **1985**. 107. 1118.

139. I. Molecular Simulations, *WebLab ViewerPro 3.7*. 2000: San Diego.

140. B.T. Ibragimov and S.A. Talipov, *Gossypol*, in *Encyclopedia of Supramolecular Chemistry*, J.L. Atwood and J.W. Steed, Editors. 2004, Marcel Dekker, Inc.: New York. p. 606.

141. R. Adams, T.A. Geismann, and J.D. Edwards, *Chem. Rev.*, **1960**. 60. 555-574.

142. B.T. Ibragimov, S.A. Talipov, and T.F. Aripov, *J. Inc. Phen. Macrocycl. Chem.*, **1994**. 17. 317.

143. C.D. Gutsche and M. Iqbal, *Org. Synth., Col. Vol.*, **1993**. 8(75).

144. A. Arduini and A. Casnati, eds. *Macrocyclic Synthesis, A Practical Approach (The Practical Approach to Chemisty Series)*. ed. D. Parker. **1996**: Oxford, England.

145. P.K. Thallapally, B.P. McGrail, S.J. Delgarno, H.T. Schaef, J. Tian, and J.L. Atwood, *Nature Materials*, **2008**. 7. 146.

146. D.H. Brouwer, S. Alavi, and J.A. Ripmeester, *Phys. Chem. Chem. Phys.*, **2008**. 10. 3857.

147. J.L. Daschbach, P.K. Thallapally, and B.P. McGrail, *Chemical Physics Letters*, **2008**. 453(4-6). 123.

148. E.B. Brouwer, G.D. Enright, K.A. Udachin, S. Lang, K.J. Ooms, P.A. Halchuk, and J.A. Ripmeester, *Chem. Commun.*, **2003**. 1416.

149. J.L. Atwood, L.J. Barbour, G.O. Lloyd, and P.K. Thallapally, *Chem. Commun.*, **2004**. 922.

150. C.D. Gutsche, *Calixarenes: Synthesis and Historical Perspectives*, in *Encyclopedia of Supramolecular Chemistry*, J.L. Atwood and J.W. Steed, Editors. 2004, Marcel Dekker, Inc.: New York. p. 153.

151. H.-K. Liu, J. Hu, T.-W. Wang, X.-L. Yu, J. Liu, and B. Kang, *Dalton Trans.*, **2001**. 23. 3534.

152. L. Dobrzanska, G.O. Llloyd, H.G. Raubenheimer, and L.J. Barbour, *J. Am. Chem. Soc.*, **2006**. 128. 698.

153. J.M. Adams, D.A. Haselden, and A.W. Hewat, *J. Solid State Chem.*, **1982**. 44. 245.

154. J.J. Pluth and J.V. Smith, *J. Am. Chem. Soc.*, **1980**. 102. 4704.

155. I. Sigma-Aldrich. http://www.sigmaaldrich.com/Brands/Aldrich/Tech_Bulletins/AL_143/Molecular_Sieves.html.

156. H.R. Allcock and E.J. Walsh, *Inorg. Chem.*, **1971**. 10. 1643.

157. P. Sozzani, S. Bracco, A. Conotti, L. Ferretti, and R. Simonutti, *Angew. Chem. Int. Ed*, **2005**. 44. 1816.

158. R.M. Barrer and R.M. Gibbons, *Trans. Farad. Soc.*, **1965**. 61. 948.

159. Y. Belmabkhout, M. Frere, and G. De Weireld, *Meas. Sci. Technol.*, **2004**. 15. 848.

160. R.J. Silbey, R.A. Alberty, and M.G. Bawendi, *Physical Chemistry*. Fourth Edition ed. **2005**, NJ: John Wiley & Sons, Inc.

161. L.R. Nassimbeni and T. Le Roex, *Private Communication, University of Cape Town, Rondebosch, 7701, South Africa*, **2008**.

162. B. Guo, L. Chang, and K. Xie, *J. Nat. Gas Chem.*, **2006**. 15. 223.

163. S.A. Talipov, B.T. Ibragimov, G.B. Nazarov, T.F. Aripov, and A.S. Sadikov, *Khim. Priv. Soedin (Russ.) (Chem. Nat. Compd.)*, **1985**. 835.

164. A. Khelifa, Z. Derriche, and A. Bengueddach, *Microporous Mesoporous Mater.*, **1999**. 32. 199.

165. R.V. Siriwardane, M.-S. Shen, E.P. Fisher, and J.A. Poston, *Energy Fuels*, **2001**. 15. 279.

166. R.J. Harper, G.R. Stifel, and R.B. Anderson, *Can. J. Chem.*, **1969**. 50. 419-433.

167. *www.molecularsieve.org*.

168. R.H. Petrucci and W.S. Harwood, *General Chemistry Principles and Modern Applications*. 6th ed. **1989**: Prentice-Hall International.

169. R.E. Morris and P.S. Wheatly, *Gas Storage in Nanoporous Materials. Angew. Chem. Int. Ed*, **2008**. 47. 2-20.

170. M.E. Brown, *Introduction to Thermal Analysis*. **1988**, London: Chapman & Hall.

171. J.R. Manning, *Diffusion Kinetics for Atoms in Crystals*. **1968**, Princeton, NJ.: D. van Nostrand Company, Inc.

172. R.W. Balluffi, S.M. Allen, and W.C. Carter, *Kinetics of Materials*. **2005**, New York: John Wiley & Sons, Inc.

173. J.L.C. Rowsell and O.M. Yaghi, *Angew. Chem. Int. Ed*, **2005**. 44. 4670.

174. P.K. Thallapally, K.A. Kirby, and J.L. Atwood, *New J. Chem.*, **2007**. 31. 628-630.

175. P.K. Thallapally, B.P. McGrail, and J.L. Atwood, *Chem. Commun.*, **2007**. 1521.

176. H. Sun, *Macromolecules*, **1995**. 28. 701.

177. H. Sun, *J. Comp. Chem.*, **1994**. 15. 752.

178. H. Sun, S.J. Mumby, J.R. Maple, and A.T. Hagler, *J. Am. Chem. Soc.*, **1994**. 116. 2978.

179. H. Sun, S.J. Mumby, J.R. Maple, and A.T. Hagler, *J. Phys. Chem.*, **1995**. 99. 5873.

180. J. Schatz, F. Schildbach, A. Lentz, and S. Rastatter, *J. Chem. Soc., Perkin Trans.2*, **1998**. 75.

181. R.M. Williams, J.M. Zwier, and J.W. Verhoeven, *J. Am. Chem. Soc.*, **1994**. 116. 6965-6966.

182. B.F. Graham, J.M. Harrofield, R.D. Tengrove, A.F. Lagalante, and T.J. Bruno, *J. Inclusion Phenom. Macrycyclic Chem.*, **2002**. 43. 179-182.

183. D.H. Brouwer, I.L. Moudrakovski, K.A. Udachin, G.D. Enright, and J.A. Ripmeester, *Cryst. Growth Des.*, **2008**. 8. 1878.

184. L.J. Barbour, *Private Communication, University of Stellenbosch, Matieland, South Africa.*, **2007**.

185. J.L. Atwood and L.J. Barbour, *Cryst. Growth Des.*, **2003**. 3. 3.